Spring 1998

Source and acceleration of energetic He(+) ions at the Earth's bow shock

Kemei Wang
University of New Hampshire, Durham

INFORMATION TO USERS

This manuscript has been reproduced from the microfilm master. UMI films the text directly from the original or copy submitted. Thus, some thesis and dissertation copies are in typewriter face, while others may be from any type of computer printer.

The quality of this reproduction is dependent upon the quality of the copy submitted. Broken or indistinct print, colored or poor quality illustrations and photographs, print bleedthrough, substandard margins, and improper alignment can adversely affect reproduction.

In the unlikely event that the author did not send UMI a complete manuscript and there are missing pages, these will be noted. Also, if unauthorized copyright material had to be removed, a note will indicate the deletion.

Oversize materials (e.g., maps, drawings, charts) are reproduced by sectioning the original, beginning at the upper left-hand corner and continuing from left to right in equal sections with small overlaps. Each original is also photographed in one exposure and is included in reduced form at the back of the book.

Photographs included in the original manuscript have been reproduced xerographically in this copy. Higher quality 6" x 9" black and white photographic prints are available for any photographs or illustrations appearing in this copy for an additional charge. Contact UMI directly to order.

UMI

A Bell & Howell Information Company
300 North Zeeb Road, Ann Arbor MI 48106-1346 USA
313/761-4700 800/521-0600

SOURCE AND ACCELERATION OF ENERGETIC HE+ IONS AT THE EARTH'S BOW SHOCK

BY

Kemei Wang

B.A., Xinjiang Agriculture College, P.R.China, 1982

M.S., University of New Hampshire, USA, 1994

DISSERTATION

Submitted to the University of New Hampshire

in Partial Fulfillment of

the Requirements for the Degree of

Doctor of Philosophy

in

Physics

May, 1998

This dissertation has been examined and approved.

Dissertation director, Eberhard S Möbius
Research Professor of Physics

Martin A Lee
Solar-Terrestrial Theory Group
Professor of Physics

Philip A Isenberg
Solar-Terrestrial Theory Group
Associate Research Professor of Physics

Lynn M Kistler
Associate Professor of Physics

Dawn C Meredith
Associate Professor of Physics

October 30, 1997

Date

This dissertation is dedicated to

my parents Shifen Wang and Youyi Pan,

my brother Keye Wang and my sister Keyin Wang,

my husband Yuanding Zhang and my son Chang Zhang,

whose love and spiritual supports made this work possible.

ACKNOWLEDGMENTS

I would like to express my sincerest thanks to my research advisor, Professor Eberhard Möbius. Without his thoughtful guidance, extraordinary patience and invaluable help for 6 years, this thesis would never have been possible. I am grateful to professor Marty Lee for his thoughtful and helpful suggestions and his critical reading of this thesis. Many thanks to Dr. Phil Isenberg and Dr. Lynn Kistler for their sincere discussions and help. I would also mention the helpful and enjoyable discussions with Professor Dawn.

To Professor John Mulhern, I offer my genuine appreciation and deepest gratitude. He is the first professor I met when I entered UNH. His concern and encouragement shed light on my life when I struggled in depression. Warmest thanks to Dot Kittredge and Li Tang for their assistance and friendship during these years. Douglas Larson deserves my special recognition for his help in scanning the color plot. I am very grateful to Babara Briggs for her support and friendship.

I am indebted to Yongqing Jiang, my best friend. Her everlasting love, loyal friendship and constant understanding supported me to finish the last sentence of this thesis.

Finally, I would like to very grateful acknowledge the love and dream given to me through the years by my family. To them I dedicate this thesis.

TABLE OF CONTENTS

LIST OF FIGURES

LIST OF TABLES

ABSTRACT

SOURCES AND ACCELERATION OF ENERGETIC HE^{+} IONS AT THE EARTH'S BOW SHOCK

By

Kemei Wang

University of New Hampshire, May, 1998

This thesis have presented the first detailed study of the sources and the acceleration of energetic He^{+} ions in front of the Earth's bow shock, using data from AMPTE/IRM and AMPTE/CCE.

Based on observations of energetic He^{+} ions during an event when the bow shock was an almost perfect perpendicular shock, we compared the results of a simulation to the observed event. The model provides a good quantitative description of the phase space distribution of the gyrating ions. A large portion (approximately 63%) of the incident pickup ions are reflected and gain energy in the interaction. It is also consistent with their spatial distribution in front of the shock. It is shown that a significant fraction of the upstream ions undergo more than one reflection at the bow shock, and gain substantial energy in this interaction.

At the quasi-parallel shock, by calculating the omnidirectional distributions of H^{+}, He^{2+}, He^{+} and O^{+} ions upstream of the shock, as well as a comparison of the observed spectra upstream of the shock and in the magnetosphere with results from the calculations, we concluded that He^{+} is locally accelerated. The subsequent modeling of

the injection and diffusive acceleration at the shock presented evidence that pickup ions can be injected and accelerated more efficiently than solar wind plasma

These results have important implications concerning acceleration of pickup ions and anomalous cosmic rays.

CHAPTER 1

INTRODUCTION

Acceleration of energetic particles at collisionless shock waves is of great importance in interplanetary space as well as on a large scale in our galaxy. The bow shock in front of the Earth's magnetosphere provides an ideal laboratory for studying the shock acceleration process in detail. First observations of energetic particles in the region upstream of the Earth's bow shock were reported by Asbridge et al. [1968], Lin et al. [1974], West and Buck [1976], and Fan et al. [1976]. By the early 1970's, a significant fraction of the qualitative phenomena associated with the region containing the energetic ions from the Earth's bow shock and the low frequency waves (called the foreshock region [Greenstadt et al., 1976]) was identified.

After the successful launch of the International Sun Earth Explorer (ISEE) spacecraft missions in 1977 and 1978, ISEE 1, 2 and 3, a new era in the study of upstream phenomena was opened. The ISEE 1 and 2 satellites with their highly eccentric orbits and the ISEE 3 satellite in a halo orbit around the libration point greatly enhanced our knowledge of upstream particles and waves. For example, in the foreshock region several

different types of suprathermal ion distributions were discovered: (1) Field-aligned beams [Asbridge et al., 1968] travel upstream along the interplanetary magnetic field. They have sharply peaked spectra and narrow pitch angle distributions, and generally do not extend in energy much above ~ 10 keV, which corresponds to a beam speed of a few times the solar wind speed. Field-aligned beams are observed to originate predominantly from the the quasi-perpendicular bow shock, i.e., where ϑ_{Bn} (the angle between the shock normal and the upstream magnetic field) is larger than 45^0. (2) 'Gyrating ions' or specularly reflected ions have a large component of this motion perpendicular to the upstream magnetic field. They are observed both within the foot of quasi-perpendicular shocks [Paschmann et al., 1987] and upstream of the quasi-parallel shock (ϑ_{Bn} is small) [Gosling et al., 1982]. (3) 'diffuse ion' with a pronounced high energy tail and nearly isotropic pitch angle distributions. Paschmann et al. [1979] have demonstrated that the diffuse component is well correlated with the presence of large amplitude low frequency magnetic fluctuations. Scholer et al. [1979] have shown that upstream particle events at energies ≥ 30 keV are in general the high energy tail of the diffuse ion component, although later Scholer et al. [1980a] also found reflected particles extending in energy well above 30 keV. Diffuse ion events occur when the observation point is connected to the quasi-parallel portion of the bow shock. Scholer et al. [1980a] have shown that the rate of occurrence of upstream particle events increases with decreasing angle between the interplanetary magnetic field and the radial direction and have concluded that the bow shock connection time of a field line controls the occurrence of upstream particles. The first composition

measurements of diffuse upstream ions were reported by Ipavich et al. [1979]. They reported two events during which at equal energy per charge the proton to alpha particle ratio at 30 - 130 keV/Q was constant and similar to the ratio in the solar wind.

Soon after the discovery of the upstream bow shock ions, it was recognized [e.g., Barnes, 1970] that the motion of these ions relative to the solar wind would be unstable and would generate low-frequency waves. Generally, the energetic particles in the upstream region are accompanied by hydromagnetic waves in the frequency regime 10^{-2} - 7×10^{-1} Hz. First indications of hydromagnetic waves upstream of the shock were reported by Fairfield [1969] using Explore 34 data. Hoppe et al. [1981] demonstrated that there is a one-to-one correlation between the presence of diffuse upstream ions and the occurrence of hydromagnetic wave in the foreshock region. The simultaneous presence of diffuse ions and hydromagnetic waves in the upstream region led to the widely adopted picture of an intense interplay between the waves and energetic ions. The waves are thought to constitute scattering centers for the ions which provide for a diffusive transport and Fermi acceleration at the bow shock [e.g., Axford et al., 1977]. Lee [1982] explicitly included the excitation of hydromagnetic waves by the energetic particle population in his self-consistent model of the wave-particle interaction. In a preliminary study, Möbius et al. [1987] demonstrated that the relation between wave and particle energy density derived by Lee [1982] holds for a few selected events. Many of the observed features of the diffuse ions, such as their general directional distributions, spectra and spatial

distribution in front of the bow shock, have been successfully interpreted within models based on diffusive acceleration [Ipavich et al., 1981; Scholer et al., 1981].

With the improved instrumentation on the AMPTE/IRM spacecraft, the origin of energetic particles has been an interesting question, i.e., whether the ions are bow shock associated or of magnetospheric origin. Interpretations in terms of bow shock acceleration were reviewed by Scholer [1985], and interpretations in terms of magnetospheric origin were reviewed by Krimigis [1985]. Sarris et al. [1976] and Scholer et al. [1981] presented evidence that energetic magnetospheric ions can traverse the magnetosheath and escape into the upstream region. Detailed ion composition measurements help to differentiate between the two interpretations with respect to the origin of the particles. In a statistical study Ipavich et al. [1984] compared the He^{2+}/H^{+} ratio in diffuse ion events with the same ratio observed simultaneously in the solar wind and in the ring current near the magnetopause during the same orbit. They found a high correlation with the ratio in the solar wind and a much weaker correlation with that in the ring current population. It is thus confirmed that He^{2+} energetic ions are the shock associated populations. Möbius et al. [1986] presented strong evidence that energetic O^{+} ions are magnetospheric bursts, but also that O^{+} behave substantially different from He^{2+}. This supports the view that both sources contribute simultaneously with varying efficiency to the energetic upstream ions.

A third possible source of energetic ions at the bow shock are supplied by interstellar pickup ions. Using a time-of-flight mass spectrometer, interstellar pickup He^{+} was first

detected at 1 AU in 1985 [Möbius et al., 1985]. More recently other pickup ions, such as H^+, He^{2+} , N^+, O^+, and Ne^+, were discovered [Gloeckler et al., 1993; Geiss et al., 1993] with the Solar Wind Ion Composition Spectrometer [Gloeckler et al., 1992] on Ulysses. Interstellar pickup ions have been a subject of interest for some years. The ions are expected to form the dominant internal pressure in the solar wind in the outer heliosphere, and thus can affect the solar wind flow [e.g., Axford, 1972; Holzer, 1977] and the structure of the termination shock, where the solar wind becomes subsonic. Pickup ions originate in the solar wind when slowly moving interstellar atoms are ionized and picked up by solar wind electromagnetic field. Being charged, these newly born interstellar pickup ions are now subjected not only to a variety of plasma processes, but are also accelerated by interplanetary shocks as they propagate outward. The most abundant pickup ion species at 1 AU is He^+.

The importance of a study of pickup ions as a source for energetic upstream ions is two fold: Firstly, pickup ions represent a source with a velocity distribution much different from the solar wind, and thus a comparison of the acceleration of solar wind and pickup ions can provide further insight into the acceleration mechanism. Secondly, pickup ions are thought to be the source of the anomalous cosmic rays(ACR). The ACR were discovered two decades ago [Garcia-Munoz et al., 1973; Hovestadt et al., 1973; McDonald et al., 1974] and represents an enhancement of He, N, O, Ne and Ar relative to their nominal abundance in low-energy galactic cosmic rays. This component in effect constitutes a background that masks the low-energy properties of certain elements of

galactic cosmic rays. These relatively low energy, high-rigidity singly charged particles provide a valuable additional means for studying both modulation and the properties of the region in the outer heliosphere where these single ionized ions are accelerated. Interstellar pickup ions are believed to be the source of the ACR component [Fisk, et al., 1974] and thus studying the acceleration of He^+ pickup ions at the bow shock can help us to learn about the acceleration process of ACR. On the other hand, we cannot rule out the possibility that the energetic He^+ ions could also be magnetospheric He^+ ions which traverse the magnetosheath and escape into the upstream region as energetic O^+ ions.

Therefore, the main goals of this work are to determine the source and to study the acceleration of energetic He^+ ions at the Earth's bow shock. This is accomplished by using data from the AMPTE/IRM (Active Magnetospheric Particle Tracer Exploreres /Ion Release Module) spacecraft for individual event analysis and statistical studies, which are compared with numerical simulations. The work is divided into two parts. One part is restricted to an almost perfect perpendicular bow shock and focuses especially on the specular reflection process. In the second part we will turn to the quasi-parallel shock, determine the source of the energetic He^+ ions, and then focus on diffusive acceleration.

To put the studies of this work into context, it is useful to review briefly observations and models of suprathermal ion distributions upstream of the Earth's bow shock. Types of ion distributions and their possible sources, such as leakage from the magnetosphere into the upstream or bow shock associated particles, are described in chapter 2. In chapter

3 the basic features of pickup ions, their observations and the modeling of their distribution function are reviewed. A description of the instruments on AMPTE/IRM and AMPTE/CCE can be found in chapter 4.

The first main topic of this work is devoted to a numerical simulation of the He^+ ion distribution, that is formed by specular reflection of pickup He^+, at a perpendicular shock. The model as well as comparisons with the measurements are presented in chapter 5.

The second objective of this work is a thorough analysis of diffuse He^+ ions at the quasi-parallel shock. Composition measurements and abundance ratios between several ions are used to determine the relative importance of the two possible sources, the magnetosphere, and acceleration of pickup ions at the shock. Diffusive theory using the standard convection-diffusion cosmic ray transport equation is reviewed in chapter 6. Two models are constructed that use the same diffusion-convection equation with two different boundary conditions for further quantitative analysis. The first model is based on the assumption that all particles are magnetospheric ions traversing the magnetosheath and escaping into the upstream region. The contradicts from the comparisons of the satellite observations with the results of model 1 confirm quantitatively that the energetic He^+ ions are not magnetospheric ions. The second model treats pickup He^+ ions as the source of energetic He^+ ions. Calculations of injection efficiency are the second emphasis of chapter 6. Finally, conclusions are drawn in chapter 7.

CHAPTER 2

CLASSIFICATION AND DESCRIPTION OF SUPRATHERMAL ION DISTRIBUTIONS UPSTREAM FROM EARTH'S BOW SHOCK

The foreshock region contains a variety of suprathermal ion distributions. The spatial location of these distributions and the location of the quasi-parallel and quasi-perpendicular bow shock regions are shown schematically in Figure 2.1 [from Fuselier,1994] for the Parker spiral interplanetary magnetic field (IMF) orientation. From early observations it was clear that the regions upstream and downstream from the quasi-parallel and quasi-perpendicular bow shock differed considerably. Here, the shock is considered quasi-perpendicular shock when ϑ_{Bn} is greater than 45^0, where ϑ_{Bn} is the angle between the average upstream magnetic field (averaged over an appropriate time interval to remove the fluctuating magnetic field) and the shock normal. The shock is considered quasi-parallel shock when ϑ_{Bn} is less than 45^0. In Figure 2.1, magnetic field lines are shown upstream from the shock, while in the magnetosheath downstream from the shock, streamlines are labeled with their upstream value of ϑ_{Bn} at the shock [see also Russell et

al., 1983]. The region containing ions backstreaming from the Earth's bow shock is called the foreshock region [Fusilier, 1994].

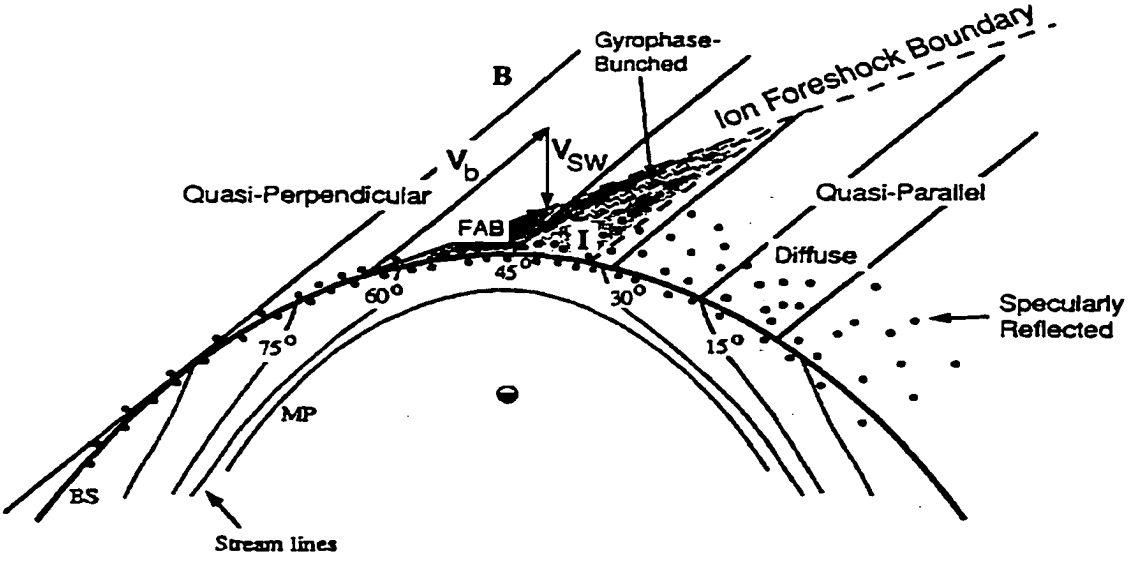

Fig. 2.1. Schematic of the foreshock and magnetosheath. The magnetic field is shown upstream from the bow shock and streamlines labeled with their ϑ_{Bn} are shown downstream from the shock. The ion foreshock is bounded by the Earth's bow shock and the ion foreshock boundary. The foreshock boundary is not the magnetic field because ion beam speeds along the magnetic field (V_b) are comparable to the convection speed of the solar wind (V_{sw}). In the foreshock region, field-aligned beams (FAB), gyrophase-bunched, intermediate (I), diffuse, and specularly reflected distributions are observed.

In the quasi-perpendicular foreshock, field-aligned beams (FAB in Figure 2.1) with a sharply peaked energy spectrum seldom extending much above 10 keV are observed. The quasi-parallel foreshock contains a variety of distributions including intermediate with properties intermediate between those of the field-aligned beams and the diffuse ions, (I in Figure 2.1), diffuse ions with relatively flat energy spectra extending well above 10 keV

and falling off more steeply above 100 keV, and specularly reflected ion distributions (with energies of approximately a few keV). As will seen in the next two sections, there are profound differences between the suprathermal ion distributions in these two regions.

Following the initial report of ions observed backstreaming away from the Earth's bow shock with energies of several kilovolts, considerable theoretical and experimental attention has been given to the problem of upstream ions. There are two basic types of suprathermal ion distributions upstream and downstream from the Earth's quasi-perpendicular shock.

2.1 Review of Observations and Models at Quasi-Perpendicular Bow Shock

2.1.1) specularly reflected ions

One type of suprathermal ion distribution that is observed immediately upstream and downstream of the quasi-perpendicular bow shock is the specularly reflected ion distribution [Paschmann et al., 1982]. An example of a specularly reflected ion distribution near the quasi-perpendicular bow shock is shown in Figure 2.2 [from Fuselier et al., 1986a]. The contours in this figure show the phase space density of ions in the ecliptic plane with two contours per decade of phase space density. The V_x direction

(toward the Sun) is to the left and the V_y direction (duskward) down. The center of the contour plot is zero velocity in the spacecraft frame. The tightly space contours in the -V_x direction are the solar wind ion distribution . The magnetic field direction is identified by the arrow labeled $\bar{B}$ in each contour plot and this magnetic field line is connected to the Earth's bow shock in the -$\bar{B}$ direction.

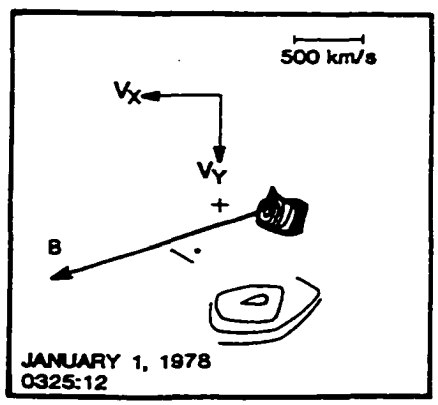

Fig. 2.2 An example of a specularly reflected ion distribution observed near the the Earth's quasi-perpendicular bow shock. In this plot, the center of the panel is zero velocity in the spacecraft frame. Positive Vx and Vy point sunward and duskward, respectively. **B** in the figure is the magnetic field direction and the direction to the shock is along -**B**. The tightly spaced contours in the -Vx direction are the solar wind. The more loosely space contours in the -Vy direction are the specularly reflected ions.

In specular reflection, the component of the incident solar wind ion velocity normal to the shock is reversed but the component tangential to the shock and the total speed remains the same. The initial trajectory of a specularly reflected ion depends crucially on θ_{Bn}, [Gosling et al., 1982]. For $\theta_{Bn} > 45^0$, specularly reflected ions have guiding center motions which are directed downstream. In this geometry, specularly reflected ions gyrate into the upstream region, gain energy by moving parallel to the solar wind electric field, and return to the shock with considerably more energy than when they left it. These higher energy ions cross the shock and gyrate into the downstream region, where they contribute importantly to downstream thermalization. The ion distributions are confined to within one gyro-radius upstream from the shock [Gosling and Robson, 1985]. Particles

may suffer further encounters with the shock due to the combined action of the interplanetary electric field and the Lorentz force. The resulting ion distribution can have a large component of its motion perpendicular to the upstream magnetic field. Paschmann et al. [1982] have presented observations of gyrating ions within the foot region of a quasi-perpendicular bow shock, i.e. $\vartheta_{Bn} > 45^0$.

2.1.2) Field-Aligned Beams

Field aligned beams were the first type of suprathermal ion distribution observed in the upstream region [Asbridge et al., 1968]. An example of a field-aligned beam is shown in Figure 2.3 [from Fuselier and Thomsen, 1992]. The format is similar to that of figure 2.2 with the tightly spaced contours representing the solar wind distribution and the more open contours representing the suprathermal ion distribution. The contours in the upper part of the plot along the magnetic field are field-aligned ion beams propagating away from the shock with a speed of approximately two to three times the solar wind speed in the spacecraft frame. They generally do not extend in energy much above ~10 keV. Field-aligned beams in the upstream region have densities on the order of 1% of the solar wind proton density [Bonifazi and Moreno, 1981a, b].

Recent analysis of field-aligned beams has shown that they are indeed composed almost entirely of protons. Integrating over 23 events, Ipavich et al. [1988] obtained a very low

He^{2+} to H^+ average ratio (5×10^{-4}) in the field-aligned beams, which is almost two orders of magnitude less than the nominal solar wind ratio. A similar result was obtained by Fuselier and Thomsen [1990] using 14 events observed with ISEE 1 and 2. They found that in field-aligned beams, He^{2+} is depleted by a factor of 10 or more relative to H^+.

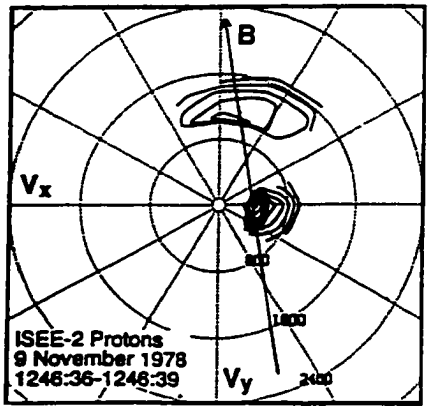

Fig.2.3 An example of a field-aligned beams observed upstream from the Earth's bow shock . The format is the same as in Figure 2.2.

Field-aligned beams were first thought to originate through reflection of the incident solar wind proton distribution at the quasi-perpendicular bow shock [Sonnerup, 1969]. Probably for this reason, they were first called "reflected ions" [Gosling et al., 1978]. The first quantitative model for field-aligned ion beams upstream of the bow shock was presented by Sonnerup [1969], who studied ion reflection for arbitrary angles between the magnetic field, solar wind and shock normal with all 3 vectors in the same plane. In this model no assumptions on the nature of the reflection process are made, and only the guiding center motion of the particle is considered. The model describes the resulting beam energy in simple geometrical terms, and therefore made it very suitable for an experimental test. Paschmann et al. [1980] extended Sonnerup's two-dimensional calculations to three dimensions and showed that the predictions of the model are

consistent with the observations of energetic ion beams over a wide range of angles between the shock normal and the upstream magnetic field. It has been found that the best agreement between model and the observations is obtained for $\delta = 0.9$, where δ is defined as $V_{//r} / V_{//i}$ in H-T frame and $V_{//r}$ and $V_{//i}$ are the velocity components of reflected ion and incident ion parallel to the magnetic field, respectively. The value is between 0 and 1, δ = 1 stands for reflections that conserve the magnetic moment of the particles. However, based on a limited data set, there is evidence [from Schwartz and Burgess, 1984] that field-aligned proton beams may be produced by either an adiabatic reflection mechanism at the shock or by leakage of a small portion of the hot proton population from the magnetosheath into the upstream region. Further researches have been needed.

In summary, 'gyrating ions' or specularly reflected ions are observed within the upstream of Earth's bow shock ramp. A fairly large fraction (up to ~20%) of the solar wind ions specularly reflected off the quasi-perpendicular shock. Field-aligned beams can propagate a significant distance from the shock and convect with the solar wind into the quasi-parallel foreshock as they are scattered, as illustrated in figure 2.1. Field-aligned beams consisting almost entirely of protons are produced by reflection of a portion (~1%) of the solar wind ion distribution incident on the shock or by leakage of a portion of the hot magnetosheath plasma back into the upstream region [Schwartz and Burgess, 1984]. The evolution of these beams the suprathermal ion distributions is discussed in the next section for the quasi-parallel bow shock.

2.2 Review of Observations and Models at Quasi-Parallel Bow Shock

The scattering of field-aligned beams and the generation of low frequency waves nominally begin in the quasi-perpendicular foreshock but evolution of field-aligned beams and the waves they generate are really seen in the quasi-parallel forshock region [Fuselier, 1994]. In this region there are three basic types of suprathermal ion distributions.

2.2.1) Intermediate ion distributions

An example of an intermediate ion distribution is shown in Figure 2.4 [from Fuselier et al., 1986a]. The format of Figure 2.4 is similar to that of Figure 2.2. Comparing the intermediate ion distribution and the field-aligned beams in Figure 2.3, it is evident that the difference between the two types of distributions is simply that the intermediate ion distribution extends over a much larger angular range than the field-aligned beam. Initially, a field-aligned beam generates a small amplitude magnetosonic wave which eventually grow to sufficient intensity to pitch angle scatter the ions into the less anisotropic intermediate ion distribution. The evolution of field-aligned beams to produce intermediate ion distribution was first confirmed by spacecraft observations [Thomsen et al., 1985; Fuselier et al., 1986c] and the simulations [Lee and Skadron, 1985, Hoshina and Terasawa, 1985]. The intermediate ion distribution is always associated with transverse large amplitude, less compressional hydromagnetic waves.

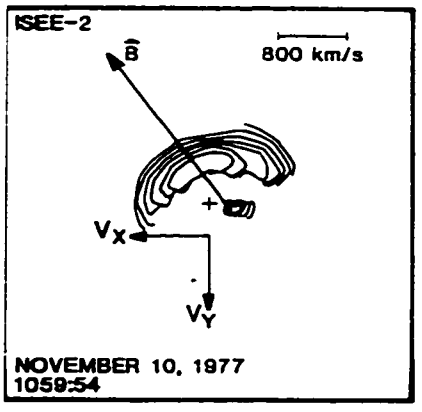

Fig. 2.4 An example of an intermediate ion distribution. This distribution evolved from a field-aligned beam similar to the one shown in Fig.2.2.

2.2.2) Specularly reflected ions

Specularly reflected ions are another distribution observed at quasi-parallel bow shock. The guiding center motion of ions specularly reflected off the Earth's bow shock is determined by the incident solar wind velocity and the shock geometry. For a steady quasi-parallel geometry, $\vartheta_{Bn} < 45^0$, the guiding center motion of specularly reflected ions is directed upstream and these ions will not return to the shock. Specularly reflected ion distributions that fit this description have been observed at large distance (i.e., more than several ion gyro-radii) from the shock [Gosling et al., 1982]. An example of such a distribution is shown in Figure 2.5 [from Fuselier et al., 1986a]. The format of Figure 2.5 is similar to that of Figure 2.2. Unlike the specularly reflected ion distributions near the quasi-perpendicular shock, these distributions are observed at larger distance than one ion

gyro-radius upstream of the quasi-parallel bow shock. They have typical densities on the order of a few percent of the solar wind density and are gyrotropic.

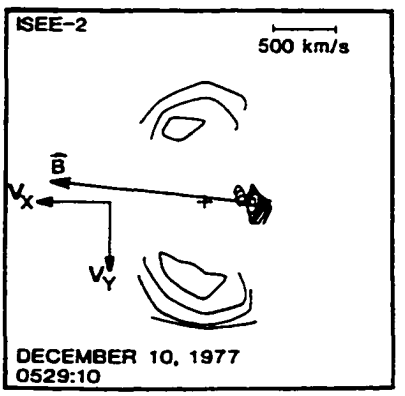

Fig. 2.5 An example of a gyrotropic distribution produced through specular reflection at the quasi-parallel bow shock in the upstream region. The format is similar to that of Fig. 2.2. The suprathermal distribution is nearly gyrotropic but appears as two separate distributions because the measurments give a 2-dimensional cu through the distribution.

2.2.3) Diffuse ion distributions

Diffuse ion distributions such as the example in Figure 2.6 [from Gosling et al., 1989b] appear to represent fully scattered intermediate distributions. The format of Figure 2.6 is similar to that of Figure 2.2. In energy space diffuse upstream ion distributions extend from solar wind energy to 100 or even 200 keV/Q with a peak at about 10-20 keV/Q, i.e., diffuse ions have a pronounced high energy tail. Beyond 30 keV/Q the energy spectra are characterized by an exponential in energy per charge [Scholer et al., 1979; 1981]. The diffuse upstream ions have typically a nearly isotropic distribution in the frame of the spacecraft. In additional, diffuse ion distributions are always observed in association with large-amplitude hydromagnetic waves [Paschmann et al., 1979].

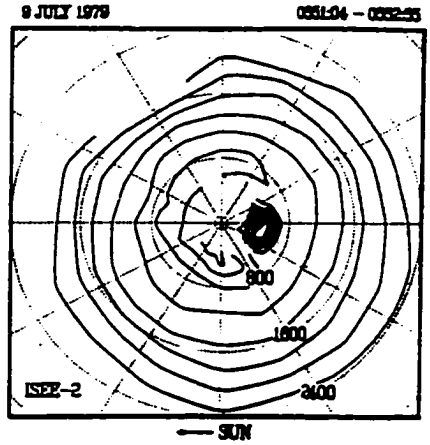

Fig. 2.6 An example of a diffuse ion distribution observed when the magnetic field cone angle was nearly zero. The format is similar to that of Fig. 2.2.

The character of broad angular distributions indicates that the diffuse ion distributions have undergone considerable pitch angle and energy scattering in the turbulent regions upstream and downstream from the quasi-parallel bow shock. The main theoretical acceleration model for diffuse ions is the first-order Fermi or diffusive acceleration model. In this model it is assumed that particles are scattered approximately elastically at scattering centers. The elastic scattering is due to small-angle pitch angle scattering by hydromagnetic waves that convect approximately with the local flow speed. The particles which are scattered back toward the bow shock in the upstream medium can gain considerable energy in the shock frame. The particles are possibly reflected back from the shock front or are scattered back by downstream waves.

From the early observations, it was believed that diffuse ion distributions represented the final evolution of field-aligned beams initially produced at the quasi-perpendicular shock

[e.g., Gosling et al., 1978; Paschmann et al., 1979; Bame et al., 1980]. Several features of these distributions seemed to support this belief. Field-aligned beams, intermediate, and diffuse ion distributions all have typical densities of ~ 1% of the solar wind proton density, are never observed simultaneously, and typically exhibit smooth transitions from one type to another. Diffuse ion distributions like the one in Figure 2.7 which is a cut through the distribution along the Sun-Earth direction (the x axis) extend to much higher

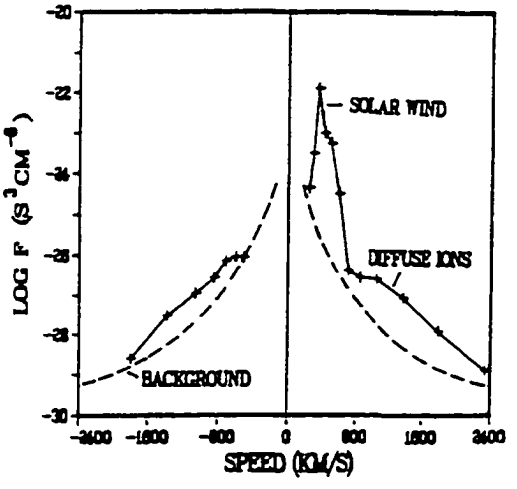

Fig. 2.7 The plot shows a cut through the diffuse distribution in the plasma flow direction. The diffuse distribution represents a nearly fully evolved ion distribution (i.e., one that has undergone severe pitch angle and energy diffusion).

energies (~ 200 keV/Q) than the intermediate distributions and field-aligned beams. Also, most of the energy of the distribution is thermal energy and typical energies of these distributions are several keV/Q. The higher energies of these distributions, compared to the ~ 5 keV/Q mainly kinetic energy of the field-aligned beams and intermediate distributions, suggest energy as well as angular diffusion of the initial field-aligned beam. Finally, the fluctuating magnetic field amplitudes increase from nearly solar wind level in association with field-aligned beams to their highest levels in association with diffuse ion

distributions [e.g., Gary et al., 1981]. The large amplitude fluctuations in the quasi-parallel foreshock ($\delta B/B \sim 1$) are responsible for the rapid acceleration of solar wind ions to high energies to form the energetic ion tail of the diffuse ion distributions [e.g., Lee, 1982].

While it might be true that the intermediate ion distributions evolve from field-aligned beams, it is clear that the beams cannot be the only source of diffuse ion distributions in the quasi-parallel foreshock. As pointed out in the previous section, field-aligned beams are composed almost entirely of protons with very little solar wind He^{2+} present. In contrast, diffuse ion distributions like the one in Figure 2.6 contain a significant fraction of solar wind He^{2+}, especially for higher Mach numbers [Ipavich et al., 1984]. When compared on an equal velocity basis, the composition of diffuse ion distributions is similar to that of the solar wind. This is one of the most important pieces of evidence that the diffuse ion distributions in the energy range from a few keV/Q to ~ 200 keV/Q are predominantely from the solar wind and that field-aligned beams, which contain very little solar wind He^{2+}, may not be an important source of diffuse ion distributions.

Specularly reflected ion distributions like the one in Figure 2.5 are a free energy source for further wave growth in the upstream region. Their density and ability to propagate upstream into the quasi-parallel foreshock make them prime candidates for a source of diffuse ions in that region. Composition measurements appear to support this contention.

Unlike field-aligned beams upstream from the quasi-perpendicular bow shock, which contain little or no solar wind He^{2+}, specularly reflected ion distributions near the quasi-parallel bow shock appear to contain He^{2+} at approximately solar wind concentrations [Fuselier et al., 1990]. However, recent numerical simulations [Scholer and Terasawa, 1990; Scholer and Burgess, 1992] suggest that the specularly reflected ions lead to shock re-formation [e.g., Onsager et al., 1991; Scholer and Burgess, 1992]. Reflected ions travel upstream until they encounter a wave crest. Deflection of the reflected ions, steepening of the wave crest, and deceleration of the incoming solar wind then lead to the emergence of a new shock front. Simulations of the quasi-parallel bow shock structure revealed that the shock is in a state of constant reformation. Observations support this picture and show that the local ϑ_{Bn} of the shock varies considerably as large amplitude magnetic field fluctuations in the quasi-parallel foreshock convect into the shock structure [Greenstadt and Mellott, 1985]. Therefore, it is believed that specularly reflected ions and solar wind ions constitute subsequently the new hot downstream distribution [Thomas et al., 1990] although specularly reflected ions themselves do not provide the bulk of the downstream ion thermalization at the stable quasi-parallel shock.

Another proposed source for the diffuse ions is the thermal leakage of the downstream particle population associated with the quasi-parallel shock. Such a population consists of hot magnetosheath ions moving fast enough to escape upstream [Ellison, 1981]. The leakage model is able to predict quantitatively the measured alpha particle to proton flux ratio in upstream events from the shock parameters. On the basis of self-consistent

hybrid simulations Lyu and Kan [1990] have recently also concluded that backstreaming ions at the quasi-parallel shock are predominantly leakage ions.

In summary, there are a wide variety of suprathermal ion distributions in the quasi-parallel foreshock region. Intermediate distributions are produced by the evolution of field-aligned beams that originate in the quasi-perpendicular foreshock. Diffuse ion distributions have several possible sources including the thermal leakage ion population from the magnetosheath and the evolution of specularly reflected ion distributions. Detailed ion composition measurements help to differentiate between these sources for diffuse ion distributions. In the next section, we review investigations to determine the origins of the diffuse ion population.

2.3 Different Source Distributions For Diffuse Ions

There has been an ongoing debate as to the relative contribution of two sources - magnetospheric bursts and bow shock-associated particles - to the upstream particle population. Sarris et al. [1976] and Scholer et al. [1981] have presented evidence that energetic magnetospheric ions can traverse the magnetosheath and escape into the upstream region. Also the detection of energetic sulfur ions upstream of the Jovian bow shock implies that particles from inside the Jovian magnetosphere can escape into the interplanetary medium [Zwickl et al., 1981]. However, observations at Venus, which does

not have a magnetosphere, show also the occurrence of energetic ions upstream of the bow shock [e.g., Moore et al., 1989; Frank et al., 1991]. This is strong evidence for the ions being accelerated at a bow shock and that a magnetosphere is not the only source providing upstream ions. A good indicator for magnetospheric bursts at the Earth's bow shock are energetic O^+ ions observed during upstream particle events. These ions are of ionospheric origin and can be clearly differentiated from those of solar wind origin [Möbius et al., 1986].

An important indicator for the solar wind is the relative abundance of diffuse alpha particles upstream of the shock. The first composition measurements in upstream energetic particle events were reported by Ipavich et al. [1979]. They discussed two events during which the alpha particle to proton ratio He^{2+}/H^+ at 30-130 keV/Q was constant and similar to that in the solar wind. A more comprehensive study was performed by Ipavich et al. [1981]. In 33 upstream events, they found that the He^{2+}/H^+ ratios in these events vary between 1% and 15% and are similar to the average ratio and variation in the solar wind. Further statistical studies by Ipavich et al.[1984] showed a high correlation(0.83) of the alpha to proton ratio in diffuse ions with the same ratio observed simultaneously in the solar wind. A large body of evidence [e.g., Ipavich, Gosling, Scholer 1984, Möbius 1986, and references therein], strongly indicates that the primary particle source for long lived diffuse ion events is the solar wind. The simulations performed by Trattner and Scholer [1991] have shown that quasi-parallel collisionless shocks can produce suprathermal upstream protons as well as alpha particles and the

density ratio of diffuse alpha particles to diffuse protons is about equal to the same ratio in the solar wind. These results are in agreement with the observations by Ipavich et al. [1984]. Hybrid simulations [Scholer, 1990; Kucharek and Scholer, 1991; Giacalone et al., 1992;1993] have shown that the majority of diffuse ions are not due to leakage of thermalized downstream ions nor due to specularly reflected ions, but they are accelerated from the incident solar wind to high energy while riding for a long period of time (~15 ion gyroperiods) close to the subshock.

A detailed statistical analysis of diffuse ion events and their related waves upstream of the Earth's bow shock was performed by Trattner et al. [1994]. The most striking result is the excellent correlation of the measured hydromagnetic wave energy density with the one predicted by the model of Lee [1982] based on the measured energy density, solar wind and Alfvén velocity. The evidence that the waves and particles are strongly coupled would also hold for energetic particles which may have escaped from the magnetosphere. Both ion components will generate low-frequency upstream waves in a similar way. The ions will be scattered by the waves and will consequently gain energy by multiple reflection between converging scattering centers at the shock. Therefore, Fermi acceleration will be applicable for both ions of solar wind and magnetospheric origin.

A number of issues require further study. As far as the acceleration mechanism at the shock itself is concerned, several questions arise. For example, what is the injection efficiency of the incident distribution extracted into the quasi-parallel bow shock? How

does it depend on species and on original distribution? Interstellar pickup ions, with a velocity distribution clearly distinguished from the solar wind, offer an additional way to study particle acceleration at the shock. We consider He^+ as a candidate to study the acceleration mechanism at the quasi-perpendicular and quasi-parallel Earth's bow shock.

As pointed out by Gloeckler and Hamilton [1987], protons are supplied by both the solar wind and the ionosphere and, while dynamically important, their mixed origin makes it difficult to use them in determining the various acceleration and transport mechanisms in the magnetosphere. Is it possible the same situation happens for He^+ in the region upstream of the shock? Since it is noted that there is a significant charge-exchange between multiply-charged ions with the neutral hydrogen in the geo-crona, much of He^{2+} converts to He^+, which causes the relative abundance of He^+ in the plasma sheet as compared to He^{2+} ($He^+/He^{2+} \approx 1.7$, Gloeckler et al., 1987). The number density ratio of He^+ to H^+ in the magnetosphere is only lower than that of O^+ whose origin is mainly the ionosphere. On the other hand, pickup He^+ ions are an important source in the region upstream of the shock, and play an important role in explaining the source of anomalous cosmic rays at the termination shock. (It is known that the interstellar pickup He^+ to solar wind He^{2+} is about 0.02). Therefore, it is important to sort out the origin of energetic He^+ ions in order to understand the acceleration mechanism. As one of the important source for energetic ions observed in upstream region from the Earth's bow shock, pickup ions will be discussed in detail in the next chapter. In chapter 6 we will use similar techniques such as composition measurements and the relative abundance of

diffuse particles upstream of the shock to distinguish between the magnetospheric He^+ and shock associated He^+ populations in front of the quasi-parallel shock.

CHAPTER 3

INTERSTELLAR PICKUP IONS

The solar system is moving with respect to the local interstellar medium (LISM) with a relative velocity of about 20 km/s, so that from the view of an observer in the heliosphere the interstellar gas is blowing as an interstellar wind through the system. Thus neutral interstellar material penetrates deeply into the heliosphere. Neutral particles in interplanetary space do not interact with the magnetic field embedded in the solar wind. However, when approaching the Sun the interstellar gas is subject to the forces of solar gravitation and radiation pressure. The latter force is substantial for hydrogen, while it is unimportant for all other species. The incoming interstellar neutrals are ionized by solar EUV radiation (dominant for He^+ and Ne^+), by charge exchange with the solar wind (dominant for H^+ and He^{2+}), and by electron collisions. The newly created ions are then immediately picked up by the combined forces of the $-V_{sw} \times B$ electric field and the interplanetary magnetic field B, and finally swept out of the heliosphere. They form a new particle population in the solar wind -- the interstellar pickup ions.

While most of the components of the interstellar gas including the bulk of hydrogen, are already ionized far beyond the orbit of the Earth, noble gases such as helium and neon

(because their high ionization potential) penetrate to less than 1 AU from the Sun [Siscoe and Mukherjee, 1972]. Therefore, a significant fraction of the helium is ionized inside the Earth's orbit. The first positive identification of interstellar He^+ pickup ions and their actual velocity distribution in the solar wind was reported by Möbius et al.[1985b].

Furthermore, the detection of interstellar H^+ [Gloeckler et al., 1993], N^+, O^+ and He^+ pickup ions has been reported [Geiss et al., 1994], as well as that of C^+ which stems mostly from local sources [Geiss et al., 1996]. In this thesis we will concentrate on He^+ ions. Therefore, a brief overview on the He^+ distributions in the solar wind is appropriate here.

3.1 Review of observations

A typical measured velocity distribution of He^+ ions is shown in Figure 3.1[Möbius, 1986]. The gray shading represents the differential energy flux while the concentric rings represent the energy steps of the SULEICA instrument, i.e., the energy of the ions indicated by the radius, the eight sectors represent the sectoring scheme in the flow direction on the ions. The Sun is to the left. The actual solar wind energy is indicated by an arrow. In the solar wind direction the He^+ ions are observed up to a certain cut-off energy, which is equal to the fourfold solar wind bulk energy of helium as determined from the 3D-plasma instrument on the satellite. The ion flux is also seen in the two adjacent sectors up to a significantly lower energy.

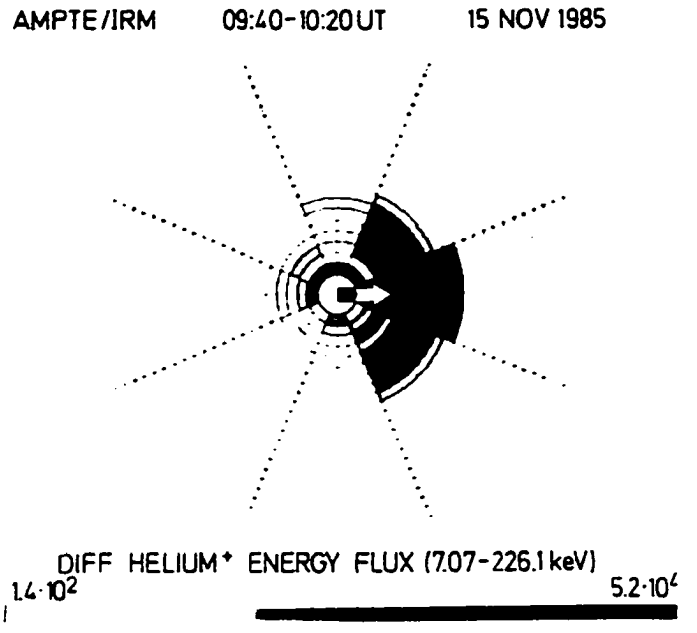

Fig. 3.1. Measured pickup ion energy distribution of He^+ ions in the plane perpendicular to the spacecraft spin axis in a gray shading representation. Each concentric ring represents one energy step of the instrument, the radial lines mark the azimuthal sectoring . The solar wind energy is indicated by an arrow.

The differential energy flux spectrum in the direction of the solar wind is shown in Figure 3.2. The spectrum is basically flat up to the cut-off energy, where the flux drops by more than two orders of magnitude.

The flux of He^+ ions which reflects the neutral density of helium shows a period of significant variation from September to December 1984. In Figure 3.3 [Möbius et all 1995a] the differential energy flux of He^+ at 20 keV is plotted against time. A maximum is reached in early December. During December the Earth is on the downwind side of the interstellar neutral wind with respect to the Sun. Here the helium is focused by the gravitational forces of the Sun and therefore the local density is significantly enhanced.

Figure 3.4 [Möbius et al., 1995a] shows a schematic representation of the neutral helium distribution in the inner heliosphere with an indication of how the data are obtained from an Earth orbiting spacecraft. Due to the gravitation of the Sun, a significant density enhancement, the so-called focusing cone, is found on the downwind side of the Sun. The density increase and the width of the cone depend sensitively on the inflow velocity and the temperature of the neutral gas.

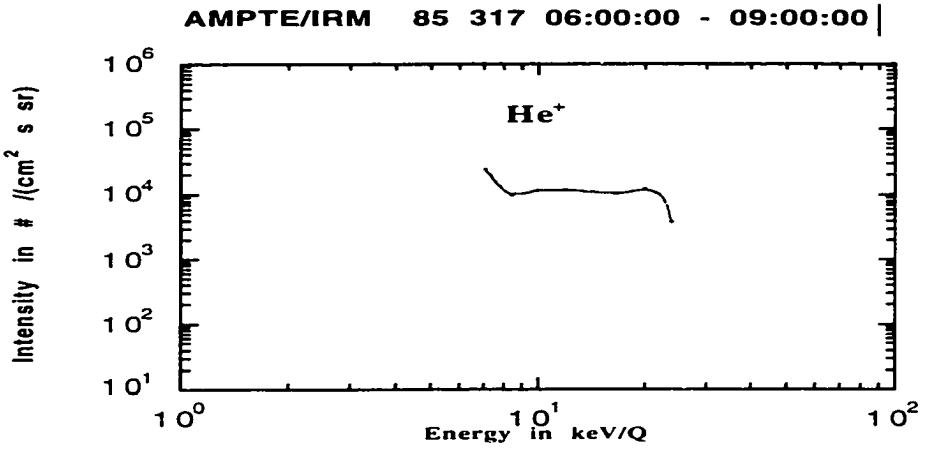

Fig. 3.2 Differential energy flux spectra of He^{+} ions taken in the sun-sector for the quasi-parallel bow shock

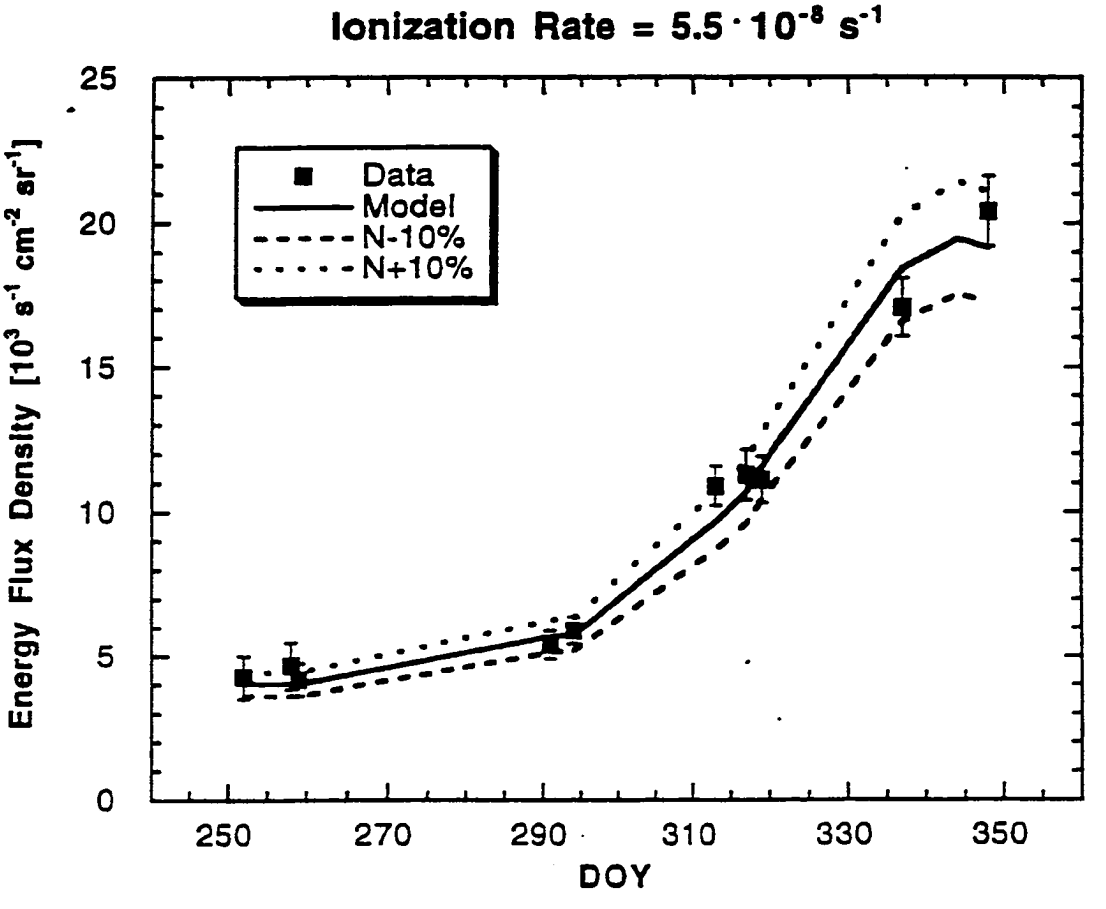

Fig. 3.3 Differential energy flux of 20-keV He^+ ions obtained in the Sun-sector for different time periods between September and December 1984.

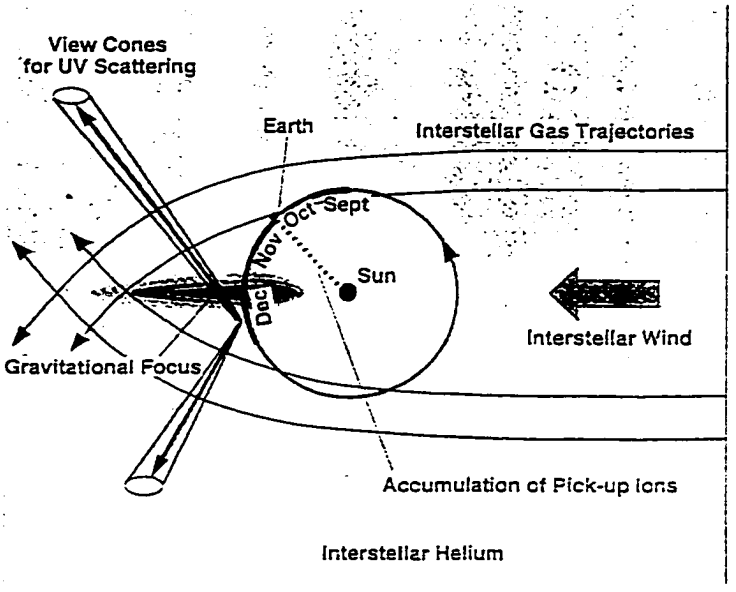

Fig. 3.4. Schematic representation of the trajectiories and the spatial distribution of interstellar helium in interplanetary space. The cones indicate the line-of-sight integrals obtained from UV backscattering measurements in the Earth's orbit. The dashed radial line indicates a cut through the spatial distribution observed in pickup ions from the Earth's orbit.

3.2 Review of the models

Vasyliunas and Siscoe [1976] presented a model of the pickup ion distribution based on instantaneous isotropization of the ions due to pitch-angle scattering and subsequent adiabatic deceleration in the expanding solar wind. The resulting distribution with a sharp cut-off at the solar wind energy, was found compatible with the helium distribution observed by Möbius et al. [1985b]. Generalizing the model by Vasyliunas and Siscoe [1976], Isenberg [1987] included the effect of energy diffusion. We will restrict ourselves to the Vasyliunas and Siscoe model because it describes the source distribution with sufficient accuracy for the work in this thesis. In this section, we review the derivation of the distribution function of pickup ions and the basic results of the model calculation.

3.2.1) Initial pick-up

In contrast to genuine solar wind ions, freshly created ions in interplanetary space are initially at rest. Immediately after ionization they are subject to the combined forces of the interplanetary $V_{sw} \times B$ electric field and the magnetic field B. In the inertial system the ions initially perform a cycloidal motion perpendicular to the local magnetic field as schematically shown in Figure 3.5[Möbius et al. 1986]. Their velocity varies between basically zero (the relative velocity of the neutral gas, ≈ 20 km/s for the interstellar gas, is neglected here compared with the solar wind velocity) and a maximum value:

$$V_{\perp max} = 2\, V_{sw} \sin \alpha \qquad (3.1)$$

α is the angle between the solar wind flow direction and the local magnetic field.

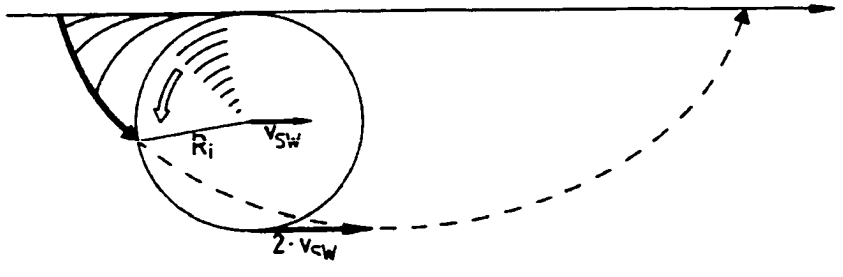

Fig. 3.5 Schematic of the cycloidal trajectory of pickup ions for perpendicular geomatry.

The maximum energy of pickup ions then is

$$E_{\perp Max} = 4\frac{m}{2}V_{sw}^2 \sin^2\alpha \tag{3.2}$$

In the solar wind frame, the distribution function is a ring in velocity space with the pitch-angle α, as demonstrated in Figure 3.6. The ions gyrate with a velocity

$$V_{\perp} = V_{sw} \sin\alpha \tag{3.3}$$

and move along the field with

$$V_{//} = V_{sw} \cos\alpha. \tag{3.4}$$

The signatures of such undisturbed ring distributions have been observed after the artificial injections of lithium clouds into the solar wind [e.g., Möbius et al., 1986].

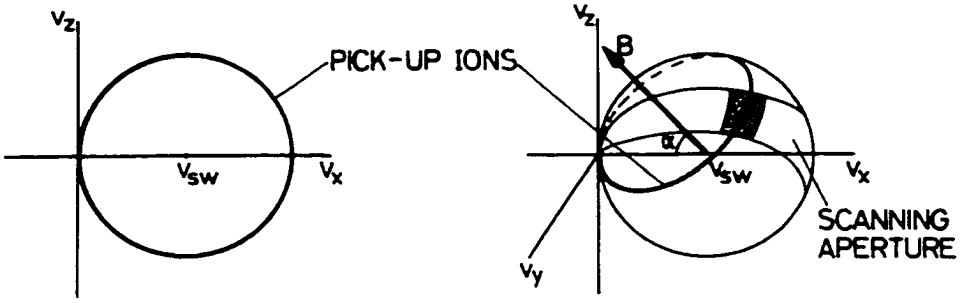

Fig..3.6 Distribution of pickup ions in velocity space; Magnetic field perpendicular to the solar wind velocity (left). Magnetic field direction oblique (right).

3.2.2) Formation of pickup ion distribution

Resonant interaction with the ambient Alfvén waves leads to an isotropization of the original ion distribution. Scattering of the ions in pitch-angle ϑ is much more efficient than diffusion in energy E, since according to quasi-linear theory the corresponding scattering efficiencies scale as $(V_A / V_{sw})^2$ for pickup ions at the solar wind velocity, where V_A is the local Alfvén velocity.

The pickup ions are scattered in pitch-angle on a typical timescale $\tau \approx \lambda / V_{sw}$, where λ is the average distance over which the ions are transported with the solar wind before being effectively pitch angle scattered. In this sense we use λ as the mean free path of scatter-free transport; its typical value has been found of the order of 0.1 AU [Möbius et al., 1988]. The scattering transforms the initial ring distribution into a spherical shell in velocity space. While the shell is convected in the anti-sunward direction, the pickup ion distribution is subject to adiabatic cooling in the expanding solar wind [Vasyliunas and Siscoe, 1976]. As shown by Möbius et al. [1988], the adiabatic cooling is significant on a time scale much longer than that for pitch-angle scattering, but acts much faster than diffusion in energy space. Thus it is reasonable to assume a distribution which results from a combination of pitch-angle scattering into an isotropic spherical shell and subsequent adiabatic cooling. In this view the distribution consists of nested shells in velocity space whose phase space density f(V) is determined by the ion production rate S_r (r) of these ions as a function of the heliocentric distance or along the Sun-spacecraft

line. Treating the pickup ion distribution as an ideal gas (adiabatic index $\gamma = 5/3$), the radius V of the spherical shell in velocity space has a relationship

$$V / V_{sw} = (r / r_i)^{-2/3} \tag{3.5}$$

where r represents the distance from the Sun, starting at the location of ionization r_i. This relation is equivalent to an unique mapping of the distance r_i from the Sun into velocity space. In a steady state the outward flux density of interstellar ions at a distance r from the Sun is found by integrating the ionization rate inside an infinitesimal solid angle segment of a sphere of radius r and dividing by its surface area. If n_i is the number density of ions of a given species, the outward flux density is

$$n_i V_{sw} = V_{sw} \int_V^{V_{sw}} 4\pi f(V') V'^2 dV' \tag{3.6}$$

That is

$$\frac{1}{4\pi r^2} \int_{r_i}^{r} S(r') 4\pi r'^2 dr' = V_{sw} \int_V^{V_{sw}} 4\pi f(V') V'^2 dV' \tag{3.7}$$

Differentiating with respect to V then gives

$$f(V) = \frac{S(r_i)}{V_{sw}(4\pi)V^2} \frac{r_i^2}{r^2} \frac{dr_i}{dV} \tag{3.8}$$

For adiabatic deceleration, this result in a velocity distribution is

$$f(V) = \frac{3S(r_i)r}{8\pi V_{sw}^4} \left(\frac{V}{V_{sw}}\right)^{\frac{3}{2}} \tag{3.9}$$

where r is the distance of the spacecraft from the Sun (here 1 AU), r_i is taken as a function of V and, therefore, leads to a simple relationship for the distribution function.

The source distribution $S(r) = N(r)\beta_{ion}(r)$ depends on the local neutral gas density $N(r)$ and ionization rate $\beta_{ion}(r)$. As mentioned before, interstellar neutrals are ionized by solar UV radiation, charge exchange with solar wind protons, and electron collisions. The solar UV flux (dominant for the ionization of interstellar helium [Holzer, 1977]) varies as $1/r^2$ with distance from the Sun and depends substantially on the solar activity [see, e.g., Hinteregger, 1976]. Hence, $\beta_{ion}(r_i) \propto \frac{1}{r_i^2}, \beta_{ion}(r_{ob}) \propto \frac{1}{r_{ob}^2}$, which lead to

$$\beta_{ion}(r_i) = \beta_{ion}(r_{ob})\frac{r_{ob}^2}{r_i^2} \tag{3.10}$$

where r_{ob} is the distance of observation point to the Sun. Therefore,

$$f(V) = \frac{3N_{He}(r_i(V))\beta_{ion}(r_{ob})r}{8\pi V_{sw}^4}\left(\frac{V}{V_{sw}}\right)^{\frac{3}{2}}\frac{r_{ob}^2}{r_i^2} \tag{3.11}$$

Let $r = r_{ob}$ (1 AU), the distribution function can be described by a production rate β_{ion} at the point of observation, while the r-dependence of the neutral density has to be maintained explicitly:

$$f(V) = \frac{3N_{He}(r_i(V))\beta_{ion}(r_{ob})r_{ob}}{8\pi V_{sw}^4}\left(\frac{V}{V_{sw}}\right)^{-\frac{3}{2}} \tag{3.12}$$

The distribution of interstellar neutral particles $N(r_i)$ in the vicinity of the Sun is basically determined by the solar gravitation, radiation pressure and removal by ionization. According to e.g., Fahr [1968], Blum and Fahr [1969]. Holzer [1972], and Axford [1972] for a cold interstellar gas the spatial distribution $N(r_i\ \theta)$ of the neutrals is given by

$$N(r_i,\theta)=\frac{N_0}{\sin\theta}\left[\frac{\partial b_1}{\partial r_i}e^{-\Lambda\theta/b_1}+\frac{\partial b_2}{\partial r_i}e^{-\Lambda(2\pi-\theta)/b_2}\right] \tag{3.13}$$

with

$$\begin{Bmatrix} b_1 \\ b_2 \end{Bmatrix}=\left[(\frac{r_i}{2}\sin\theta)^2+(1-\sigma)\frac{GM}{V_0}r_i(1-\cos\theta)\right]^{\frac{1}{2}}\pm\frac{1}{2}r_i\sin\theta \tag{3.14}$$

which is only applicable when the spacecraft is not too close to the cone. N_0 is the density at infinity, θ the angle between the direction of the Sun's motion (with velocity $V_0 \approx 20$ km/s) with respect to the interstellar medium and the line connecting the observer with the Sun, GM/r_{ion}^2 is the gravitation acceleration of the Sun (~2.2 AU/s^2) and σ is the relative contribution of the radiation pressure (which is negligible for helium, i.e., $\sigma \approx 0$). $\Lambda = r^2\beta_{ion}/V_0$ is a characteristic penetration depth of the interstellar gas, which depends on the ionization rate β_{ion} at the reference distance r and the velocity of the interstellar wind V_0. According to Möbius et al. [1988] for the interstellar pickup He ion, Λ is about 0.5 AU determined from comparison of these expressions with the measured energy spectra, θ is about 120^0 which is roughly estimated according to the position of spacecraft on October 9,1984.Thus, all quantities are determined except N_0 and $\beta_{ion}(r_{ob})$.

Knowing the velocity distribution of He^+ ions, the source strength $S \propto N_0\,\beta_{ion}$ of the pickup ions can be obtained from the measured differential energy flux at a fixed energy. For a direct comparison with the measurements, the ion distribution must be transformed

into the spacecraft frame of reference and then integrated over the instrument field of view $\Delta\Omega$ and energy range ΔE to determine the differential energy flux $EdJ/d\Omega dE$:

$$\frac{EdJ}{d\Omega dE} = \frac{V_{sw}^4 E}{\Delta\Omega\Delta E}\int_{\Delta\Omega}\left[\int_{\Delta E} f'(w',\vartheta,\varphi)w'^3 dw'\right]d\varphi\cos\vartheta d\vartheta \qquad (3.15)$$

$f'(w',\vartheta,\varphi)$ is the distribution function in the spacecraft frame, with the viewing direction (φ,ϑ) with respect to the solar wind flow and $w' = V'/V_{sw}$ where V' is the transformed velocity which is a function of the measured particle energy E. It is assumed here that the distribution is sufficiently isotropized in the solar wind frame, and therefore no pitch-angle dependence has been included. The limits of the integration are taken according to a specific energy step ΔE and solid angle segment viewed by the SULEICA instrument during one spin sector. This procedure is performed numerically. A full description of this procedure is given in Möbius et al.[1988].

3.2.3) Modification in the Modeling of the ion distribution

The current interpretation of pickup ion distributions and their translation into interstellar gas parameters contains several assumptions that have simplified the analysis. They seemed valid for the early pickup ion results. However, according to more recent observations and their analysis, modifications to the model presented above are required. Its simplifying assumptions can be maintained as long as the mean free path length for pitch-angle scattering is short compared with any other relevant scale length in the

evolution of the observed pickup ion distributions, i.e., for adiabatic deceleration and spatial variation of the source. The assumption of very efficient pitch-angle scattering implies that the pickup ion distribution is nearly isotropic in the solar wind frame [e.g.,Vasyliunas and Siscoe, 1976] so that an accurate determination of the total pickup ion flux and thus the local neutral gas density is possible, even from a fraction of the distribution. Recently, studies of anisotropies in the velocity distribution of pickup H^+ in unperturbed high-speed solar wind [Gloeckler et al., 1995] have indicated that the mean free path for pitch-angle scattering of pickup ions can be much larger (on the order 1 AU, or comparable with the size of the inner heliosphere). The significant reduction of the pickup ion flux in the anti-sunward hemisphere of the distribution that has been observed during radial IMF conditions in comparison with pickup during perpendicular IMF [Möbius et al., 1995b] can be explained in the same way.

Except in cases when the IMF is oriented perpendicular to the solar wind direction, the revised view of the pickup ion distribution predicts a substantial reduction of the flux in the anti-sunward heliosphere. In the solar wind frame all pickup ions are injected with a velocity $-V_{sw}$. For radial magnetic field conditions all ions will have to be transported to the anti-sunward hemisphere of the velocity distribution solely by pitch-angle scattering. Because of instrumental constraints, the pickup ion flux and thus the source neutral density has been derived mostly from the anti-sunward portion of the distribution. This restriction applies to the SULEICA sensor with its lower energy threshold at 5 or 10 keV/charge. Therefore, to derive an accurate neutral gas density from the anti-sunward

hemisphere of the pickup distribution observed by SULEICA, modifications seem necessary for a radial shock.

CHAPTER 4

THE AMPTE-MISSION AND ITS INSTRUMENTS

The data for the following analysis were obtained with the Active Magnetospheric Particle Tracer Explorers (AMPTE). This mission was designed to study the access of solar wind ions to the magnetosphere, the convective - diffusive transport and energization of magnetospheric particles, and the interactions of plasmas in space. The mission consisted of three spacecraft: the Ion Release Module (IRM) provided by the Federal Republic of Germany, the United Kingdom Subsatellite (UKS) and the Charge Composition Explorer (CCE) developed and built by the United States. The IRM provided multiple ion release in the solar wind, the magnetosheath, and the magnetotail, with in situ diagnostics of each.

The IRM was equipped with instruments well suited not only to study the interaction of the artificial ion cloud with the ambient medium, but also to investigate the magnetospheric boundary regions and the natural plasma composition. The spacecraft worked successfully for two years before it became inoperational on 14 August 1986. The UKS served as a subsatellite of the IRM spacecraft. Its purpose was to help

distinguish between spatial structure and temporal changes in the plasma phenomena initiated by ion releases from IRM and in the natural magnetospheric environment. The spacecraft operated for ≈ half year before its power supply failed on January 15, 1985. The measured quantities were similar on both IRM and UKS including magnetic fields, positive ions, electrons, and plasma waves. In additional, IRM has ion composition capabilities.

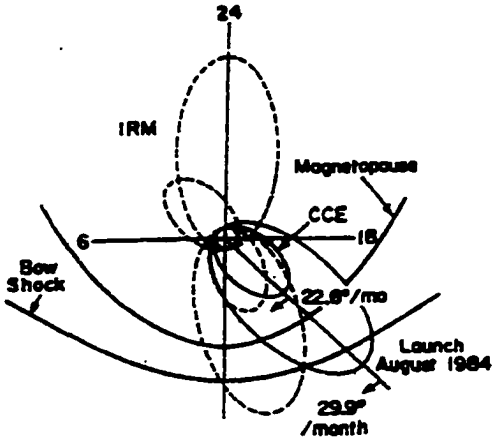

	CCE	IRM
Apogee	8.8 R_E	18.7 R_E
Period	15.6 hrs	44.3 hrs
Inclination	<5°	28.8°

Fig. 4.1. Orbit of the IRM and CCE spacecraft at launch (August 1984) and at two subsequent periods.

The CCE was instrumented to detect those lithium and barium tracer ions that were released from the IRM and transported into the inner magnetosphere. A magnetometer and plasma wave spectrometer complemented the particle measurements. The CCE was

operated for five years before it encountered command module/power supply problems at the beginning of 1989, and failed on 12 July 1989.

4.1 Orbit

All three spacecraft were launched by a Delta 3924 launch vehicle from the Kennedy Space Center in August 1984, into a 29^0 inclined elliptical orbit with an apogee 9.0 R_e geocentric. The IRM and UKS stayed together and on the second orbit were boosted to an apogee of an 18.7 R_e by the IRM kick motor. The CCE also contained a kick motor, which was fired at apogee to reduce the CCE orbit inclination to near 0^0.

The orbits of the CCE and IRM spacecraft are shown in Figure 4.1 [Gloeckler and Hamilton, 1987] at launch and for two later time periods. CCE is in a near equatorial orbit with an apogee of about 9.0 R_e and a 15.6 h period. This orbit is ideal for sampling the ring current. During interplanetary disturbed times, it takes the spacecraft into the daytime magnetosheath and occasionally beyond the bow shock into interplanetary space. CCE's spin axis points roughly at the Sun and its spin period is about 6 s.

IRM has 29^0 inclination, 18.7 Re apogee orbit with a 44 h period. This orbit allows good sampling of the magnetosheath, bow shock and interplanetary space, as well as the ring current region and near-Earth plasma sheet. Its spin axis was initially in the ecliptic plane,

but later it was adjusted with magnetic torqueing to be at right angles to the ecliptic. The spin period is ≈ 4.3 sec. In addition to the diagnostic instrumentation which consisted of a 3D plasma analyzer for electrons and protons, a suprathermal energetic ionic charge analyzer SULEICA, a magnetometer and plasma wave detector, the IRM satellite carried 16 canisters with a mixture of Li and CuO or Ba and CuO for the active ion release experiments. For all the release experiments in the solar wind and the magnetosphere the SULEICA instrument was the only sensor on the spacecraft to evaluate the in situ energetic particle population before and during the ion releases.

The investigations in this thesis are tied to observations upstream of the Earth's bow shock that relied mainly on the instrumentation aboard IRM. For comparison with the composition in the magnetosphere, data from the CHEM instrumentation on CCE are also used. The instrumentation used for our study will now be discussed in more detail.

4.2 Instrumentation on board AMPTE/IRM

To study the origin of particles in and around the magnetosphere, their heating acceleration and transport mechanisms, it is essential to have measurements of the ionic mass, charge and energy distribution and electromagnetic field environment in various regions of the magnetosphere. Therefore, the instrumentation for the in situ measurements on board AMPTE/IRM consisted of

1. a fluxgate magnetometer

2. a 3D plasma instrument

3. a time-of-flight spectrometer

4. a plasma wave instrument

For this investigation the fluxgate magnetometer provided the magnetic field data, the 3D plasma experiment the solar wind density and velocity, and the time-of-flight spectrometer the distribution and composition of the upstream particles. We will restrict ourselves to the description of instruments 1 through 3.

4.2.1) The Fluxgate Magnetometer

The *three-axis fluxgate magnetometer* was developed by the Technische Universität Braunschweig in collaboration with the Max-Pianck-Institut für extraterrestrische Physik (MPE) and the NASA Goddard Space Flight Center. Important features of the instrument were its wide dynamic range from 0.1 nT to 60000 nT and its temporal resolution of 1/32 sec. For detailed information see Lühr et al. [1985].

4.2.2) The 3D plasma Instrument

The *3D plasma instrument* was developed by MPE and the University of California, Berkeley. The instrument consisted of three sensors, two of which measured the complete 3D velocity distribution function of ions and electrons for every spacecraft revolution (4.35 sec). A Langmuir probe was added for low energy measurements.

The basic principle of the first two sensors, hemispherical top-hat electrostatic analyzers, is illustrated in Figure 4.2 [Paschamnn et al., 1985]. Each analyzer had three concentric spherical section elements: an inner hemisphere with radius R_I to which the deflection voltage was applied, an outer hemisphere (with radius $R_I + \Delta$) with a circular hole at its zenith, and a small top cap section (with radius $R_I + 2\Delta$). The gap between the top-hat and the outer hemisphere defined the entrance aperture. Sample trajectories for the three different polar angle directions are shown in Fig.4.2.

The measured distribution was accumulated into 30 energy bins and 128 angles evenly distributed over the 4π solid angle sphere. The instrument covered the energy range from 15 eV to 30 keV for electrons and 20 eV/charge - 40 keV/charge for ions. The basic moments (density, velocity, temperature tensor and heat flux vector) of the distribution functions of ions and electrons were computed in real time by dedicated microcomputers

and were available with a 1 spin time resolution. For a detailed description of the instrument see Paschmann et al. [1985].

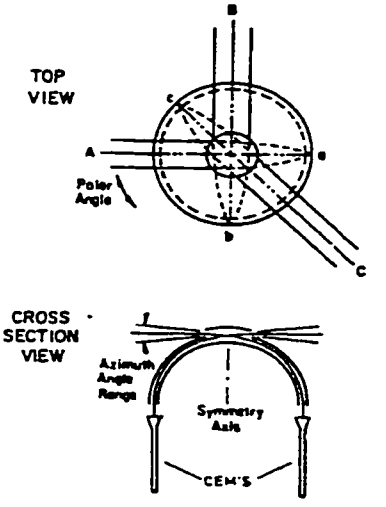

Fig. 4.2. The basic priciple of the 3D plasma experiment (Paschmann et al., 1985).

4.2.3) The Time-of-Flight Spectrometer SULEICA

The SULEICA instrument was designed at MPE and the University of Maryland (UoMd) and was able to distinguish all major ions from H to Fe in the energy range from 5 keV/charge to 270 keV/charge [Möbius et al., 1985]. The entrance aperture had an opening angle of $40^0 \times 10^0$. The distributions were sampled in the spin plane of the satellite in 16 sectors for H^+ and He^{2+} and 8 sectors for all other ions. A complete summary of the capabilities of the instrument is presented in Table 4.1 [from Trattner, 1992]. To determine the ionic charge and mass of incoming ions, the SULEICA sensor

combined the techniques of electrostatic deflection, time-of-flight (TOF) and residual energy measurement. A schematic view of the sensor is presented in Fig. 4.3 [from Möbius et al., 1985].

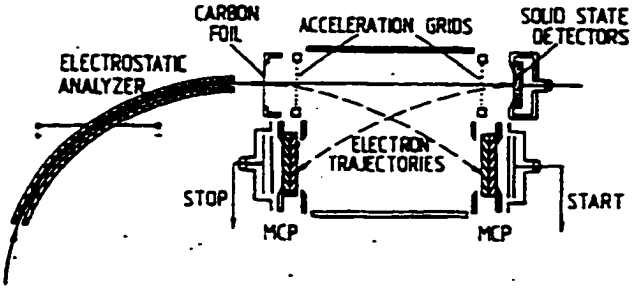

Fig. 4.3. Schematic view of the SULEICA measuring techniques (Möbius et al., 1985).

The electrostatic deflection system consisted of two concentric 75^0 by 40^0 spherical segments with a center radius of 20 cm and a plate distance of 0.5 cm. The resulting geometrical factor of the analyzer was $4.3 \cdot 10^{-2}$ $cm^2 \cdot sr$ and the energy resolution $\Delta E/E \sim 0.097$ [Möbius et al., 1985]. The surface of the analyzer plates was coated with CuS black to suppress the penetration of UV radiation into the sensor. The energy range of 5 - 270 keV/Q was divided into 24 logarithmically spaced ($\sqrt[4]{2}$) steps which were incremented after each complete spin period. The sequence of energy stepping was adapted to the needs of regions encountered by the spacecraft. For high time resolution, the instrument was in a mode with six energy steps incremented by a factor of 2 after completion of a full spacecraft spin. One full energy cycle lasted for six spacecraft spins (~25 s). This analyzing technique selected the incoming particles according to their energy E per charge Q.

After passing the electrostatic analyzer, the ions entered the time-of-flight system as a parallel beam with the shape of a cylindrical section where the velocity was measured between two secondary electron-detector assemblies (SEDA's). The start SEDA consisted of a thin (3.7 $\mu g/cm^2$) grid-supported carbon foil and two microchannel-plate (MCP) assemblies, while the stop SEDA was provided by the gold surface of 4 solid-state detectors and another two MCP assemblies. The distance between the carbon foil and the solid state detector was d = 13 cm. An ion which entered the time-of-flight section penetrated the carbon foil and finally hit the solid-state detector. The start and the stop signals for the measurement of the time of flight τ were provided by secondary electrons which were emitted from the carbon foil and the detector surface. The electrons were accelerated by thin wire grids with 97 percent transmission and then deflected by radial electric fields such that they hit the MCPs with an energy of ~ 1600 eV. In order to prevent detection of secondary electrons emitted from the walls, the front side of the MCPs was set to a negative-bias voltage of ~ 300 V with respect to the walls.

Finally, the ions were stopped in one of four silicon surface barrier detectors of trapezoidal shape where E^*, a known fraction $1/\alpha^*$ of the residual energy, was determined. α reflects the nuclear defect and the energy loss in the dead layers of the detector and thus depends on particle species and incident energy. The thickness of the detectors was 0.5 mm with a sensitive area of 700 mm^2.

These measurements were then combined to determine the mass, charge and energy of the ions in the following way: the energy per charge (E/Q) as selected by the electrostatic analyzer and the measured velocity (d/τ) were used to determine the mass per charge M/Q of the ion according to:

$$\frac{M}{Q} = 2 \cdot \frac{E}{Q} / \left(\frac{d}{\tau}\right)^2 \cdot \beta \tag{4.2}$$

where β accounts for the energy loss in the carbon foil. The energy measured by the solid state detector E^*, and the measured velocity (d/τ) were used to determine the mass M according to:

$$M = 2 \cdot E^* \cdot \alpha^* / \left(\frac{d}{\tau}\right)^2 \tag{4.3}$$

The calculated M/Q from equation (4.2) and M from equation (4.3) yield the charge Q. The signal of the solid-state detector is too low to determine the total energy of ions with energies < 30 keV/Q and low charge state (e.g. He^+, O^-). In this case their charge state can only be inferred.

After combining all geometrical effects, grid transmission, MCP and foil efficiencies, the total detection efficiency of the time-of-flight section varied between $\eta = 0.28$ for oxygen ions with E > 400 keV and $\eta = 3 \times 10^{-2}$ for protons of 10 keV (see table 4.1).

The conversion factor g from count rate to differential flux for the SULEICA instrument is then:

$$g = (a \cdot \Delta\Omega \cdot \frac{\Delta E}{E} E \cdot \eta)^{-1} / [cm^2 \cdot sr \cdot keV / Q]^{-1} \quad (4.4)$$

where a $\Delta\Omega = 4.3 \cdot 10^{-2}$ $cm^2 \cdot sr$.

The energy loss in the c-foil and in the dead layers of the solid state detectors as well as all the efficiencies were calibrated during ion measurements with a radioactive α-particle source and at an ion accelerator of the Max-Planck Institut für Aeronomie.

The measurement techniques of the Charge-Energy-Mass Spectrometer (CHEM) on CCE are based on a combination of electrostatic deflection and post acceleration of up to -30 kV followed by a time-of-flight and energy measurement which is very simillar to SULEICA. Here the details are omitted. (see Gloeckler et al.date for a full description, 1985).

SULEICA Instrument Characteristics		
Energy range	in (24) 20 energy steps	(5) 10 to 270 keV/Q
Energy resolution (analyzer)	$\Delta E/E$	0.097
Energy resolution (detector)	ΔE	30 keV
Mass per charge resolution	40 keV/charge $\Delta(M/Q)/(M/Q)$	0.13
	270 keV/charge $\Delta(M/Q)/(M/Q)$	0.12
Charge resolution	40 keV ΔQ	1 (unit charge)
Geometrical factor	$a \cdot \Delta\Omega$	0.043 cm^2 sterad
Efficiency of TOF unit	40 keV	p: 0.07
		O^+: 0.04
	270 keV	p: 0.11
		O^+: 0.27
Temporal resolution	17 steps (5–80 keV)	73.78 sec
	18 steps (10–230 keV)	78.12 sec
	6 steps	26.04 sec
Angular resolution	p, α	16 azimuthal sectors
	other ions	8 azimuthal sectors
Instantaneous view angle in elevation/azimuth		$\pm 20°/\pm 5°$

Table 4.1 Summary of SULEICA instrument characteristics (after Möbius et al., 1985).

CHAPTER 5

ENERGIZATION OF PICKUP HE+ BY REFLECTION AT THE EARTH'S QUASI-PERPENDICULAR BOW SHOCK

Ion reflection is a general characteristic of high Mach number collisionless shocks [e.g., Biskamp,1973] and provides an important channel of dissipation in the region ahead of the shock. As discussed in chapter 2, there are two types of reflected ion distributions in front of the quasi-perpendicular shock: field-aligned beams and specularly reflected ions. The former is essentially a beam that streams away from the shock along the interplanetary magnetic field lines. The latter is seen as a distribution of gyrating ions transverse to the magnetic field which extends over the foot region of the magnetic field profile near the shock. Paschmann et al. [1982] have presented observations of gyrating ions within the foot region of a quasi-perpendicular bow shock, i.e. $\theta_{Bn} > 45^0$. They performed simple orbit calculations to demonstrate that the guiding center motion and gyrational speed of these ions are consistent with simple geometrical considerations for specular reflection. In the case of gyrating ions, the detailed gyration of the particle is important, and the concept of the first adiabatic invariant has no meaning. In this process the (unmagnetized) ions are simply bounced off the shock potential, reversing their velocity component along the shock normal, while maintaining the velocity component

parallel to the shock surface. Particles may suffer further encounters with the shock due to the combined action of the interplanetary electric field and the Lorentz force

These previous studies have been limited to the interaction of solar wind ions with the bow shock and no multiple shock encounters were addressed. Pickup ions represent a source of ions, with a characteristically broad velocity distribution and a sharp upper limit of twice the solar wind speed, clearly distinct from the solar wind. Studying their acceleration at the Earth's bow shock and at interplanetary shocks will allow us to test acceleration models and to compare ion acceleration efficiencies for different source populations at shocks. Furthermore, a better understanding of the interaction of pickup ions with Earth's bow shock can also be applied to the presumed acceleration of the anomalous cosmic ray component (ACR) at the solar wind termination shock, since the interstellar pickup ions are believed to be the source of ACR.

In this section we will present the first observations of gyrating He^{+} ions at a perpendicular bow shock($\theta_{Bn} = 90^{0}$). We will also offer a quantitative model of the reflection process at the bow shock and compare its results with the observations.

5.1 Basic Observations

For this investigation, a time period on October 9, 1984 has been chosen, when the AMPTE/IRM spacecraft was near the subsolar point of the bow shock, and the IMF was approximately perpendicular to the shock normal. An overview of the event is presented in Figure 5.1. Shown from top to bottom are: the magnetic field strength B (in nT), the direction of the magnetic field in azimuth Φ_B and in elevation θ_B in GSE coordinates, the polar angle θ_B of the magnetic field in spacecraft coordinates, the solar wind speed V_{sw} (in km/s), the solar wind density N_p(in cm^{-3}), and the differential flux of He^+ at 40 and 80 keV/Q. During most of the time the magnetic field was almost in the ecliptic plane oriented perpendicular to the Earth-Sun line. This provides an almost perfect perpendicular shock condition. Because of the orientation of the spacecraft during the early mission, with the spin axis still close to the ecliptic plane, the magnetic field direction was nearly parallel to the spin axis of the satellite. On its inbound pass, the spacecraft crossed the bow shock at 11:28 UT, as indicated by the rapid change in solar wind velocity and magnetic field strength. The spacecraft returned to the upstream region ~ 3 minutes later and finally crossed the bow shock into the magnetosheath at 11:44 UT. At 10:42 UT, still at a substantial distance upstream of the shock, the first energetic He^+ ions were observed with energies of 40 keV in sector 6 at 90^0 with respect to the solar wind (see the sector scheme inserted in Fig. 5.3). After 11:08 UT more energetic ions

were seen with energies up to 80 keV. It should be noted that the maximum energy (E_{cut}) in the solar wind direction of the pickup ion distribution for V_{sw} = 750 km/s is 46 keV.

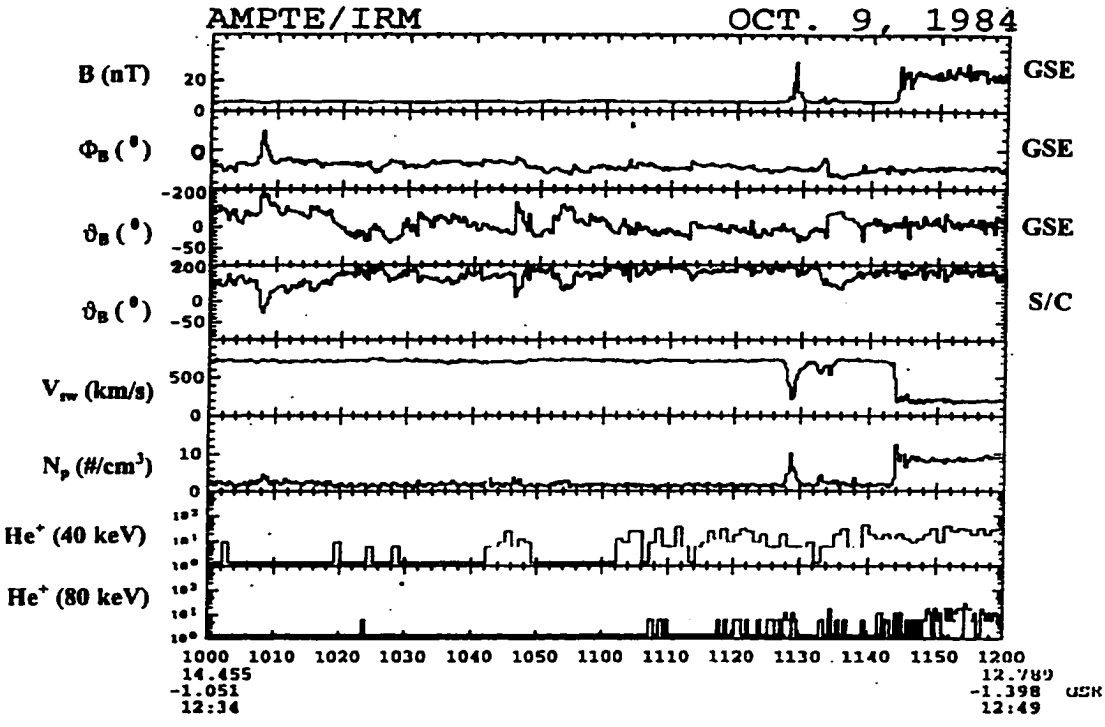

Fig. 5.1. Variations of interplanetary magnetic field strength B, direction in azimuth Φ_B, and elevation ϑ_B in GSE and SCC coordinates, respectively, the solar wind speed V_{sw}, the solar wind density N_p, and the differential flux of He^+ at 40 and 80 Kev/Q.

Figure 5.2 shows a 2-D cut of the directional distribution of He^+ energy-angle spectra in the plane perpendicular to the spacecraft spin axis during three consecutive 20 minute time intervals. The rings represent the energy steps at 10, 20, 40, and 80 keV/Q

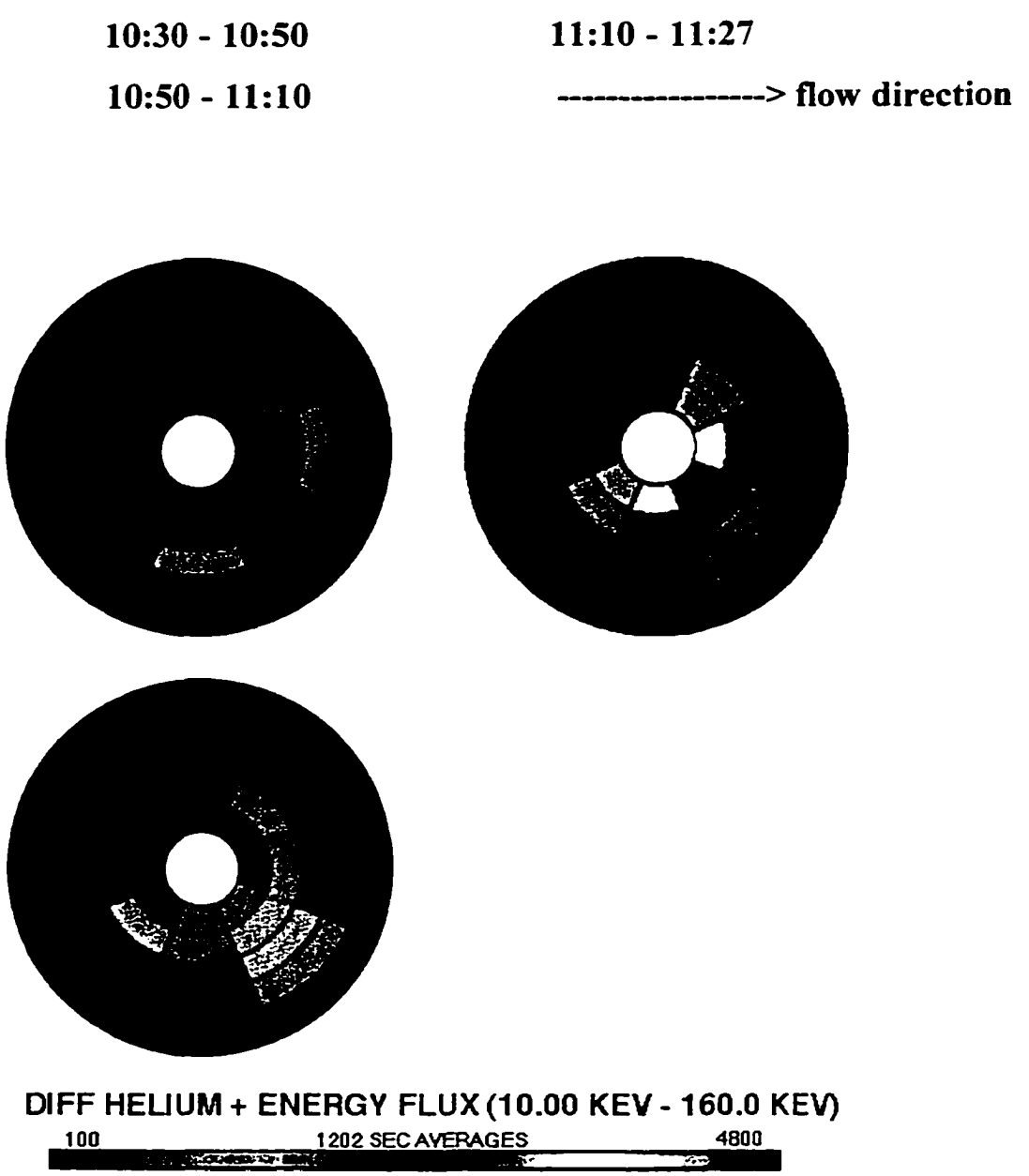

Fig. 5.2. Directional colored spectrograms of He^{+} in the plane perpendicular to the S/C spin axis for the time period 10:00-10:30 UT (a), 10:50-11:10 UT (b) and 11:10-11:27 UT (c). Note that the magnetic field direction is almost parallel to the S/C spin axis.

outwardly from the center. The orientation of the distribution can be obtained from the sector scheme inserted in the the Fig. 5.3. The flow direction of the ions is shown and the cut-off energy for the event is 46 kev. As pointed out above, the magnetic field was oriented almost parallel to the spin axis so that the observation conditions were ideal for ion fluxes perpendicular to the magnetic field. The figure presents a sequence of events changing from (a) an almost pure pickup ion distribution at (10:30-10:50 UT) via (b) (10:50-11:10 UT) to (c) (11:10-11:27 UT), when the spacecraft was very close to the bow shock and He^+ ions appeared from different directions at progressively higher energies.

A typical pickup He^+ distribution can be recognized by ion fluxes only in the solar wind sector(4) and two adjacent sectors(3 and 5) [Möbius, 1986]. Already during the first time interval additional energetic ions are found in sector 6, i.e., flowing parallel to the shock plane. As the spacecraft moves toward the shock (in Figure 5.2(b) and 5.2(c)) more energetic ions with energies up to 80 keV are observed in sector 5, and the energy in sector 6 is increased to 40 keV. Finally the ion flux increases substantially and also ions coming from the shock are observed (in sector 7) as the spacecraft approaches the bow shock. A substantial fraction of the ion distribution upstream of the bow shock clearly reaches much higher energies than the maximum for pickup ions. These ions fill a much wider range in angles, including ions coming direct from the shock direction.

5.2 Model

A schematic view of the situation under consideration with pickup ions incident on a perpendicular shock in the plane normal to the magnetic field is depicted in Fig. 5.3. Incident ions may be reflected in the shock potential. After leaving the shock into the upstream direction the ions undergo a partial gyration about $\vec{B}$ and then reencounter the

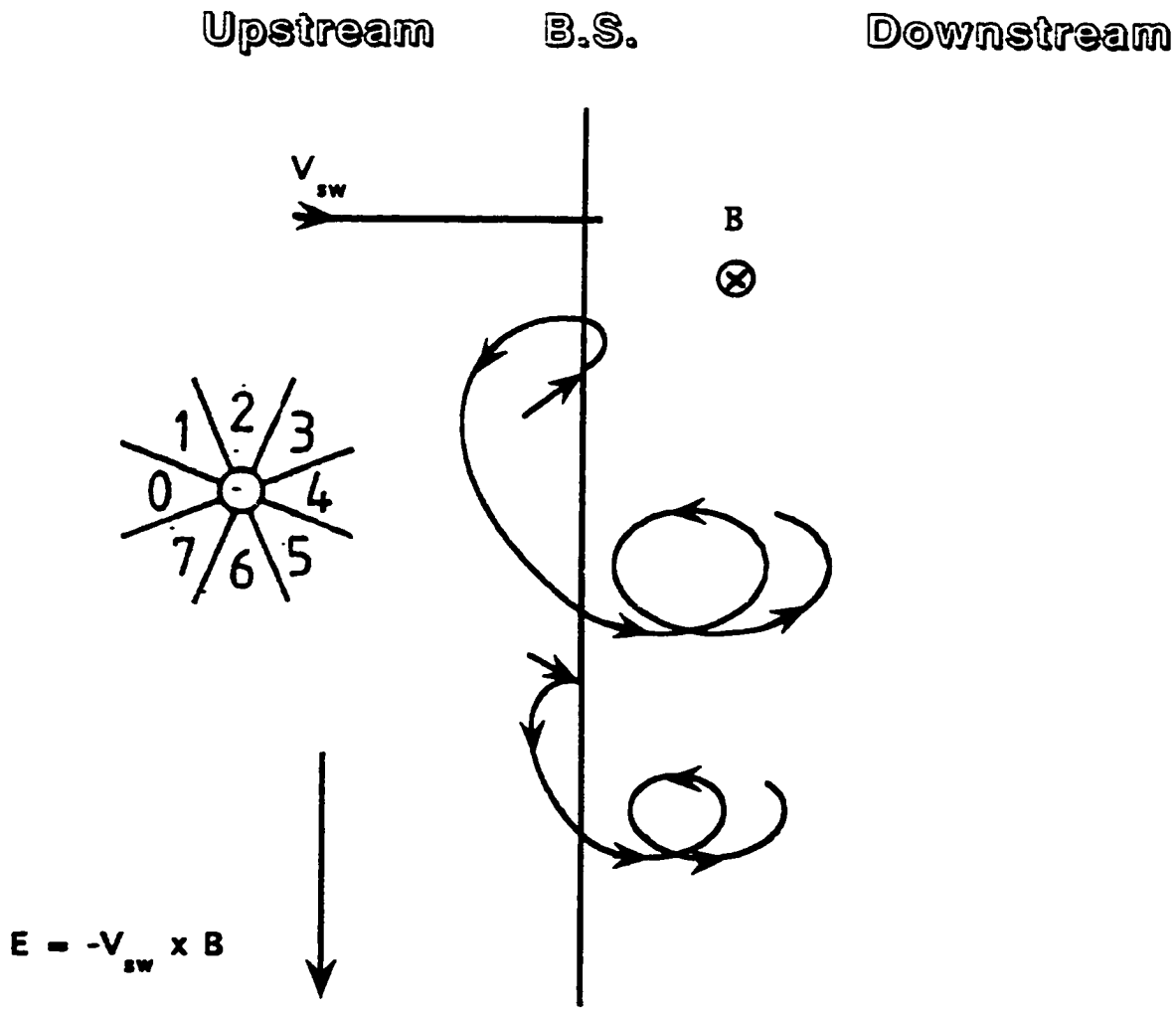

Fig. 5.3. Schematic representation of ion trajectories after reflection at the shock.

shock, or penetrate briefly into the downstream region, undergo a partial gyration about $\vec{B}$ downstream of the shock and then emerge upstream again. On the part of the trajectory upstream of the shock, the convective electric field $\vec{E} = -\vec{V}_{sw} \times \vec{B}$ accelerates the ions parallel to the shock surface. As a consequence, the ions return to the shock with a higher speed and a reduced angle with respect to the shock surface. Therefore, they also appear in sectors 7 and 6. Closer to the shock more and more particles with higher speeds will appear in sectors 6 and 5. When they finally return to the shock, the ions have gained substantial energy in the electric field and may now be able to pass the potential barrier.

5.2.1) The shock potential

The shock potential is a consequence of the different gyroradii of electrons and protons. Typically the electric potential jump at the bow shock is somewhat less than the proton ram energy of the solar wind:

$$q\Delta\Phi = 1/2\ M_p\ V_{sw}^2\ \gamma \qquad (5.1)$$

Where the $\gamma < 1$. In our model we will start with the crude assumption ($\gamma = 1$) and then test the possible influence of a variation in γ.

5.2.2) The orbit of the reflected ions in the upstream region

The shock thickness ΔL is of the order of $c/\omega_i \sim 155$ km for the actual upstream magnetic field of 6 nT, where ω_i is the ion plasma frequency. Thus the transit time for a solar wind parcel through the shock, $\Delta t = \Delta L/V_{sw}$ [Russell and Greenstadt, 1979], is ~ 0.4 s for the given solar wind speed of 750 km/s, which is short compared with the actual ion gyroperiod $T_g \sim 10.9$ s. As a result, the shock potential can be considered as stationary, and it is reasonable to assume infinitesimal shock thickness. For simplicity it is also assumed that there are no fluctuations of $\vec{B}$, although typical solar wind fluctuations are present in the upstream region. We also restrict our model to motion in the plane perpendicular to the magnetic field for the time being. We will discuss the effects of a velocity component parallel to $\vec{B}$, which is not altered in the interaction with the shock, at a later stage in this thesis.

Working with a purely perpendicular shock allows us to evaluate the problem in two dimensions, i.e. the ion distribution is independent of Z, and V_Z is conserved. In addition, we assume a planar shock of infinite extension. In a coordinate system with its origin at the incident point at the shock, its $\vec{x}$ axis parallel to the shock normal $\vec{n}$, $\vec{z}$ parallel to $\vec{B}$, and $\vec{y}$ chosen to complete a right-handed system, the equation of motion is

$$m\frac{d\vec{V}}{dt} = q\vec{E} + \frac{1}{c}\vec{V}\times\vec{B} = \frac{1}{c}(\vec{V} - \vec{V}_{sw})\times\vec{B} \qquad (5.2)$$

in the shock rest frame and the orbit of the reflected ion in the upstream region is described by

$$X(t) = V_o[\sin(\omega_I t - \theta_o) + \sin\theta_o]/\omega_I + V_{sw}[\sin(\omega_I t) - \omega_I t]/\omega_I \quad (5.3)$$

$$Y(t) = V_o[\cos(\omega_I t - \theta_o) - \cos\theta_o]/\omega_I + V_{sw}[\cos(\omega_I t) - 1]/\omega_I. \quad (5.4)$$

where $\omega_I = qB/(mc)$ is the gyrofrequency, V_o the original speed of the ion, θ_o the acute angle between $\vec{V}_0$ and $\vec{n}$, and t the time since reflection. An ion reencounters the shock at a time t*>0 when X(t*) = 0. At this time the particle has a velocity $\vec{V}_0(t^*)$. If $1/2mV_x^2(t^*)$ is greater than $q\Delta\Phi$, the particle will overcome the potential barrier, and its motion continues in the downstream region. Of course, it may recross the shock after a partial gyration in the downstream region. Alternatively, energies less than $q\Delta\Phi$ result in reflection at the shock and one or more additional encounters. During multiple encounters with the shock an ion can gain a substantial amount of energy. This "surfing" of ions along a quasi-perpendicular bow shock has been described by Lee et al.[1996] as an important process to produce energetic ions.

5.2.3) Three different classes of particles in the pickup ion distribution

As a consequence of these various types of shock encounters, we can divide the incoming ion distribution, by calculating the trajectory of ions in the model, into three classes of particles which may be discussed separately as follows. Figure 5.4 shows a schematic view of the two-dimensional cut with $V_z = 0$ through the pickup velocity distribution perpendicular to B. It is separated into three different areas with characteristic orbits for the three different types of interaction with the shock.

A -- Electrostatically reflected ions

Ions, whose energy contribution from the x component of the velocity is lower than the shock potential (indicated by region A), will be reflected at the shock, then gain energy from the electric field and finally gyrate downstream. For a considerable fraction of these ions, the energy along the shock normal is not sufficient after the first reflection to penetrate the potential barrier. They will be reflected several times and gain higher energies. In our simulation we count them separately as types A(1), A(2), and A(3), etc., where the digits represent the number of reflections at the shock.

B -- Magnetically reflected ions

A part of pickup ions that have enough energy to penetrate the shock barrier will be magnetically reflected. They "dive" downstream first, however, after less than one gyroperiod, they can emerge again upstream with the assistance of the downstream magnetic field. These ions (found in region B) of the distribution also gain energy in the convection electric field, and finally gyrate downstream with higher energies after a maximum of two shock encounters.

C -- Transmitted ions

The remainder of the total pickup ion distribution (shown in region C) will pass into the downstream region with their energy reduced by the shock potential and simply gyrate further downstream.

In our simulation we follow the trajectory of every particle from the source into the final energetic ion distribution starting with the first reflection at the shock. In order to normalize the ion energy flux in the simulated distribution for a quantitative comparison with the observations, we have to establish the distribution function of the pickup ions. As discussed in section 3.2, we will use the analytic expression by Vasyliunas and Siscoe [1976], which includes the injection of newborn ions into the solar wind, rapid pitch-angle scattering, and adiabatic cooling due to the radial expansion of the solar wind. This leads to an isotropic velocity distribution in the solar wind frame. We use equation (3.12) for this distribution function. In order to establish the absolute value of $R_o * \beta_i (r_{ob}) * N_0$, the

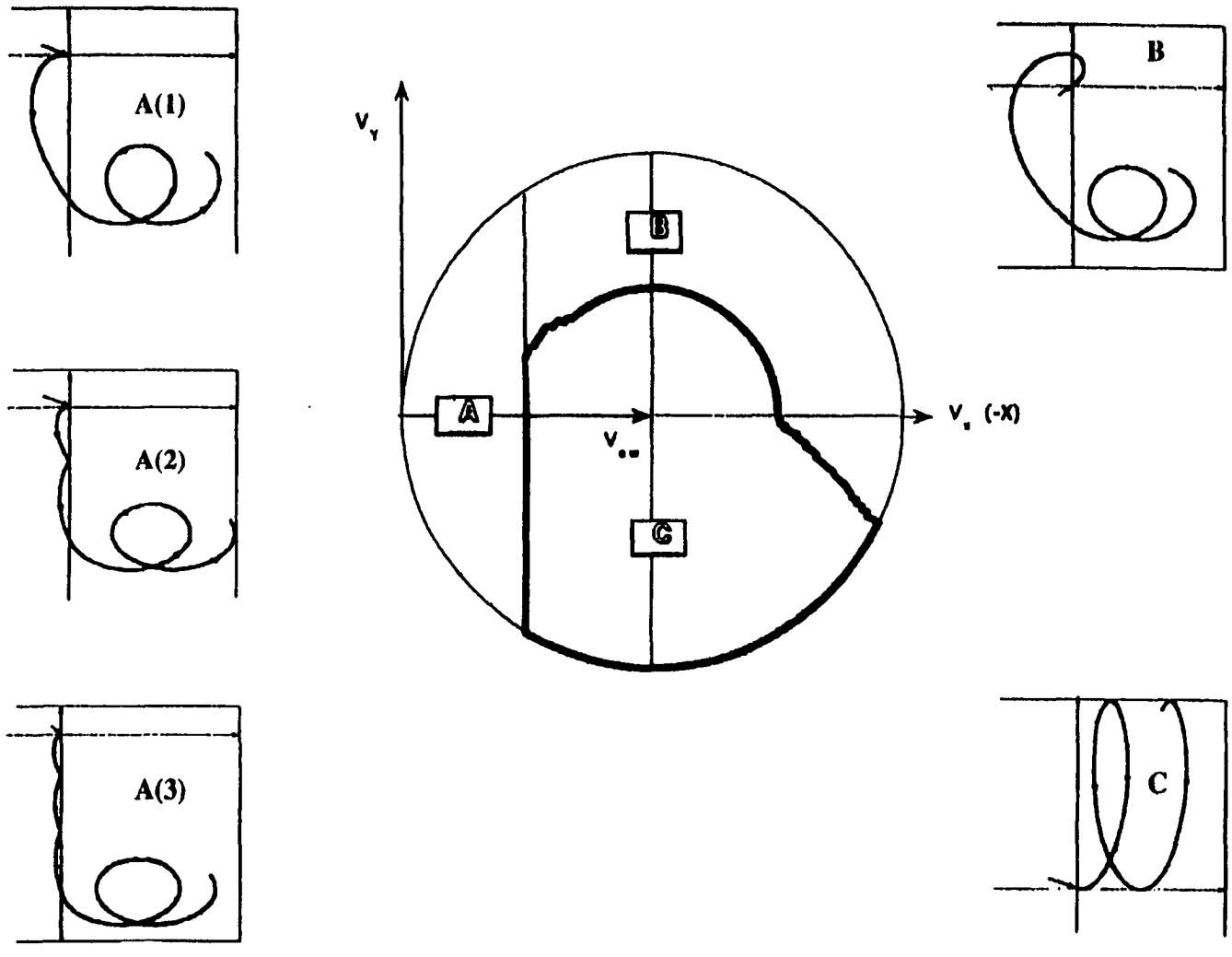

Fig. 5.4. Projection of pickup ion distribution into the plane perpendicular to the magnetic field separated into regions with different behavior during shock encounters.

incident pickup ion distribution in our simulation is normalized to the average pickup flux as observed by Möbius et al. [1995a] for the time period of the investigation. For comparison with the measurements, the differential flux of the energetic ions obtained in this simulation is averaged over the field-of-view of the instrument in each of its individual azimuthal sectors. However, a higher energy resolution is maintained.

5.2.4) Normalization of reflected ions

According to Liouville's theorem, the distribution function is constant along a particle trajectory, and the volume occupied by the particles in phase spase also remains unchanged. That is, the shape of the volume in phase space can be distorted or squeezed along the particle trajectory, but an increase in one phase space dimension must be precisely compensated by a decrease in the other dimensions. It is equivalent to say the phase space density should not increase or decrease during the acceleration process, although the velocity of the particles changes along their trajectories. Therefore, our simulation is simple because the pickup ion phase space density is known as the spherical distribution expressed by Vasyliunas and Siscoe [1976] and it will not change during the later acceleration process.

Fig. 5.5 shows how we choose the simulation grid for the pickup ion distribution in the plane with $V_z = 0$. In order to make use of the intrinsic symmetry of the initial pickup ion distribution and to translation this into the frame of the measurements, let us use (V_0, ϑ_0)

and (V_0', ϑ_0') to represent the original ion velocity cylindrical coordinates for a grid element in the inertial reference frame and the solar wind frame, respectively. The two set of coordinates are clearly related by

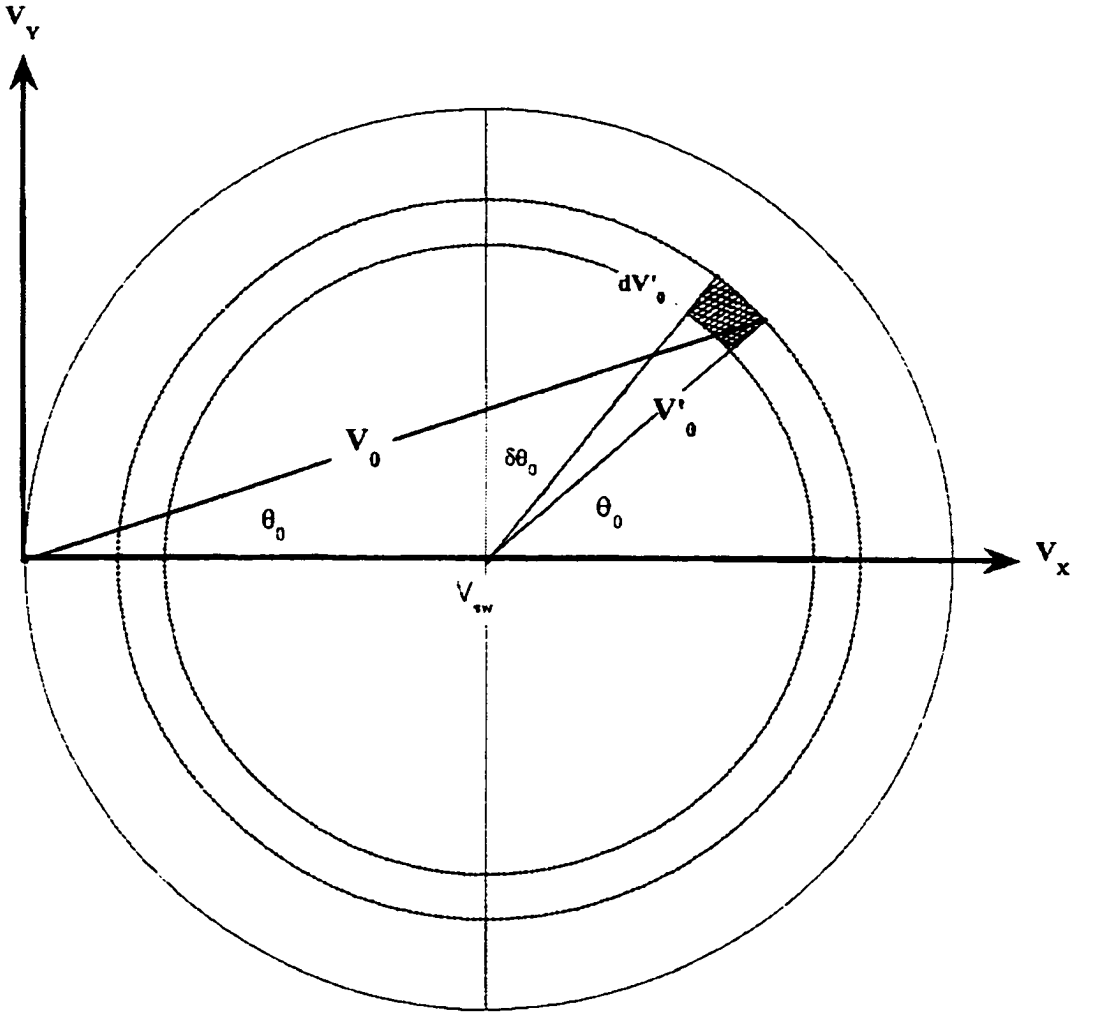

Fig. 5.5 The plot shows a cut through the pickup ion distribution in the plane ($V_z = 0$). (V_0, θ_0) and (V'_0, θ'_0) are the coordinates of an ion's velocity in the spacecraft frame and in the solar wind frame, respectively.

$$V_0^2 = V_{sw}^2 + V_0'^2 + 2V_0' \cos\vartheta_0'$$
$$\sin\vartheta_0 = \frac{V_0'}{V_0}\sin\vartheta_0' \tag{5.5}$$

The ions in every element starting at the shock surface (x = 0) follow a fixed trajectory. Then we catalogue all such trajectories for all V_x',V_y' in the circle. For a definite V_z, we have a set of circles whose radius extends from 0 to $\sqrt{V_{sw}^2 - V_z^2}$, while V_z can be extended from 0 to $\pm V_{sw}$. In this way, all of the grid elements cover the whole sphere of pickup ion distribution.

As Fig. 5.6 shows, recording the velocity information for each crossing of a trajectory on the line x for all trajectories, regardless of y, it gives us a discrete set of $\vec{V}$'s, with associated $f(\vec{V})$ for each element in the initial distribution. Averaged the distribution $\bar{f}(\vec{V})$ in every computation grid in the frame of the observer after the reflection, we calculate the average particle number in every volume element of velocity space as

$$\Delta N_i = \bar{f}(V_i) V_i dV_i d\vartheta_i dV_z \tag{5.6}$$

where V_i is the average observed velocity in the velocity space, $d\vartheta_i$ is the polar angle taken by the grid.

In order to allow a quantitative comparison of the model ion spectrometer results with the measured quantities, the differential flux density is first calculated over the individual sector as

$$\left(\frac{\Delta J(x,E_i,\Omega)}{\Delta E_i \Delta\Omega}\right)_{\substack{1\,sector \\ 1\,finerenergystep}} = \sum_{grids} \frac{2E_i}{m^2} \frac{\Delta N_i}{V_i^2 dV_i \Delta\Omega} \tag{5.7}$$

$\Delta\Omega = 45^0$. Then we integrate them over individual instrument channels with $\Delta E/E \approx 0.1$ in the spacecraft frame. For all our simulations, we assume an infinite planar shock and a homogeneneous distribution in y and z.

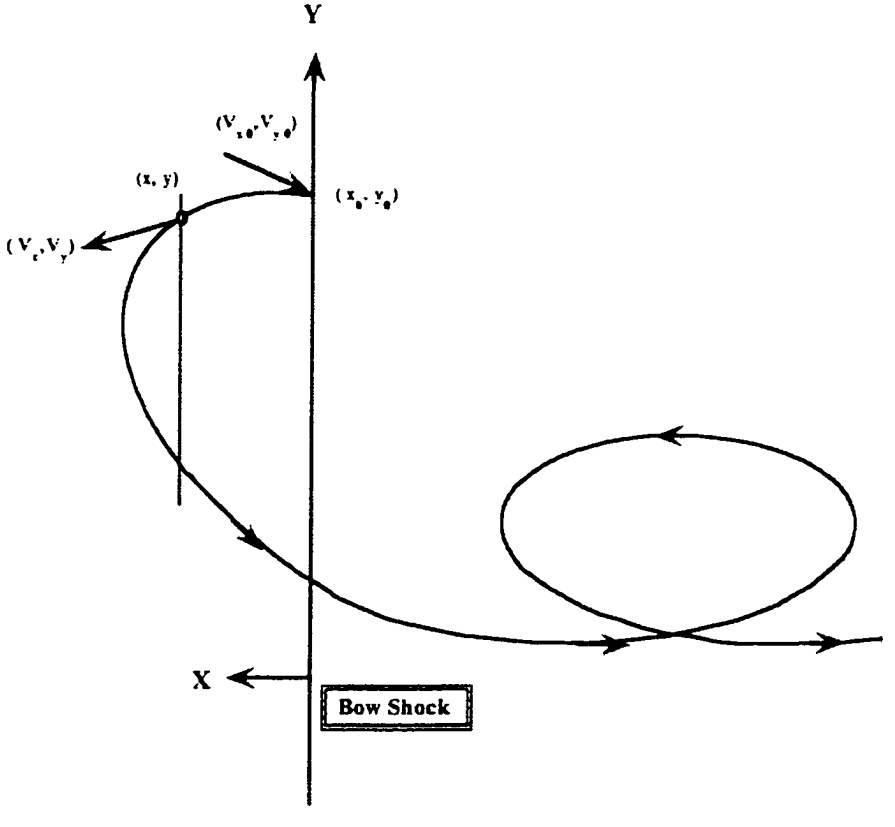

Fig. 5.6 A satellite at (x, y) records the information of the velocity (V_x,V_y) for specularly reflected ion when the particle was reflected at $(x_0 = 0, y_0)$ in the shock surface with a velocity (V_{x0}, V_{y0}).

5.2.5) Implication of the 2-D model

The velocity distribution of pickup ions forms a full sphere centered at the solar wind velocity. Therefore, a 3-dimensional problem has to be solved. However in the event under study, $\vec{B}$ was not only perpendicular to the shock normal, but also parallel to the spin axis of the spacecraft. With the aperture of the SULEICA instrument viewing exactly perpendicular to the spin axis, this would in principle lead to a simpler model considering only the ion motion perpendicular to the magnetic field, because the velocity parallel to B is not altered by the acceleration. For an instrument that only accepts particles exactly perpendicular to $\vec{B}$, we just need to integrate over the V_x - V_y plane of the distribution with $V_z = 0$. For an instrument that covers the full angle space, we cut the sphere of the velocity distribution function into several thin pieces in the V_x - V_y plane and treat every piece in two dimensions. This would be equivalent to a projection of the entire sphere into the x-y plane.

The entrance aperture of the electrostatic analyzer on the AMPTE/IRM covers a finite opening angle of 40^0 in elevation symmetric to the plane perpendicular to the spacecraft spin axis. Thus the sensor detects particles with $|\vartheta| = \tan^{-1}(v_z/\sqrt{V_x^2 + V_y^2}) \leq 20^0$. Because the velocity component perpendicular to B is increased in the acceleration process while V_z remains constant, the sensor will be able to detect particles that start at a larger angle ϑ

in the original distribution. However, some of the particles in the reflected distribution will still miss the sensor, because their final V_x and V_y components are too small. These particles tend to come from the polar pieces in the original spherical pickup ion distribution. In order to compare the results of this model quantitatively with the measurements, we have to subtract particles, whose angle after reflection at the shock is larger than 20^0, from the simulated flux.

5.3 Simulation Results

As we have seen in Fig. 5.4 the original pickup ion distribution is clearly divided into separate regions according to what happen to the ions at the shock. As a first result of our simulations we find that ~15% of ions in the distribution are electrostatically reflected at the shock (type A), ~48% are magnetically reflected ions (type B), and ~37% are transmitted directly into the downstream region (type C). After establishing our model for the ion reflection at the bow shock we will now present energy spectra from a simulation with input parameters characteristic of the time period of our observations.

Figure 5.7 shows separately the original pickup ion energy spectra (the left) and spectra of specularly reflected He^+ (the right) - mixed ions of type A and B - in all sectors. The He pickup ions are concentrated in the solar wind direction (sector 4) with their spectrum extending up to the cut-off energy (in this case, E_{cut} = 46 keV for a solar wind speed of

750 km/sec). Reduced ion fluxes are seen in the two adjacent sectors (sectors 3 and 5). After interacting with the bow shock, energetic ions are found in all sectors except 2, 3 and 4. The typical energy of the ions is increasing from sector 1, through 0, 7 and 6, to sector 5. This is in accordance with ions that emerge from the shock and are turned around by the IMF while being accelerated in the convection electric field. These findings are in basic agreement quatitatively with the observations presented in Fig. 5.2. The observed distribution is a combination of the pickup and the reflected ions.

5.3.1) Contributions of ions from the different classes of ions to the spectra

In order to gain further insight into the energy gain of "specularly reflected" ions at collisionless shocks, we have separated the contributions of ions from the different classes of particle orbits to the spectra in sectors 5, 6 and 7. As can be seen from Fig. 5.4 the multiply reflected ions are concentrated very close to the shock. Here, ions from all different classes contribute to the distributions. Consequently we have chosen a relatively close distance (0.04 R_c) for our detailed study. The results are shown in Fig. 5.8. The dashed lines represent the spherical distributions that the sensor with full angular coverage will see. The solid lines represent the net particle distributions that the sensor with limited acceptance angle actually received.

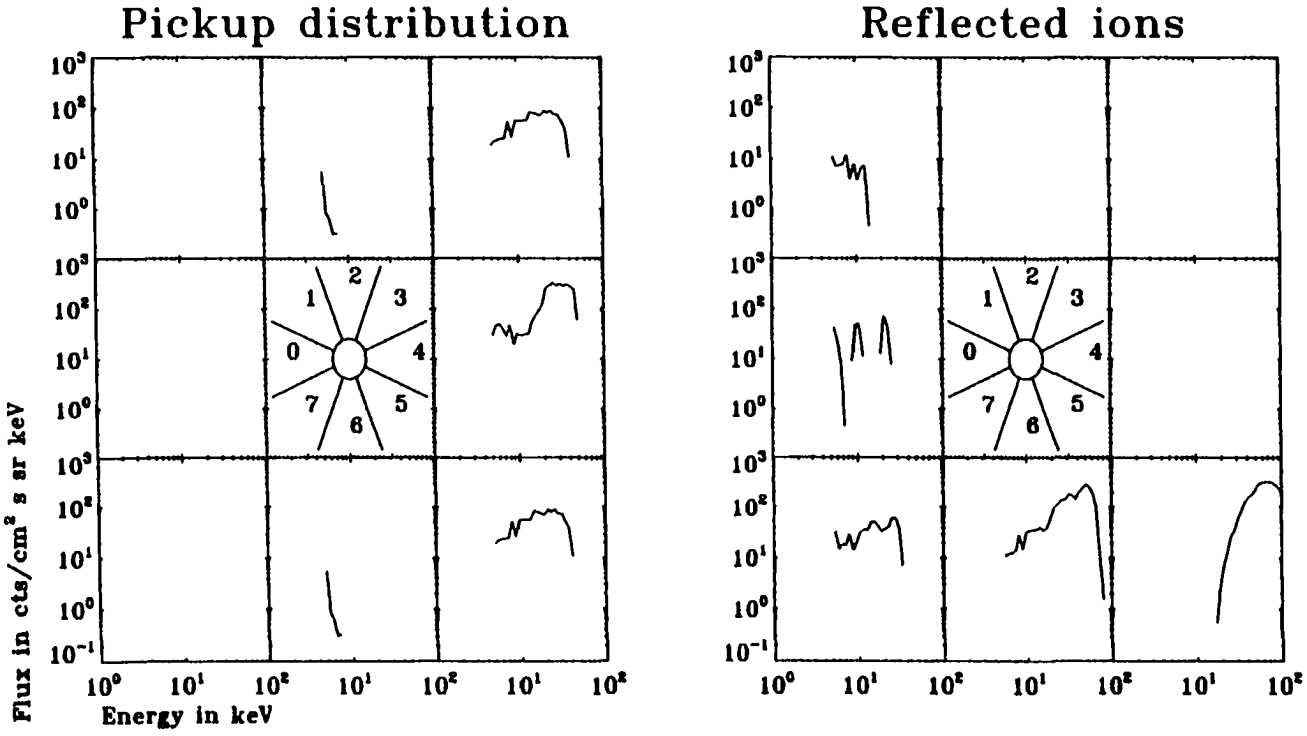

Fig. 5.7 Simulated differential flux distribution (right panel) of ions reflected at a perpendicular shock together with the incoming pickup ion distribution (left panel) for V_{sw} = 750 km/sec at 0.04 R_E from the bow shock.

For the perpendicular magnetic field direction prevalent during this event, most of the ions that emerge from the shock appear first in sector 7. Ions of type B generally start with a higher energy and produce a higher flux than type A ions. In sector 6 ions of both types have gained additional energy in the convection electric field. Here also type A ions are seen after their second and third reflection, where their contribution to the total flux seems to become dominant at high energies. Note that the highest level of fluxes are reached only after three reflections. Ions with more than three reflections are not found at this location. After more reflections the ions remain closer and closer to the shock and are less likely to play a role. Sector 5 contains those ions of types A(1) and B which have taken the largest turn upstream of the shock and thus reached the highest energy. Clearly the contribution from type B ions is most important in this sector. Multiply reflected ions are not observed in sectors 5 and 7, because their motion is almost parallel to the shock front.

Comparing the part of the ion distribution that is not observed due to the limitation in acceptance angle, with the total ion distribution, the largest effect appears in sector 7 and for the ions of type B. This is reasonable because the ions with larger angle ϑ comes from those ions which emerge from the shock out of the downstream region with smaller velocities V_x and V_y , but larger V_z. They are observed closer to the shock and fall into sector 7. They dominate the magnetically reflected ions. In all simulations we use the complete 3-dimensions model.

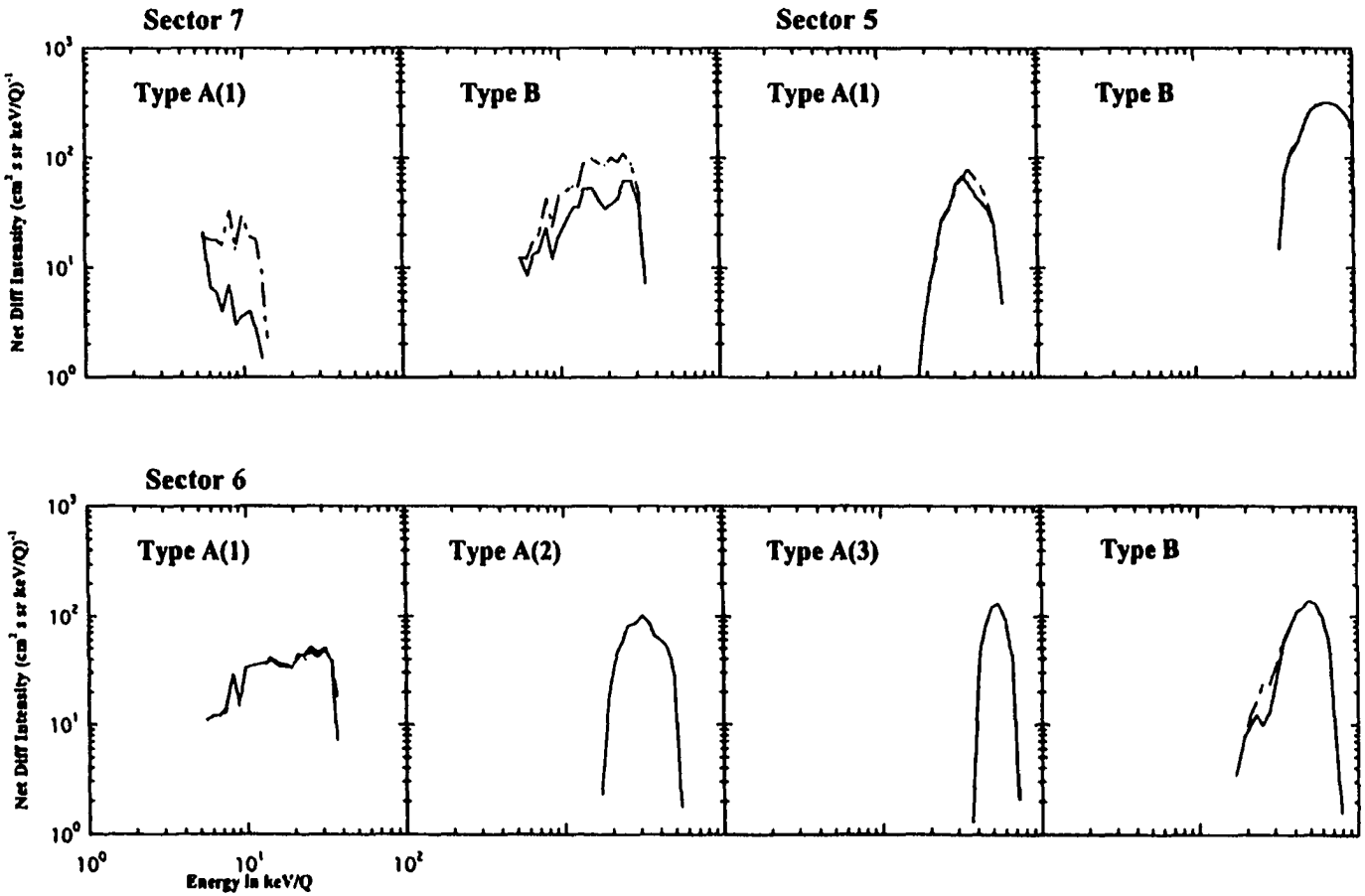

Fig. 5.8 Contribution to the spectra of reflected ions from different types of ion trajectories for sectors 5, 6 and 7. The dashed lines represent the spherical distribution which sensor with full angular will see. The solid lines represent the net particle distribution that the sensor with limited acceptance angle actually received

5.3.2 Contribution of multiply reflected ions

In order to explore the important role played by multiple reflections, we investigate the possible contribution of multiply reflected ions to the simulated spectra as a function of distance from the shock in Figure 5.9. Fig.5.9 (a),(b) and (c) are the spectra in the sectors 5, 6 and 7, respectively. Therefore, we compute separately the contributions of type A and B ions to the spectra and compare them with the data at 11:10 - 11:27 UT in the upper and lower panels, respectively, with the satellite was closest to the shock. From left to right the distance from the shock has been increased in the simulations from 0.024 to 0.08 Re. Beyond 0.072 R_e there are only singly reflected ions. If only type A particles including multiple reflections are used in the simulation (upper panel), the simulated spectrum tends to be in better agreement with the observations at 11:10 - 11:27 UT as closer proximity to the shock is assumed. The contribution of ions from the type B into the spectra drives the flux to high for the higher energies in sectors 5 and 6 and therefore leads to levels of the simulated flux that are much higher than the data (lower panel). The simulated fluxes of type B ions seems only to be consistent with the observed fluxes in sector 7. However, these data points in sector 7 have the largest error bar, because only a few ions are counted here. Hence, the constraints derived from sectors 5 and 6 should be taken more seriously. As we will see in the next section, the same constraints for type B ions apply also in the comparison with the two earlier time periods. Apparently the type

B particles do not appear with the predicted flux. Because these ions first dive downstream, they are probably most strongly affected by any magnetic fluctuations in the downstream region. If we want to take into account possible effects of magnetic field fluctuations downstream of the shock, we will may have to reduce the contribution from these ions.

Fig. 5.10 shows the comparison of simulated for choices of 10% and 100% of type B ions with the data at 11:10 - 11:27 UT in sectors 5, 6 and 7. It is clear that if we make the assumption of 10% of type B ions, the results closer to the bow shock seem to be a better match. Therefore, we assume in the following that only 10% of type B ions contribute to the simulated spectra. In accordance with what we discussed above this would also suggested that so called "surfing" of multiply reflected ions [Lee and Shappiro,1995] indeed play a visible role in the ion acceleration at the quase-perpendicular shock.

5.3.3)Variations with distance from the shock

In figures 5.11 and 5.12 we extend the comparison of our simulations with the time periods 10:50-11:10 and 10:30-10:50 UT when the spacecraft was still at a somewhat larger distance from the shock. The series of simulations in Fig. 5.11 suggests that a distance between 0.16 and 0.24 R_e provides the best match between the prediction and the data, again under the assumption that 10% or less of type B ions are contributing to

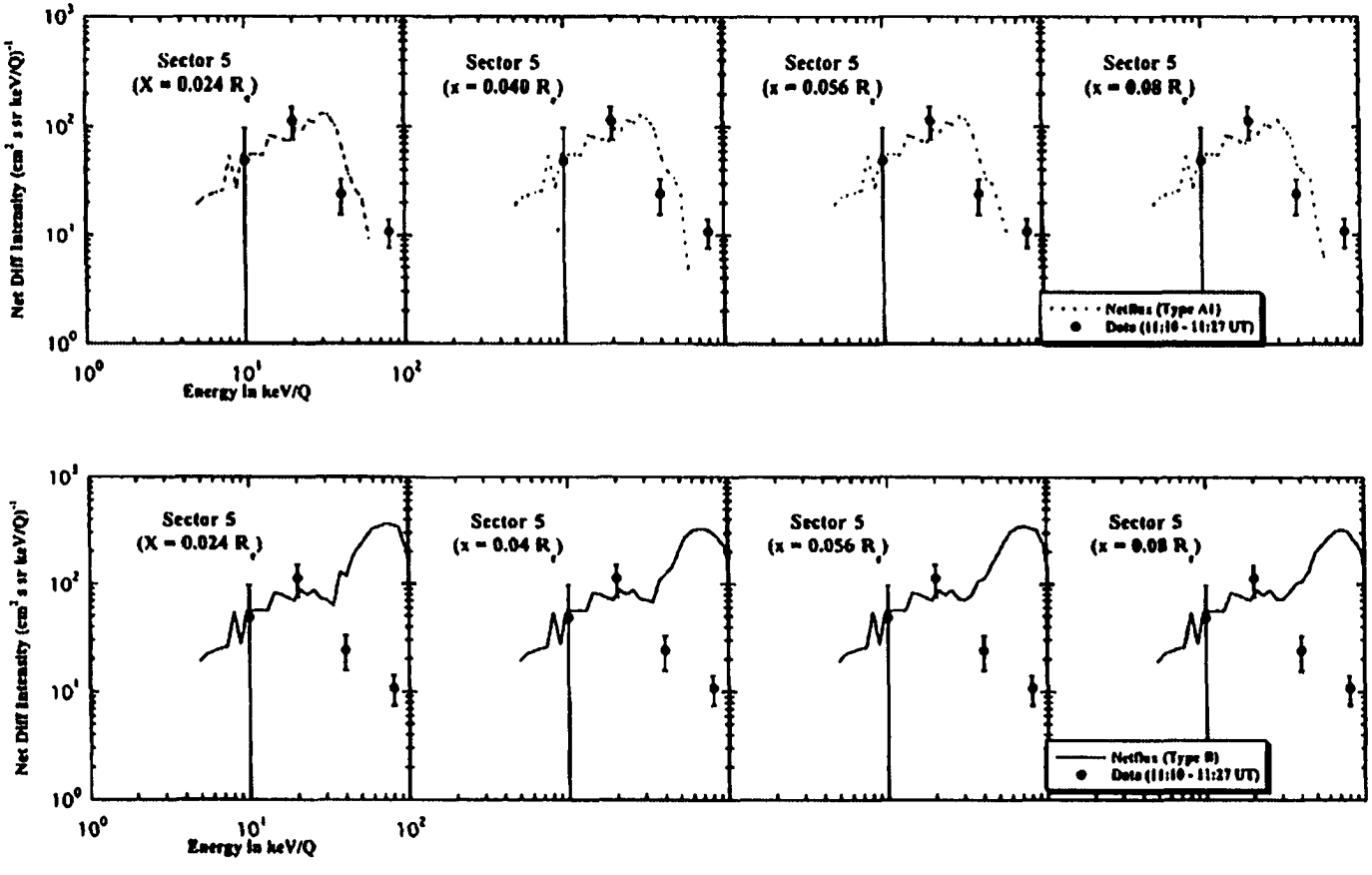

5.9 (a) Comparison of simulated spectra in sector 5 with data at 11:10 - 11:27 UT , contributions of type A (including 1, 2 and 3 reflections) and B ions to the spectra in the upper and lower panels, for various distances to the B.S.

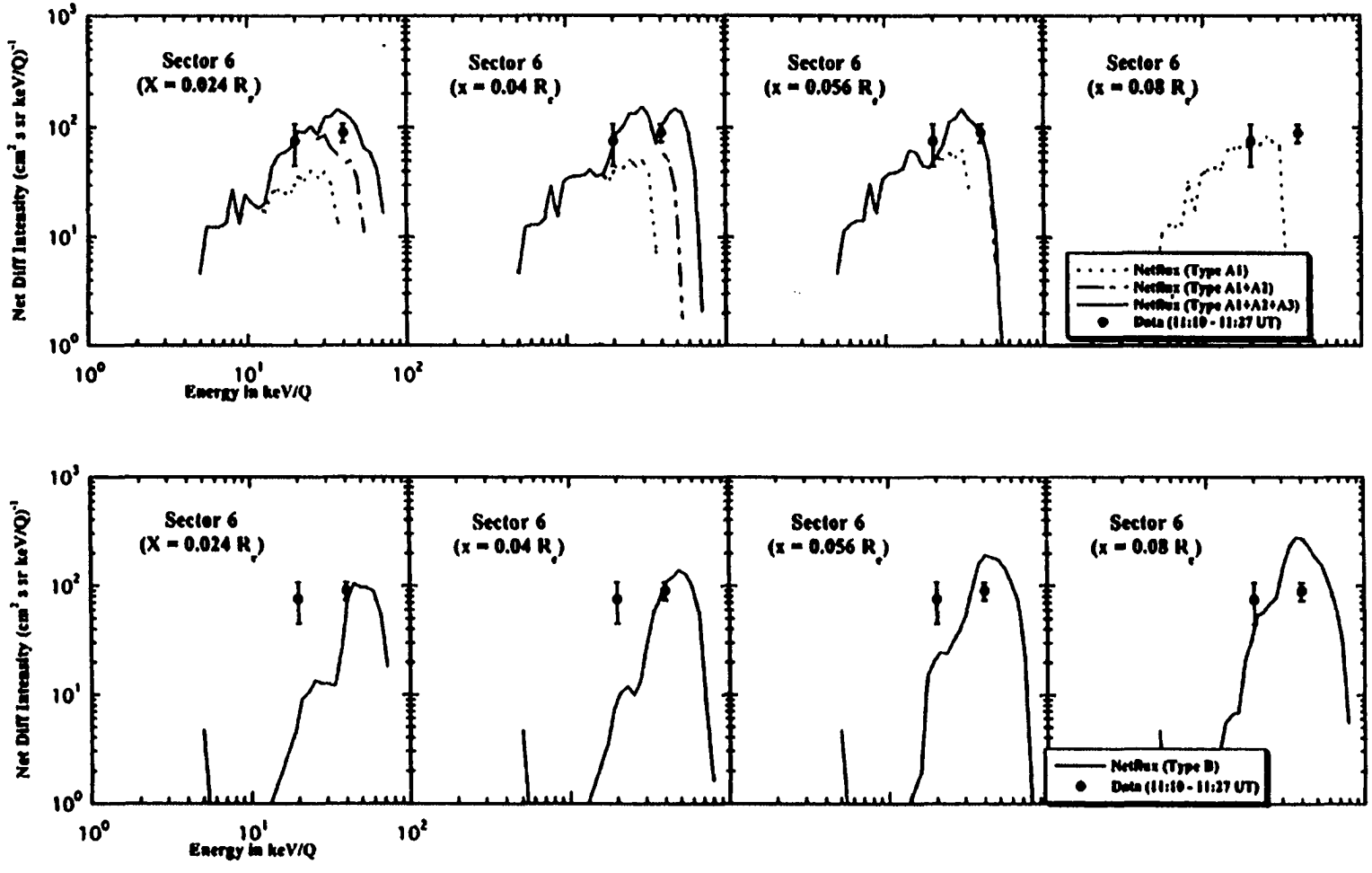

5.9 (b) The same as Fig. 5.9 (a) in sector 6.

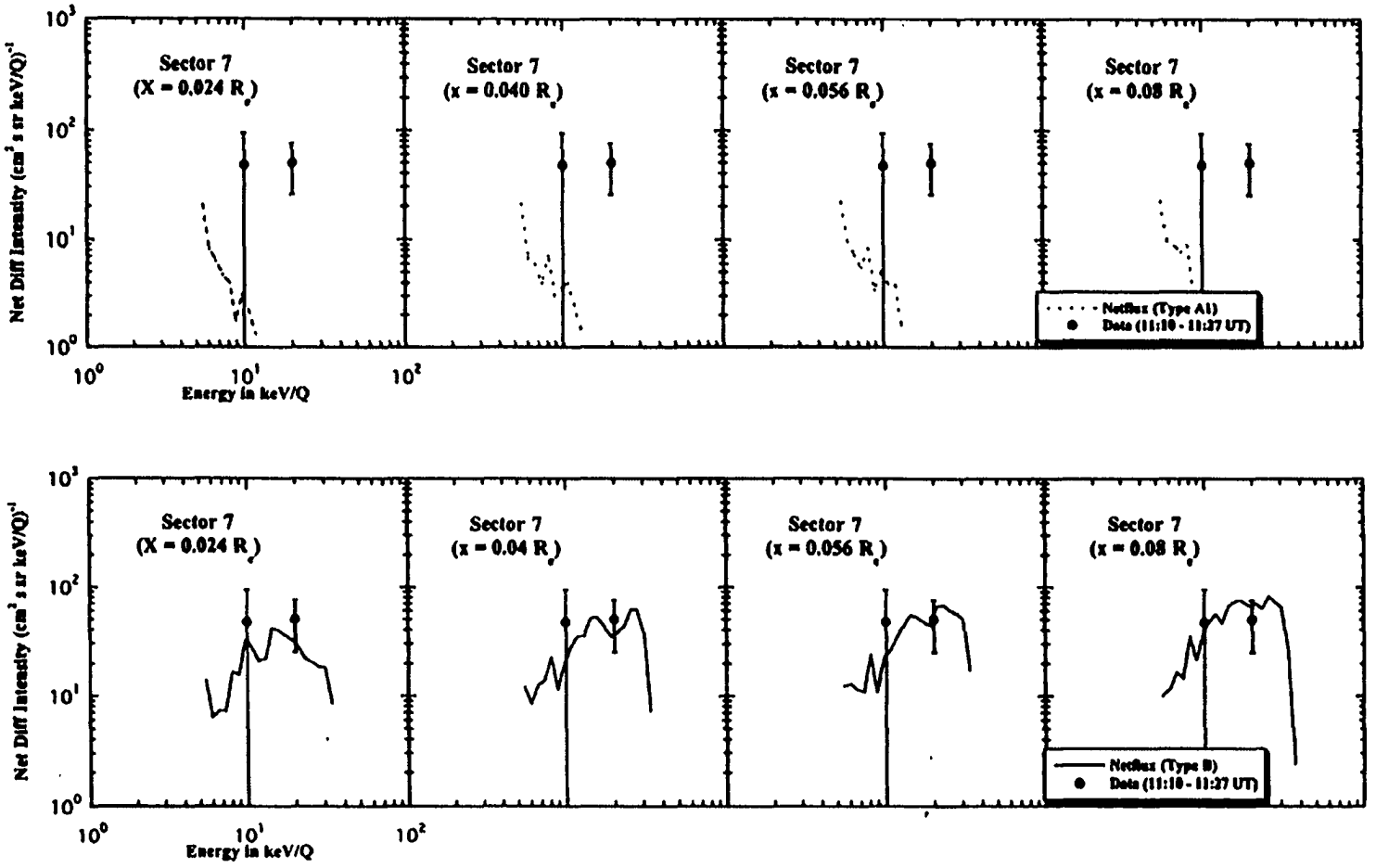

5.9 (c) The same as Fig. 5.9 (a) in sector 7.

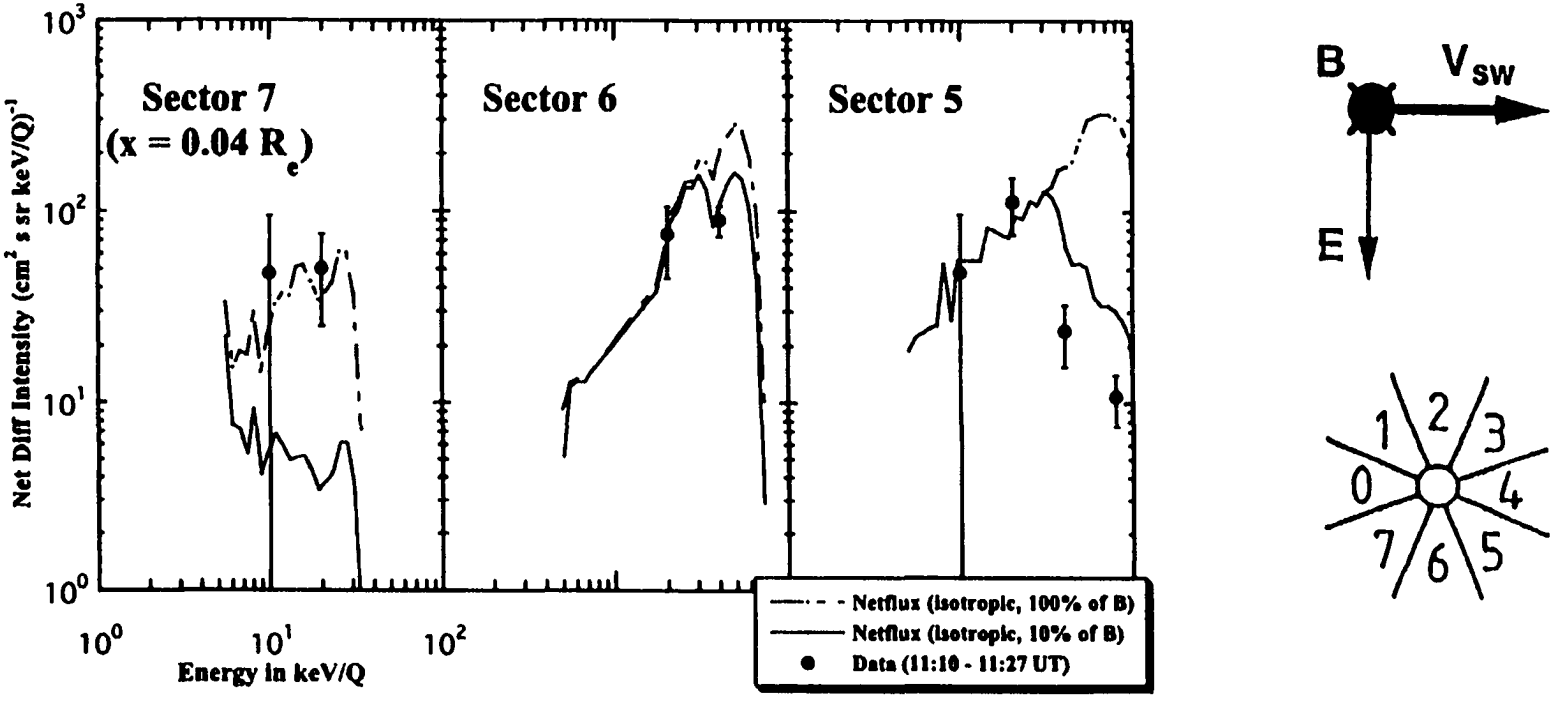

5.10 Comparison of simulated spectra (lines) with the observations at 11:10-11:27 UT for sectors 5, 6, and 7. The two lines represent the contributions from 100% and 10% of type B ions plus 100% of type A ions, respectively.

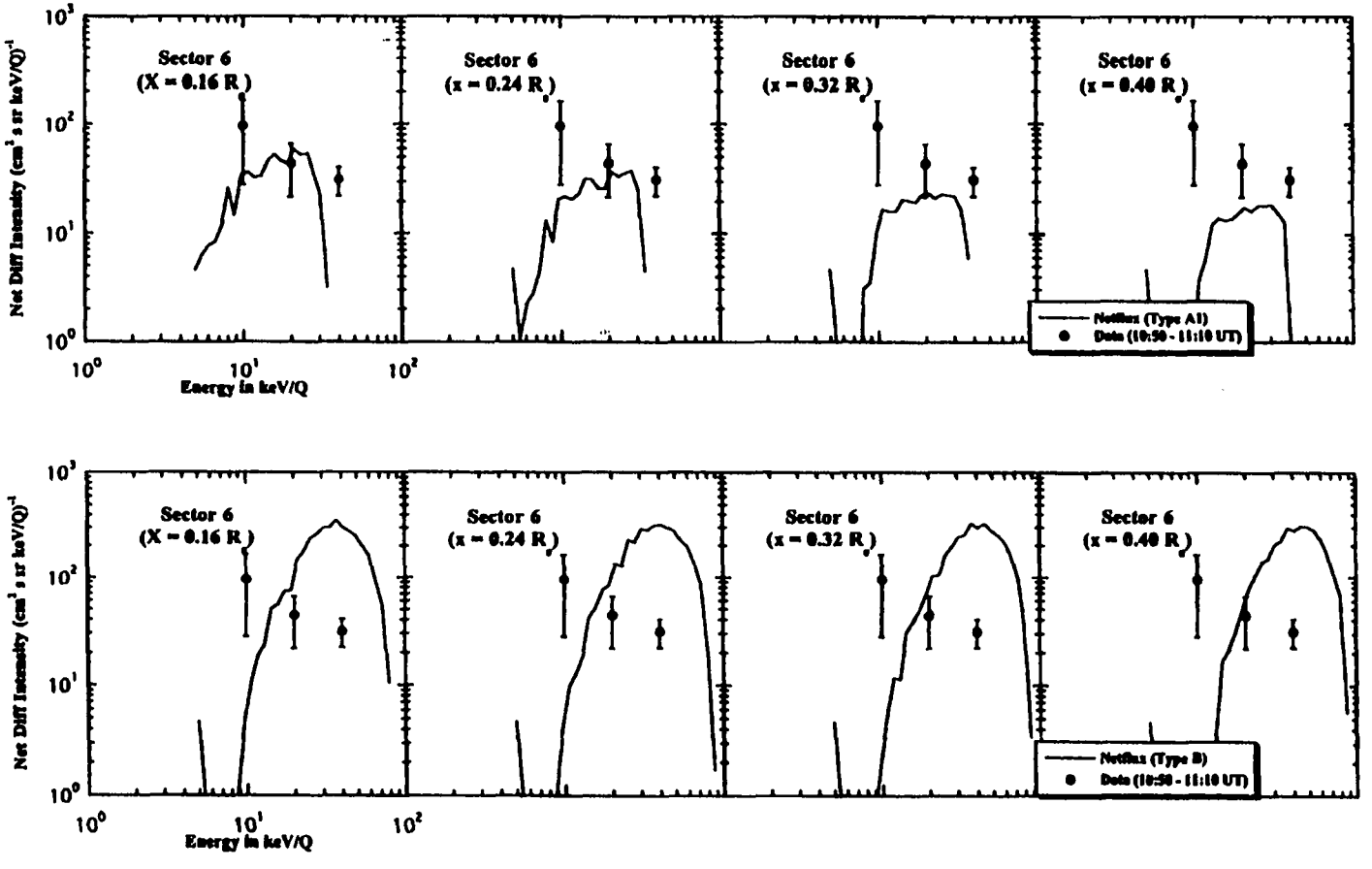

5.11 Comparison of simulated spectra of type A and B ions separately in the upper and lower panels in sector 6 with data at 10:50-11:10 UT, for various distances to the B.S.

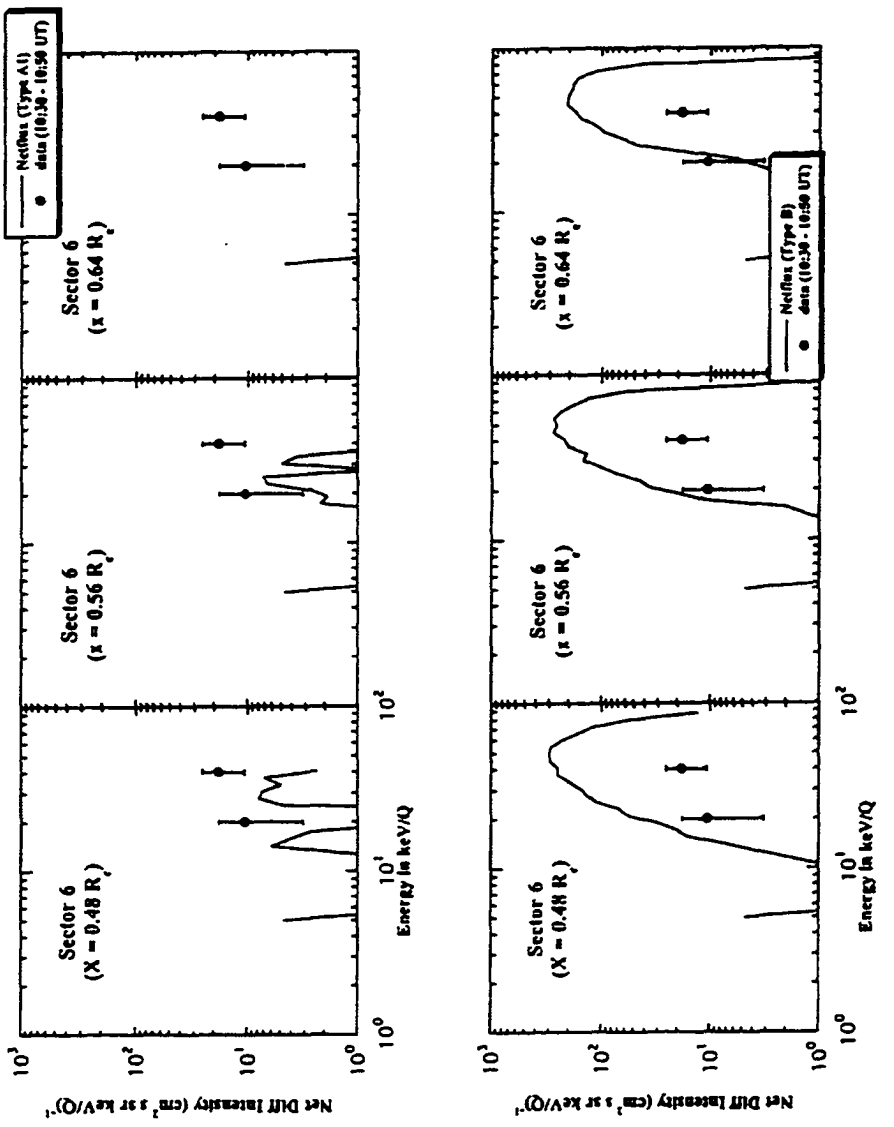

5.12 The same as Fig. 5.11 at 10:30-10:50 UT.

the spectra. Since the point at 10 keV is not a strong constraint due to its 2 counts during this time period, 0.32 R_e would also be possible. Therefore, the adopted distance range for the time period 10:50-11:10 UT are 0.16 - 0.32 R_e (0.8 - 1.6 $r_{p,L}$). For the same consideration, the distance of the observation point from the bow shock adopted for time period 10:30-10:50 UT, when no ions arrive in sector 7, is about 0.48 - 0.56 R_e (2.4 - 2.8. $r_{p,L}$.). This distance leads to the best agreement between observations and the simulation results. The full comparisons in sectors 5, 6 and 7 for the three time periods will be shown in the next section.

It is apparent that the distance from the shock is an important parameter in determining the ion spectrum. For the observation time period 11:00 - 11:27 UT best results are achieved with an average distance between 0.04 and 0.056 R_e from the shock. It would be a good test of the model, if we could determine this distance in an independent way. This is difficult in view of the shock motion during the time of multiple bow shock crossings with respect to the observing spacecraft. A simplified check of the actual distance to the shock seems to give conflicting results. To see this point clearly, we discuss two examples.

At 11:28 UT, the satellite passed the shock for the first time. For simplicity, we first assume that the shock remained stationary at the position during the entire observation period (10:30 to 11:28 UT). According to the results of the model, at distances greater than 0.88 R_e, there are no speculaly reflected ions. Therefore, the average distance

between spacecraft and bow shock at 10:30 - 10:50 UT, when we began to observe the energetic ions and the calculated flux is high enough to be detected (see Fig. 5.2), is about 0.56 R_e. Let us assume a linear relationship between time and the distance of the spacecraft (which moves uniformly towards the shock) from the bow shock (which is assumed to be static). Then a straightforward calculation returns an average distance of ~0.10 R_e for 11:10 - 11:27 UT. As indicated in Fig. 5.7, we will not be able to see any "surfing" ions at this distance which would result in a less favorable agreement between the model and the data. Even our example with marginal agreement is still closer to the shock. Therefore, we have to question our simplified assumptions.

As shown in Fig. 5.1, at 11:28 UT, the bow shock moved toward the Sun with respect to the spacecraft, which was continuously moving towards the Earth, so that the spacecraft entered the downstream region. At 11:31 UT, the returning shock passed the spacecraft moving towards the Earth so that the spacecraft found itself back upstream. Finally, at 11:44 UT the spacecraft encountered the shock once again and entered the downstream region. It appears that the shock is moving in an oscillatory motion. To test this idea, we simulated the bow shock movement as a simple oscillator which is oscillating about a firm location. However, a simple oscillatory movement failed to meet all the constraints of the observations. It is obvious that the motion of the bow shock is more complicated than an oscillator.

As already discussed above, we cannot use a linear variation of the average distance to represent the actual position of the bow shock over the observation time. Therefore, we have to rely on the best agreement between the ion data and predictions of the model to obtain the average shock distance for each time period. According to Fig. 5.9, 5.11 and 5.12, we adopt a distance of the observation point from the bow shock is in the range 0.04 - 0.056 R_c at 11:10 - 111:27 UT, 0.16 - 0.32 R_c at 10:50 - 11:10 UT, 0.48 - 0.56 R_c at 10:30 - 10:50 UT respectively. These correspond to 0.12 - 0.2 $r_{L,P}$, 0.8 - 1.6 $r_{L,P}$ and 2.4 - 2.8 $r_{L,P}$ for these three consecutive time periods.

5.3.4)Influence of the incident pickup ion distribution

Another determining factor for the flux of reflected ions is the original pickup ion flux density as the source distribution that is used for the absolute flux normalization of our simulations. Because only one energy step would coincide with the pickup ion spectrum for the instrument mode in use during our observation period, these data were not suitable to determine the pickup ion flux directly. Therefore, we used the typical pickup He^+ flux for the October time period based on a study by Möbius et al.[1995a]. These data still have some observational uncertainties. As pointed out in a subsequent paper [Möbius et al., 1996] the local neutral density and thus the total pickup ion flux may have been underestimated in the original study by a factor of 1.3-1.4, because the observations used by Möbius et al.[1995a] were made for IMF directions varying between 45^0 and 90^0 with respect to the solar wind flow. Pickup ion distributions tend to be anisotropic with

respect to the Earth-Sun direction for radial magnetic field as reported by Gloeckler et al.[1995]. This would result in reduced fluxes as observed by instrumentation such as the SULEICA sensor, which collects pickup ions only above the solar wind speed. Without better information we adopt a maximum correction factor of 1.4 over Möbius et al.[1995a] as the upper limit of the pickup ion flux.

In Figures 5.13, 5.14 and 5.15 the simulations for the time period 11:10-11:27 UT, 10:50 - 11:10 UT and 10:30 - 10:50 UT are shown for the corrected and uncorrected values of the pickup ion flux for sectors 5, 6 and 7, respectively. An additional cross check is possible in sector 5 where most of the spectrum is represented by incident pickup ions. The two curves reflect the maximum uncertainty in the normalization of the pickup ion flux. Within the errors of this measurement both curves represent the observations reasonably well except the points at 20 and 80 keV in sector 5. The fluxes at 20 keV in sector 5 fluctuate from time period to time period, while the spectrum below 21 keV in this sector should just represent the incident pickup ion distribution, which should be stable. However, in this data point there are only 2 counts for time period 10:30 - 10:50, 4 for 10:50 - 11:10, and 6 for 11:10 - 11:27, i.e., the statistics are poor. Therefore, this apparent discrepancy may be just caused by statistical fluctuations. Taking the average over all periods from 10:30 to 11:27 UT leads to a result that is in agreement with the typical pickup ion distribution for this time. In summary, in view of the simplifying assumptions of a planar exactly perpendicular shock, the agreement is relatively good, except for the points at 10 and 20 keV in sector 7 at 11:10 - 11:27 UT as well as the point

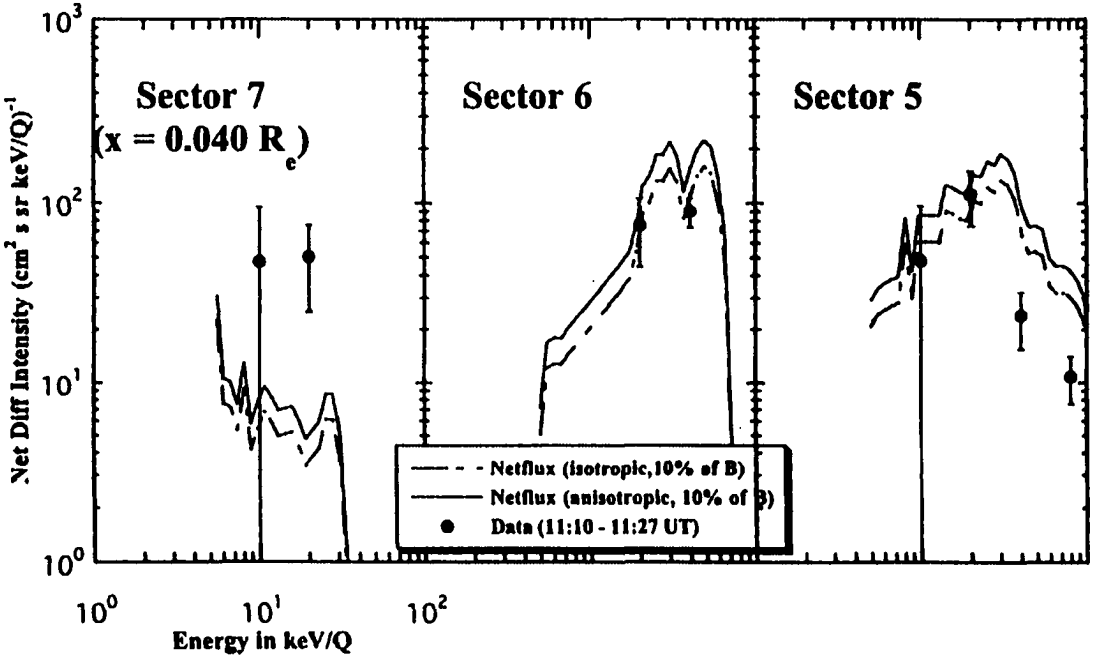

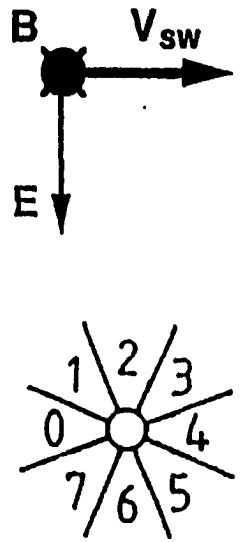

5.13 Comparison of simulated spectra (lines) with the observations at 11:10-11:27 UT for sectors 5, 6, and 7. The two lines represent two different normalizations mentioned in Fig. 5.8.

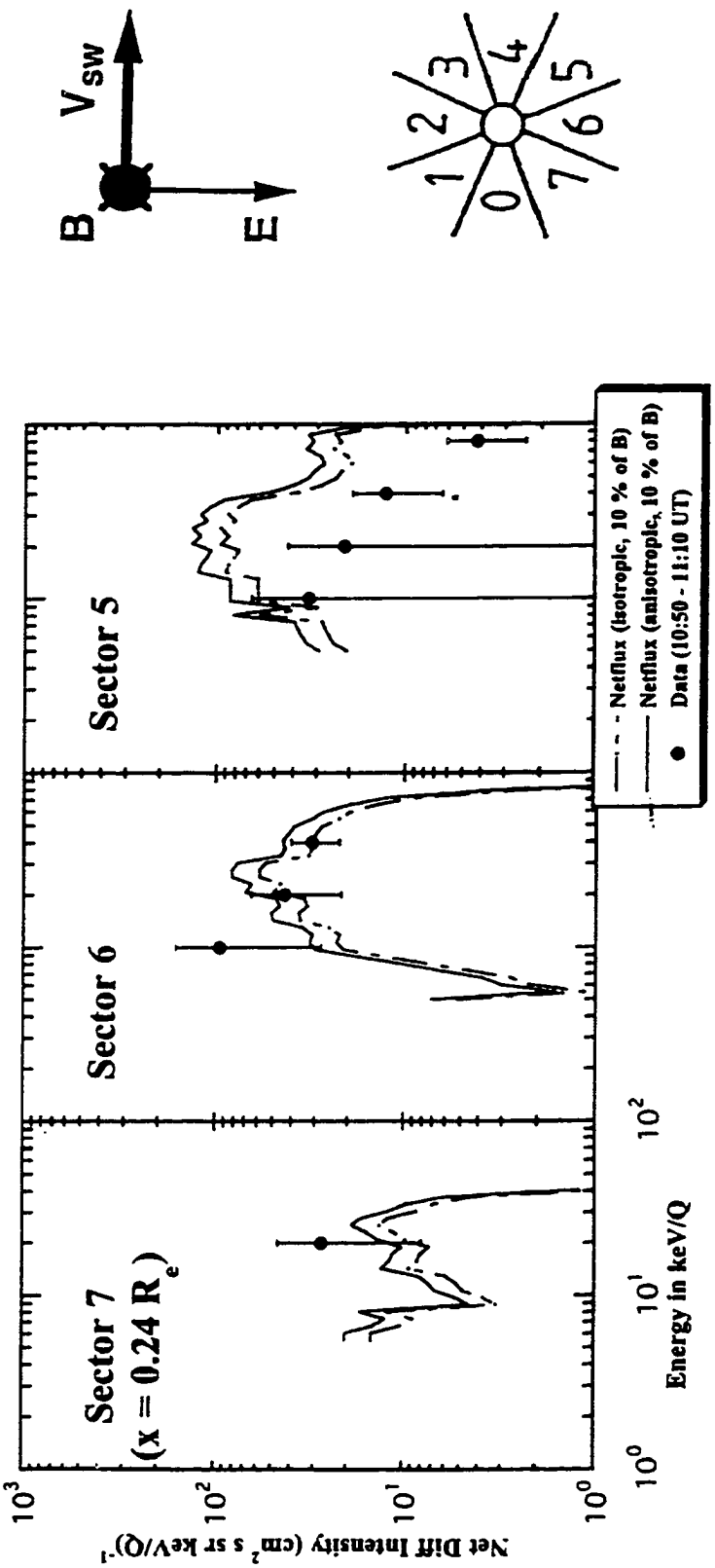

5.14 The same as Fig. 5.13 at 10:50-11:10 UT..

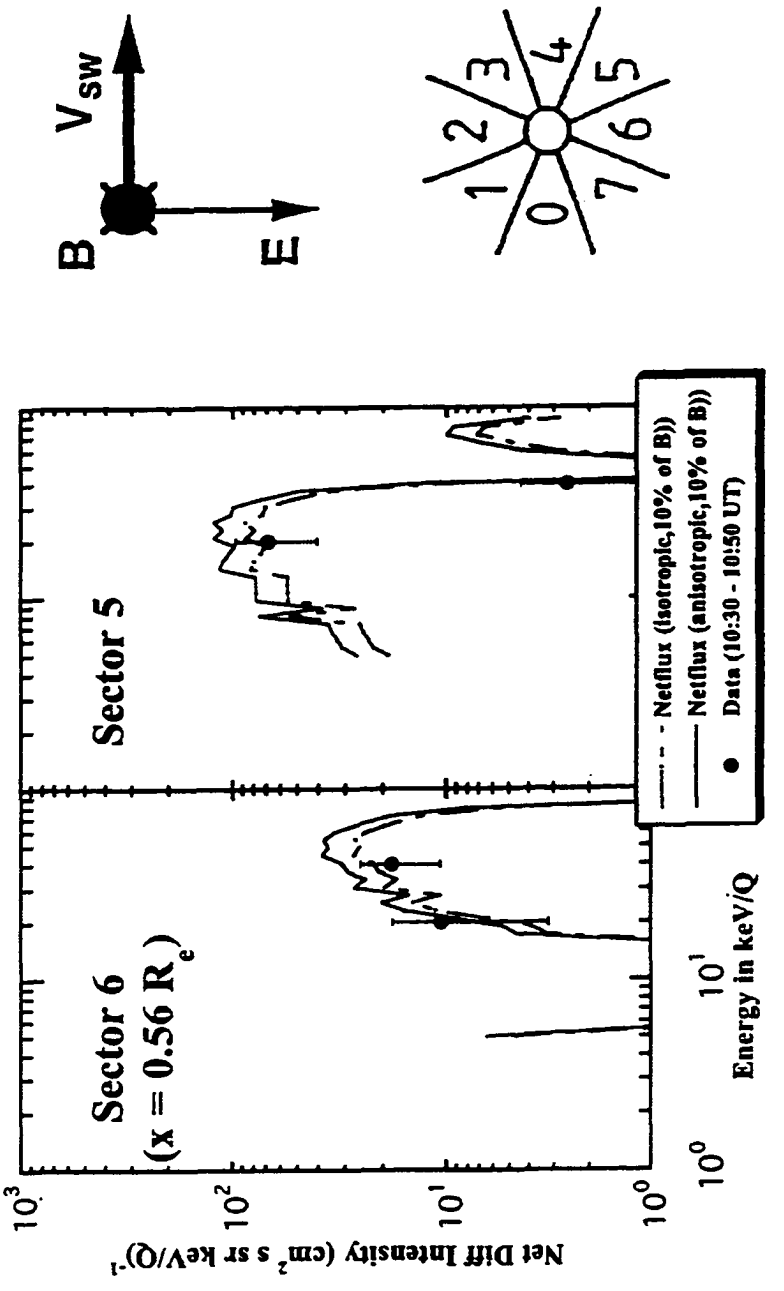

5.15 The same as Fig. 5.13 at 10:30-10:50 UT..

at 40 and 80 keV in sector 5 during the time period 10:50 - 11:10 UT and 11:10 - 11:27 UT.

5.3.5)Influence of the shock potential

So far we have assumed that the shock potential is exactly determined by the solar wind energy. To investigate the validity of this assumption we vary the shock potential by setting $q\Delta\Phi = 1/2\ m_{ap}\ V_{sw}^{2}\ \gamma$. We have performed simulations with $\gamma = 0.5$, $\gamma = 0.7$ and $\gamma = 1$ as shown in Fig. 5.16 and Fig. 5.17. The results indicate that the influence of γ on the magnetically reflected ion flux (type B) in sectors 5 and 7 is weak. Only multiple or electrostatically reflections (type A) are sensitive to γ. In Fig. 5.16, the spectra of multiple reflected ions shift moderately to the lower energy as the γ decreased from 1.0 to 0.7. The spectra from type B in sector 6 are also sensitive to γ, but the influence of γ to the sum of all the contributions of types A and B is still weak. Because the lower shock potential only causes an enlargement of the area of type B and a reduction of the area of type A in the pickup ion distributions. This leads to a visible but still weak effect in sector 6. In Fig. 5.17 the spectra of multiply reflected particles shift dramatically to the lower energy and there is even no ions with 3 reflections while the spectra of type B ions are increased dramatically in sector 6. It seems difficult to explain the observation with lower shock potential. This results seems consistent with the assumption that the shock potential is close to the full ram energy of the solar wind. However, no quantitative.

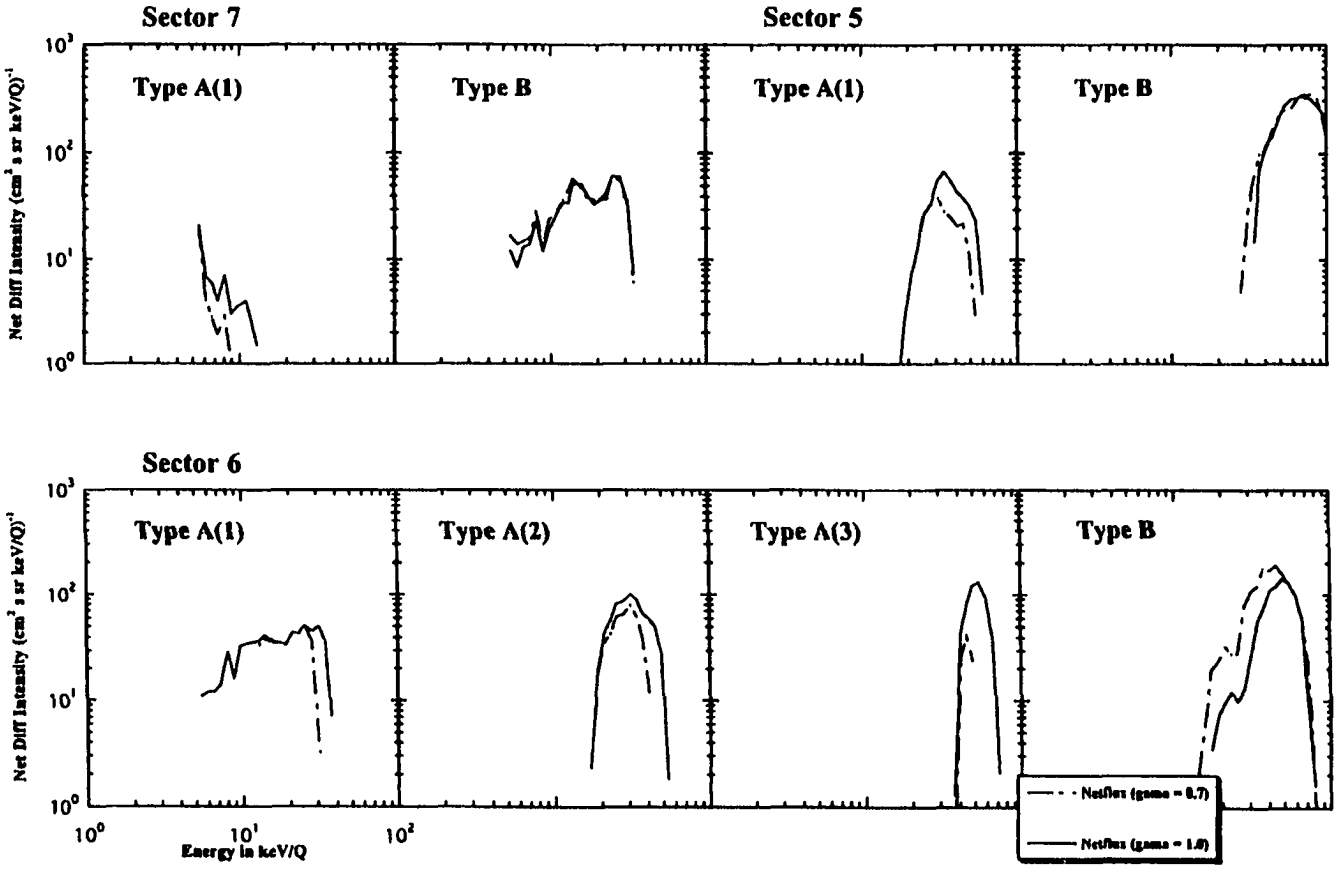

5.16 Comparison of a variation for the effective shock potential $e\Phi_s = \gamma m V_{sw}^2/2$ on simulated spectra form different types of ion trajectories for sectors 5, 6 and 7 with $\gamma = 0.7$ and $\gamma = 1.0$.

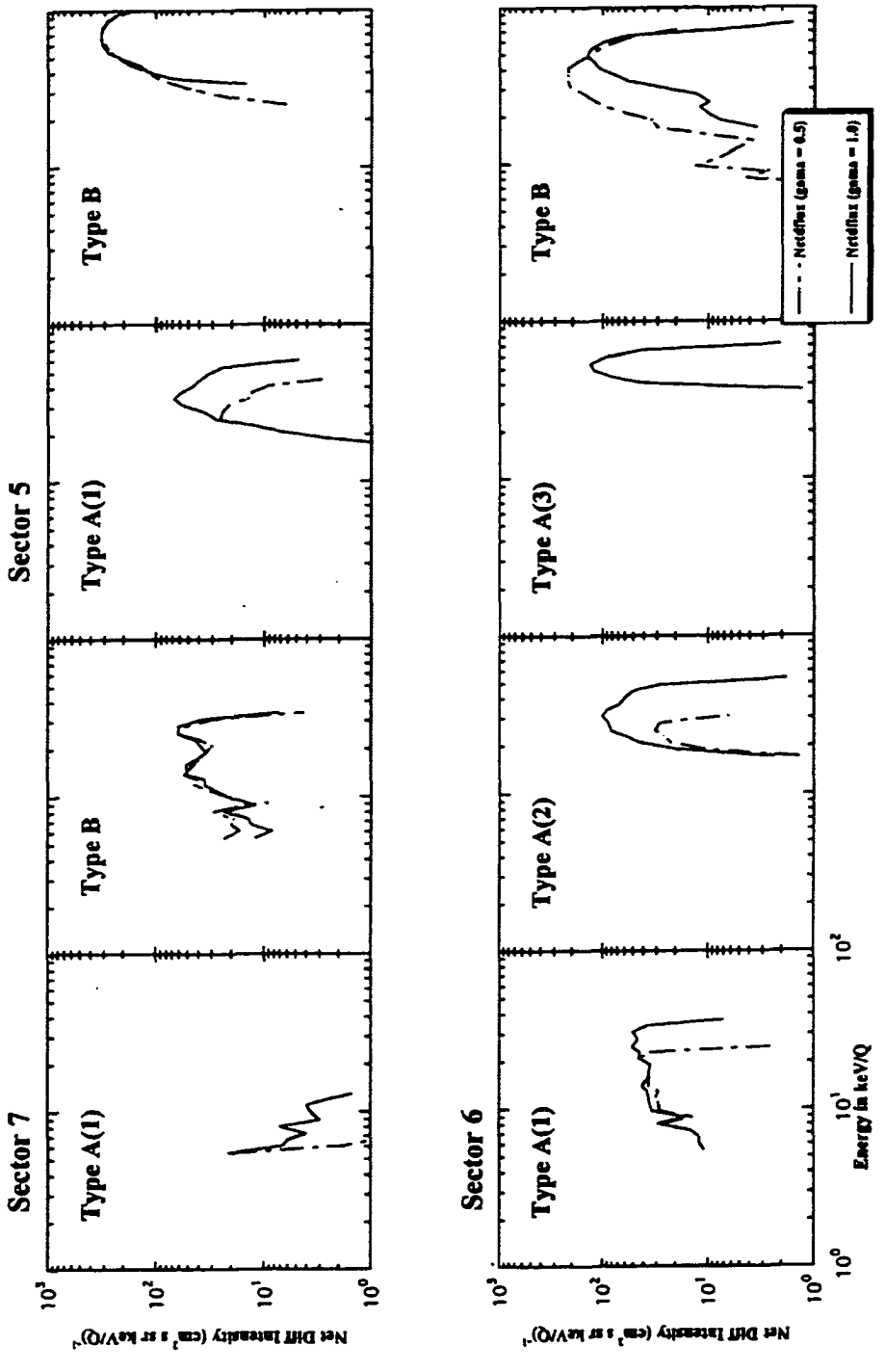

5.17 The same as Fig. 5.16 with $\gamma = 0.5$ and $\gamma = 1.0$..

conclusions on the actual value of the shock potential can be drawn from the comparison with our data, because the different curves still fall within the uncertainties of the data

5.4) Summary and Discussion

We have studied specularly reflected He^+ pickup ions in front of an almost perpendicular bow shock with AMPTE SULEICA for a time period in October 1984. We have compared the observations with a model distribution derived from trajectory calculations at a perpendicular shock. In the simulation we can distinguish three different classes of particles in the incident pickup ion distribution:

- almost 15% of the incoming ions are electrostatically reflected at the shock (type A);
- ≈48% of the pickup ions are magnetically reflected (type B);
- the remaining 37% are transmitted through the shock.

The 3 classes of ions are organized in 3 coherent regions of the incident pickup ion distribution.

The observed directional and energy distribution of the reflected ions is consistent with the simulated distribution. We could identify the contributions from the two different classes of ions (electrostatically and magnetically reflected) in the observations. The data at 80 keV in sector 5 and 40 keV in sector 6 are consistently lower than the predictions of our model for the two time periods at 11:10 - 11:27 and 10:50 - 11:10 UT with good

statistics if type B ions are counted at 100%. This behavior could be explained by taking into account the magnetic field fluctuations just downstream of the shock. Therefore, we account for this effect by a contribution of 10% from type B to the simulated spectra. Even then, the data beyond the pickup ion cut-off energy ($\geq$ 40 keV) in sector 5 are still lower than the simulation, while the data at 20 keV in sector 7 during 11:10 - 11:27 UT is higher than the result of the model. Taking into account the magnetic field fluctuation by adding only 10% of type B ions does not produce full agreement simultaneously for both sectors. These discrepancies may imply the following possibilities: First, type B ions spend a longer part of their trajectory in the upstream region of the shock than type A particles. As a consequence, a fraction of these particles may be lost along the trajectory before they reach sector 5 by scattering in magnetic field fluctuations This scattering is more important for sectors 5 and 6 than for sector 7, where the ions appear in earlier part of their trajectory. Therefore, if we would take, say 50% of type B ions into the spectra for sector 7, 10% or less for sector 6 and 5% for sector 5, the agreement between the data and the prediction of model turns out to be better. But due to the poor counting statistics in sector 7 a definite conclusion cannot be drawn. Secondly, it is possible that ions with higher energy are strongly scattered by the turbulent fields upstream and downstream of the shock. Finally, this discrepancy may be attributed to neglecting other effects in the simulations, such as a non-ideal shock geometry.

Overall the agreement of our model with the observations seems remarkably good in view

of the potential observational errors and simplifying assumptions made in the model. The observed energetic ion fluxes closest to shock can only be explained with a significant contribution from ions that undergo at least 2 reflections and possibly even 3 reflections. This seems to indicate that "surfing" of ions along a quasi-perpendicular bow shock as pointed out by Lee et al. [1996] plays an important role in the production of energetic ions at the shock. During multiple encounters with the shock the ions can gain a substantial amount of energy. However, no ions with a second or third reflection are found further than 0.07 R_E upstream of the bow shock for the observed solar wind conditions.

Because we do not have independent knowledge of the relative position of the satellite to the bow shock due to the motion of the shock, we studied the influence of variable bow shock distance on the ion spectra and then used the best agreement between the model prediction and the data to infer the distance. Finally, we studied the dependence of the energetic ion fluxes on the magnitude of the shock potential. Within 30% even 50% of the solar wind ram energy ($e\Phi = m_p/2\ V_{sw}^2$) only a very weak influence is seen.

CHAPTER 6

DIFFUSIVE HE^+ ION INJECTION AND ACCELERATION AT THE QUASI-PARALELL EARTH'S BOW SHOCK

As mentioned in chapter 2, energization of solar wind ions at the Earth's bow shock and leakage of energetic ions from the magnetosphere are two possible sources that have been proposed for energetic ions seen in the magnetosheath and upstream of the quasi-parallel bow shock. Enhanced plasma and magnetic turbulence and their associated energetic ions are coupled phenomena and are similar in the upstream and downstream regions. This suggests that they are from the same bow shock related origin [Asbridge et al., 1978]. A plausible mechanism for energization of solar wind ions is first-order Fermi acceleration at the quasi-parallel bow shock [e.g., Lee, 1982]. However, for similar magnetic field orientations that are favorable for the Fermi process, ions from the Earth's magnetosphere will also be able to travel along the magnetic field into the magnetosheath and into the region upstream of the quasi-parallel bow shock [Luhmann et al., 1984]. Therefore, it has been suggested that energetic ions are likely to leak from the magnetosphere [e.g., Sarris et al., 1976] and could form the energetic ion population upstream of the shock.

In order to distinguish between the two possible sources and to determine their relative importance, composition measurements offer an important tool. Because there is a large population of H^+ and He^{2+} in the solar wind and comparatively little in the magnetosphere, the ratio of He^{2+}/H^+ is an ideal tracer for the bow shock acceleration process. On the other hand, because of a substantial contribution of energetic O^+ in the Earth's magnetosphere and a comparatively low flux of ions with or near M/Q = 16 in the solar wind, oxygen is an ideal tracer for leakage of energetic ions from the magnetosphere. These two tracers will provide the reference base on which we will try to identify the source of energetic He^+ in the upstream ion population. If energetic He^+ stems from leakage of He^+ out of the magnetosphere, we should expect to find a similar behavior between energetic He^+ and O^+. Otherwise, we should expect to find a similar behavior between energetic He^+ and He^{2+}, i.e., if energetic He^+ is indeed shock-accelerated ions. Therefore, composition measurements of the diffuse ion population upstream of the quasi-parallel shock offer the potential to determine conclusively the origin of the energetic He^+ ions. Thus we can hope to differentiate between leakage of He^+ ions from the magnetosphere and local acceleration of He^+ ions at the shock. In this section we will first present observations of the differential fluxes, energy spectra and directional distribution of the key ions species in front of the shock and compare them with simultaneous observations in the magnetosphere. After a qualitative interpretation of these observations we will compare them with an analytical model that contains both magnetospheric leakage and acceleration of ions at the shock.

6.1 Basic observations

The following analysis of diffuse ion events is based on data from the suprathermal energy ionic charge analyzer (SULEICA) on board the AMPTE/IRM spacecraft. A typical upstream ion event, as selected for our analysis, is shown in Figure 6.1. Plotted are the magnetic field strength B, its direction in GSE coordinates in azimuth Φ_B

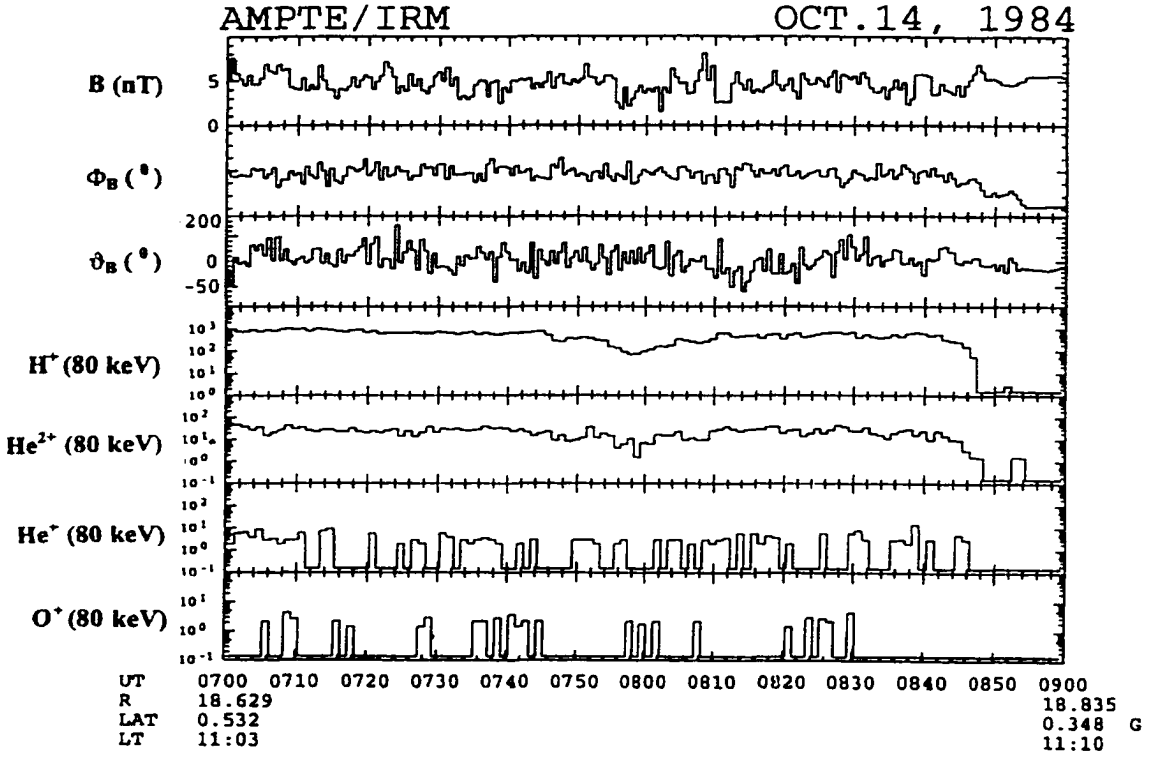

Fig. 6.1. Typical example of an upstream event at 0700 - 0900 on October 14, 1984. Plotted are variations of interplanetary magnetic field strength B, direction in azimuth ΦB, and elevation ϑB in GSE coordinates, and the differential flux of H^+, He^{2+}, He^+ and O^+ at 80 KeV/Q.

(fluctuated between $\pm 10^0$), elevation θ_B (changed between $\pm 40^0$) and the differential flux of 80 keV/Q H^+, He^{2+} , He^+ and O^+ ions as a function of time. Shown is the two-hour period from 7:00 to 9:00 UT on October 14, 1984, when AMPTE/IRM was a few Earth radii upstream of the shock at approximately 11:00 local time. The magnetic field is radial from 6:00 tc 8:46 UT. The fluxes of H^+ and He^{2+} stayed almost constant and reached a plateau from 7:00 UT to 8:46 UT with the radial field upstream. The intensity decreases when magnetic field fluctuations decrease at 8:46 UT. Before 7: 00 UT, the satellite observed a few energetic He^+ ions during a one-hour period (6:00 - 7:00 UT). The satellite encountered high energy He^+ starting from 7:00 UT, and the differential flux of He^+ is almost continuous and also constant but with poor counting statistics during this period while the flux of the energetic O^+ is continuously present.

6.1.1) Angular distribution and energy spectra

20 minutes averages of the directional distribution of H^+, He^{2+}, He^+ and O^+ at 80 keV and 160 keV(differential flux vs. flow direction) are presented in Figure 6.2. The arrow indicates the projection of the magnetic field into the plane perpendicular to the spacecraft spin. The energetic H^+ and He^{2+} ions exhibit a distribution mainly perpendicular to the magnetic field with a net anisotropy directed towards the Earth. The fluxes in the distribution are substantially depressed along the magnetic field for H^+ and He^{2+}. The He^+ ions basically mimic the behavior of the H^+ and He^{2+}, but with poor

counting statistics. At 160 keV the energetic O^+ ions are clearly streaming along the field and away from the Earth. At 80 keV the main flux of O^+ is still directed away from the Earth, but it also exhibits a strong anisotropy perpendicular to B.

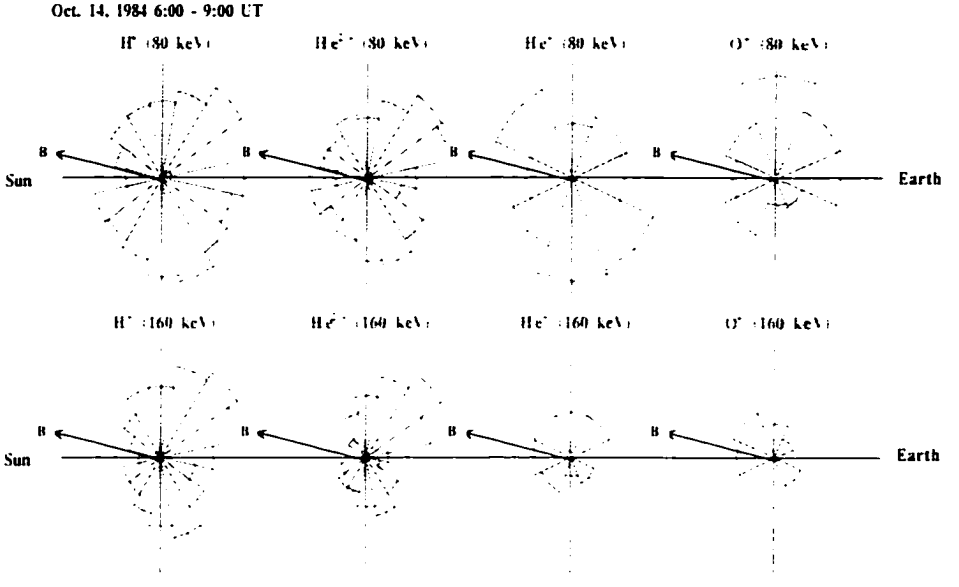

Fig. 6.2. Typical example of an upstream event at 0900 - 0920 on October 14, 1984. Plotted are averages of the angular distribution for H^+, He^{2+}, He^+ and O^+ at 80 keV/Q and 160 keV/Q (differential flux vs. flow direction).

The anisotropies of the H^+, He^{2+} and He^+ ions are typical for strong scattering in the magnetic field fluctuations. The net anisotropy in the spacecraft system into the earthward direction is an expression of the energy gain due to the Compton-Getting effect

via diffusive reflection in the solar wind [e.g., Scholer et al., 1979]. This can be taken as evidence that the particles (H^+, He^{2+} and He^+) are strongly scattered in the upstream medium and convected backward towards the shock with the solar wind velocity. First order Fermi acceleration at the shock is then an unavoidable consequence of the diffusion-convection equation [Gleeson and Axford, 1967]. The depression in the distribution along the magnetic field is possibly due to the fact that the scattering mean free path is of the order of the distance for free escape of the ions from the foreshock region [Möbius et al., 1986]. Ions with pitch angles near 90^0 experience a much longer trajectory through the scattering region.

Contrary to H^+, He^{2+} and He^+, the O^+ ions are streaming away from the earth along the magnetic field, precisely what one would expect for particles freely escaping from the magnetosphere. Thus the fact that O^+ ions are streaming away from the Earth, while the other upstream ions are strongly scattered with obvious anisotropy shows existence of two ion populations. While H^+, He^{2+} and He^+ ions in the range of a few times 10 keV/Q have a resonant frequency near the maximum in the power of the upstream waves [Hoppe and Russell, 1983], O^+ are in resonance at substantially lower frequency. The fact that O^+ ions stream away from the Earth while other ions (H^+, He^{2+} , He^+) are strongly scattered also indicates that the spatial diffusion coefficient parallel to the magnetic field for O^+ is larger than that of the other species.

These characteristics are consistent with local acceleration of H^+, He^{2+} and He^+ and escape of O^+, but a definite conclusion cannot be drawn yet. In principle, all species could come from the magnetosphere, H^+, He^{2+} and He^+ get scattered and experience further acceleration, while O^+ would be unaffected. However, scattering would also hinder the escape and could cause a depletion in the distributions of H^+, He^{2+} and He^+ along the magnetic field. In other words, these characteristics do not allow to differentiate definitively between the two possible origins of the upstream energetic He^+ ions, i.e., the pickup or the magnetosphere. We need to look for more evidence.

6.1.2) Energy spectra

Figure 6.3 displays typical differential flux energy spectra of the different ion species averaged over 20 minutes during an upstream event on October 20, 1984. The dashed line represents a exponential fit curve so that we can compare the slope of the spectra between species. The upper panel shows spectra upstream of the shock and the lower panel contains spectra in the magnetosphere that were taken during the same time period with the AMPTE/CHEM instrument. In the upstream region the spectra of H^+ and He^{2+} exhibit a similar shape, He^+ and O^+ appear to be harder than those of H^+ and He^{2+}. In the magnetosphere the spectra of H^+ and O^+ are softer than those of He^+ and He^{2+}. Also, the spectrum of O^+ in the upper panel has very similar shape with that of in the lower panel. Furthermore, the differential flux of O^+ is considerably the lowest in the region upstream of the shock, but higher than that of He^{2+} and He^+ in the magnetosphere, i.e., the

abundance of O^+ appears to be depleted upstream of the shock when compared with level in the magnetosphere.

Next we study the shape of differential flux energy spectra. The energy spectrum of O^+ in the region upstream of the shock is significantly harder than that of the other species and is similar in shape to the O^+ spectrum, which as observed with the CCE spacecraft in the magnetosphere. This lends additional support to the idea that the origin of the energetic O^+ is the magnetosphere, as suggested by the angular distributions. In order to see clearly the shape of spectrum for diffuse He^+ ions, data whose energy is greater than the cut-off energy are only shown here. The spectrum of He^+ beyond the cut-off energy (in this event, $E_{cut\text{-}off}$ = 40.5 keV) is obviously harder than that of He^{2+} and H^+ in the upstream region, while in the magnetosphere the spectrum of He^+ is similar to that of H^+ and O^+. At first glance, this seems to speak for a magnetospheric origin for He^+ contrary to the evidence of the directional distribution. However, the fact that pickup ions are the possible source for the acceleration of He^+ compared with the solar wind for H^+ and He^{2+} could lead to a harder spectrum for He^+. Therefore, we have to seek further evidence.

The fact that the O^+ flux falls off from the magnetosphere to the upstream region more than that of any other species may give us a clue. If the He^+ upstream ions were of the same origin as O^+ one would expect to see a similar feature of spectrum in the upstream

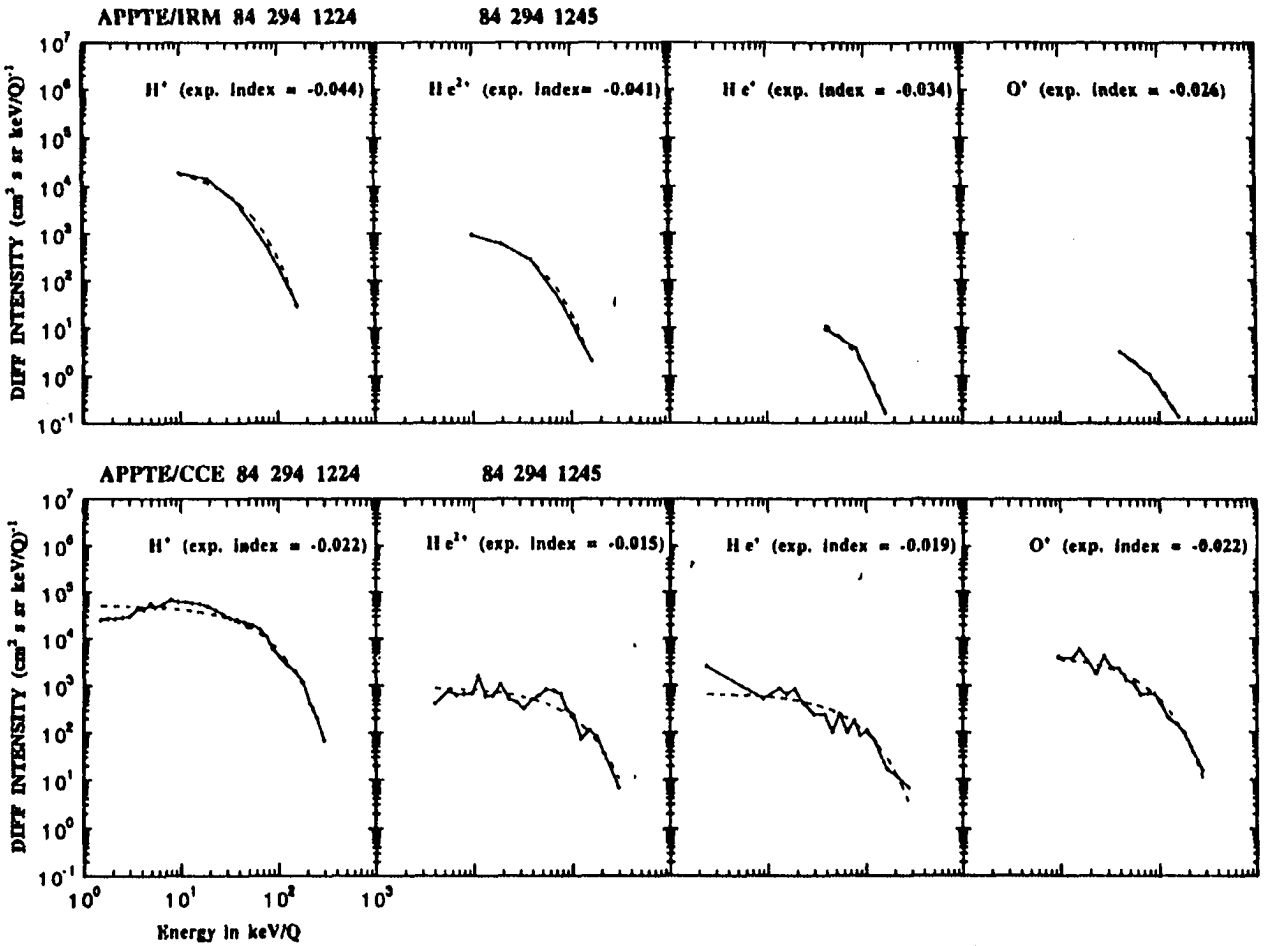

Fig. 6.3. Differential particle flux versus energy per charge for H^+, He^{2+}, He^+ and O^+. The measurements were observed with SULEICA (upper panel) as well as CCE (lower panel) instruments, respectively, for the October 12 ,1984 event averaged from 1224 - 1245. The solid line indecates the observations while the dashed line a exponantial fit curve which help us to compare the spectra.

event. Therefore, we will compare, in the next section, the ratios of the flux density in the upstream region and in the magnetosphere for H^+ , He^{2+} , He^+ and O^+ for a larger set of upstream events. We study the abundance ratios for energies higher than 40 Kev/Q, because the counts of O^+ at the lower energies are affected by background. For He^+ only ions whose energy is above the cut off energy of pickup ions are considered as belonging to the diffuse ion distribution.

6.1.3) Statistical analysis of the upstream ion distributions

We selected all time periods when the AMPTE/IRM was just upstream of the nose of the Earth's bow shock and during a time when the interplanetary magnetic field was radial. We define "radial" by requiring that the angle between the magnetic field and the normal direction of the bow shock is less than 20 degree for all events. For the purpose of our study this requirement is equivalent to that of a quasi-parallel bow shock. The selection criterion for the events was a steady flux for He^+ at energies greater than 40 keV ions for at least 10 minutes. For our survey, all events which exceed a duration of 20 minutes and exhibit a clear plateau in the energetic He^+ are subdivided into 20-min intervals. For the statistical analysis all measured quantities are averaged over 10 - 20-min time intervals. During the period September through December 1984, 38 upstream events were selected. In order to compare the ion distributions between the upstream and magnetospheric regions, we require events for which we have the spectra in the upstream selected. In order to compare the ion distributions between the upstream and

magnetospheric regions, we require events for which we have the spectra in the upstream require measured by AMPTE/IRM and the simultaneous correlated spectra in the magnetosphere recorded by the CHEM instrument ON CCE. Only 10 of the 38 events satisfy this criterion when AMPTE/CCE was in the dayside magnetosphere with a distance of 7-9 R_e from the Earth. Figure 6.4(a) shows a schematic representation of the relative position of the IRM spacecraft and bow shock as well as the magnetic field direction for a typical event. Figure 6.4(b) shows the distribution of the magnetic field directions taken for all events chosen. The details of all events are listed in Table 6.1.

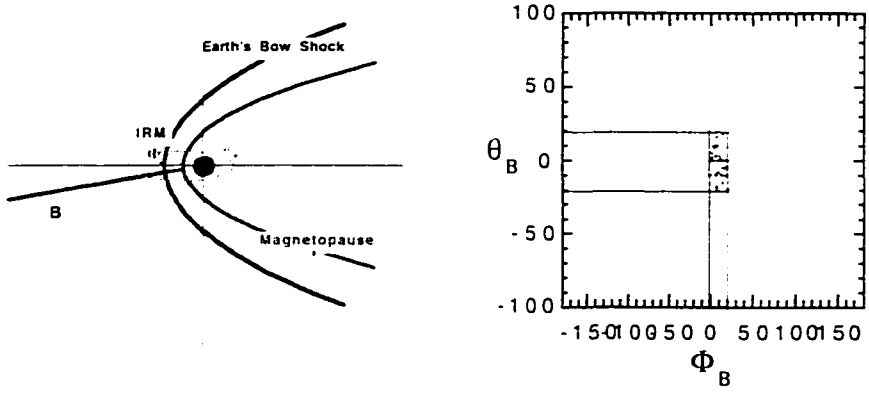

Fig. 6.4. Schematic representation of an event chosen to have the spectra in the upstream and the magnetosphere, simultaneous (a); (b) potted are the "radial" distribution of magnetic field directions for all events.

Table 6.1 Summary of events chosen at quasi-parallel Earth's bow shock by AMPTE.

Date	Time	V_{sw} km/s	ϑ_{Bn} deg	R (IRM) / Local Time		L (CCE) / Local time
10/07-1	11:26-11:36	550	7	15.97-15.87	12:27-12:28	8.84-8.87 11.51
10/07-2	11:40-11:52	550	4	15.83-15.7	12.29-12:30	8.88-8.91 11.51
10/07-3	12:00-12:12	600	0	15.61-15.51	12:31-12:32	8.93-8.94 11.51
10/09-1	08:36-08:56	700	4	15.43-15.21	12:26-12:28	8.12-8.32 10.90
10/09-2	08:56-09:10	700	4	15.21-15.05	12:28-12:29	8.33-8.43 10.90
10/09-3	09:18-09:38	700	4	14.96-14.73	12:30-12:32	8.50-8.62 10.90
10/12-1	06:08-06:34	650	20	17.37-17.55	10:50-10:52	-
10/12-2	06:44-07:06	650	4	17.60-17.73	10:53-10:54	-
10/12-3	07:06-07:26	650	4	17.73-17.85	10:54-10:56	-
10/12-4	09:40-10:00	700	20	18.44-18.51	11:05-11:07	-
10/14-1	06:00-06:14	600	18	18.45-18.50	10:59-11:00	-
10/14-2	06:24-06:40	600	8	18.53-18.57	11:00-11:01	-
10/14-3	06:40-07:00	600	2	18.57-18.63	11:01-11:02	-
10/14-4	07:00-07:20	600	2	18.63-18.68	11:02-11:04	-
10/14-5	07:20-07:40	550	2	18.68-18.72	11:04-11:05	-
10/12-6	07:40-08:00	550	12	18.72-18.76	11:05-11:06	-
10/14-7	08:00-08:20	550	12	18,76-18.79	11:06-11:08	-
10/14-8	08:20-08:45	550	20	18.79-18.82	11:08-11:09	-
10/20-1	06:34-	700	8	17.33-17.16	11:25-11:27	-

	06:58					
10/20-2	07:38-08:00	700	2	16.86-16.86	11:31-11:32	-
10/20-3	08:00-08:20	700	8	16.08-16.52	11:32-11:34	-
10/20-4	08:20-08:40	700	18	16.52-16.33	11:34-11:36	-
10/20-5	09:04-09:24	650	18	16.12-15.92	11:38-11:40	-
10/20-6	11:06-11:15	700	18	14.82-14.70	11:50-11:51	8.36-8.44 10.30
10/20-7	11:20-11:40	700	18	14.64-14.40	11:51-11:54	8.47-8.61 10.30
10/20-8	12:08-12:24	650	20	14.07-13.83	11:57-11:59	8.79-8.87 10.30
10/20-9	12:24-12:46	650	20	13.83-13.50	11:59-12:01	8.87-8.96 10.30
12/10-1	09:40-10:00	550	20	16.64-16.80	08:24-08:25	
12/10-2	10:00-10:20	550	14	16.80-16.91	08:25-08:27	-
09/12-1	13:00-13:20	575	1	14.78-15.01	12:14-12:15	-
09/12-2	13:20-13:40	575	1	15.01-15.24	12:15-12:17	-
09/12-3	13:40-14:00	575	1	17.08-17.08	12:17-12:19	-
09/12-4	18:30-18:50	600	10	17.67-17.79	12:42-12:44	-
09/12-5	18:50-19:10	600	12	17.79-17.90	12:44-12:45	
09/12-6	19:10-19:30	600	10	17.90-18.00	12:45-12:46	
09/20	00:10-00:30	525	0	16.11-16.28	11:58-12:00	-
10/10-1	07:56-08:20	675	2	16.49-16.70	10:48-10:50	
10/10-2	08:20-08:41	675	20	16.70-16.86	10:50-10:51	-

Figure 6.5 shows scatter plots of the abundance ratios for He^{2+}/H^{+} at 80 keV/Q and 160keV/Q as observed in the magnetosphere and in the upstream region. The horizontal

axis represents the abundance ratios in the magnetosphere, while the vertical axis represents the ratios in the upstream region. The line with a slope of one (indicating no ratio change) divides the plots into two regimes: the upper regime reflects the cases where the abundance ratio in the upstream region is higher than that in the magnetosphere, while the opposite is true in the lower regime. Figure 6.5 tells us that the ratios of He^{2+}/H^{+} at 80 keV are somewhat enhanced in the diffuse ions compared with those in the magnetosphere, but shows a scatter of points at 160 keV, which is similar to the result obtained by Ipavich et al. [1984].

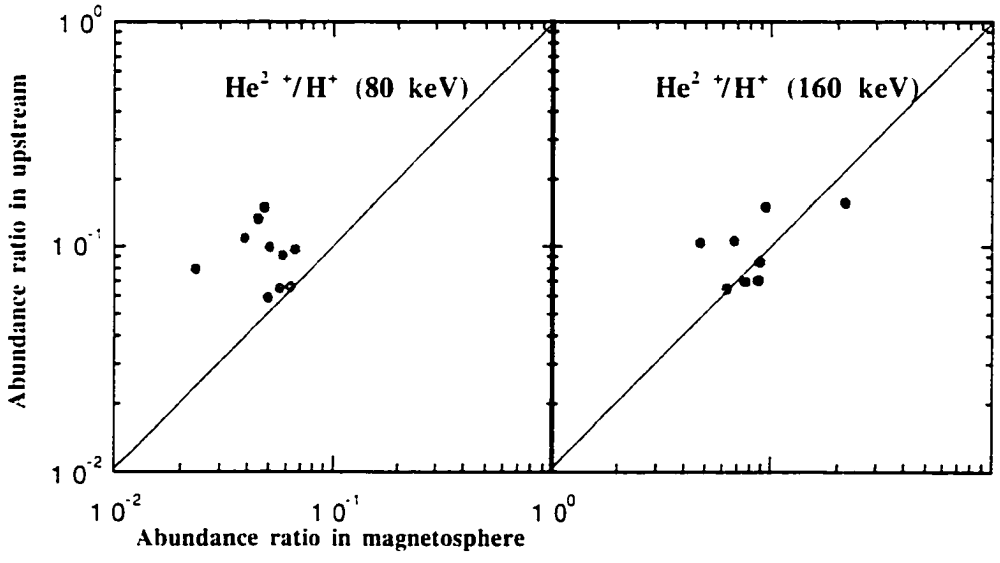

Fig. 6.5. Scatter plots of the abundance ratios for He^{2+}/H^{+} at 80 keV/Q and 160 keV/Q, respectively, as observed in the magnetosphere and in the upstream region.

Figure 6.6 shows the comparison for O^+/H^+ and O^+/He^{2+} in a similar representation. Most of the ratios fall into the lower regime indicating that O^+/H^+ and O^+/He^{2+} are depleted in the diffuse ions compared with the ion distributions in the magnetosphere. In other words, H^+ and He^{2+} are both enhanced over O^+ in the region upstream of the shock.

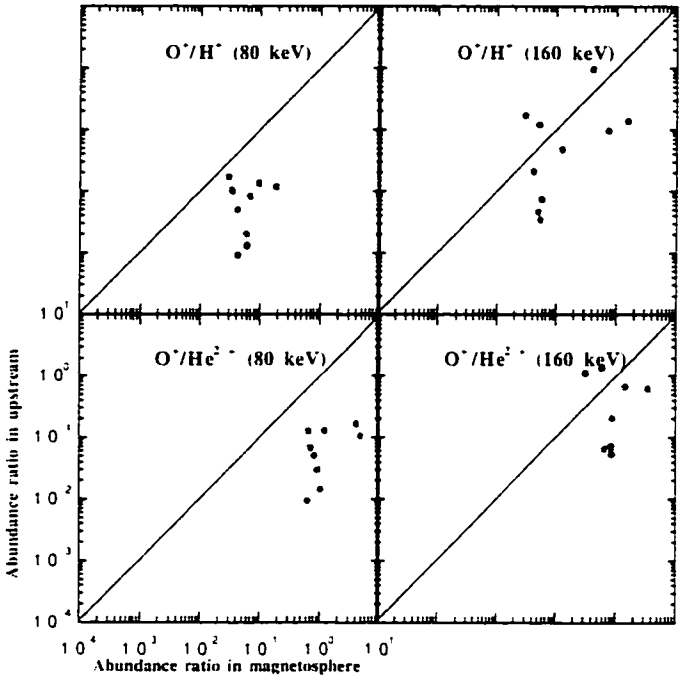

Fig. 6.6. The same as Fig. 6.5 for O^+/H^+ and O^+/He^{2+}.

Now, we study the abundance ratios of He^+/H^+ and O^+/He^+ according to the same scheme. The upper panel of Figure 6.7 shows the abundance ratios of He^+/H^+. The fact that most of the ratios fall into the lower regime, comparing with the Fig. 6.5, seems to indicate that the behavior of diffuse He^+ is different from that of H^+ and He^{2+} ions. The

lower panel of Figure 6.7 shows the abundance ratios of O^+/He^+. Most of these ratios fall into the lower regime as well. The similarity of the lower panels of Fig. 6.7 and Fig. 6.6 indicates that H^+ and He^{2+} as well as He^+ are all enhanced over O^+ in the upstream region, i.e., with respect to magnetospheric O^+ ions, energetic He^+ ions have the same trend as the H^+ and He^{2+} ions. If energetic He^+ ions were magnetospheric ions as O^+, the result of Fig. 6.7 would tell us that He^+ leak more easily into the upstream region than O^+. This seems to contradict the general idea of a rigidity dependent transport favoring high-regedity ion. In this picture O^+ should leak move easily into upstream region than the

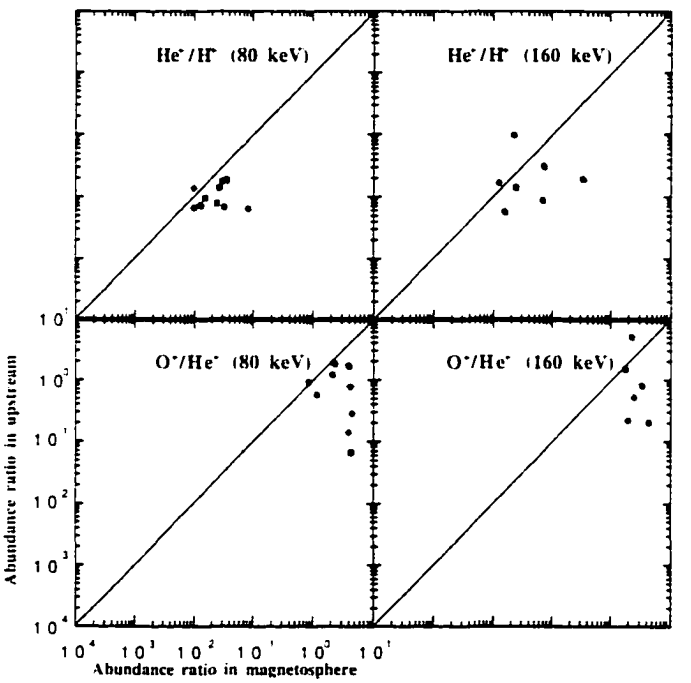

Fig. 6.7. The same as Fig. 6.5 for He^+/H^+ and O^+/He^+ .

other species due to its larger gyroradius.To test this idea, we need a more quantitative analysis.

We will apply a simplified model based on the diffusion-convection equation to this problem. Our purpose is to check two possible sources for energetic He^{+}: 1) leakage of energetic He^{+} ions in the magnetosphere and 2) acceleration of pickup ions at the bow shock. We cannot rule out the possibility of a mix of these two sources for energetic He^{+}, but we can at least hope to determine the relative importance between them. Therefore, we solve the same diffusion-convection equation with two different boundary conditions to look for an answer in two steps. The first step is to start from the assumption that all particles are magnetospheric ions traversing the magnetosheath and escaping into the upstream region. In addition to the diffusive transport, scattering of the ions by waves on either side of the shock leads also to energization by repeated shock crossings. We solve the diffusion-convection equation with a source in the magnetosphere and compare the results of the model with the observations. In this way we can quantitatively test the origin of He^{+} with the observation shown in Figure 6.7. Then, based on the conclusions in the first step, we will set up the diffusion-convection equation with injection at the bow shock thus treating the He^{+} pickup ions as the source of the energetic He^{+} ions, to see what percentage of the pickup ions encountering the shock can be fed into the shock acceleration process. Our hope is that application of this simple theoretical work will enable us to shed light on the origin of the energetic He^{+}.

6.2 Model

Diffusive theory takes into account the normal presence of magneto-hydrodynamic wave turbulence in a collisionless plasma. By scattering on these waves on either side of the shock, particles can be energized by repeatedly crossing the shock. Diffuse ions stream relative to the solar wind in the upstream direction and are therefore subject to the hydromagnetic streaming instability. This results in a growth of hydromagnetic waves which scatter the ions in pitch angle [K.J. Trattner, 1992]. The initial beam distribution is driven towards isotropy which reduces the wave growth rate. Particles which are scattered back towards the shock gain additional energy in the shock frame. They may again be reflected at the shock front or the magnetosheath so that the process can be repeated. Diffusive theory takes into account the acceleration of particles reflected at the shock and scattered back upstream by waves in the magnetosheath. Our models only consider the latter effect and can be applied to both magnetospheric leakage and acceleration, but with different boundary conditions. The statistical nature of the scattering allows some particles to reach very high energies by repeatedly crossing the shock before they are convected downstream.

6.2.1) Physical Basis of Diffusive Acceleration

In order to see how scattering in a fluid on either side of a parallel shock leads to acceleration, consider a particle of energy E in the downstream scattering frame close to the shock. In this frame, the shock front is moving at speed V_2 into the upstream direction. If the particle speed u and pitch angle ϑ are such that $u\cos\vartheta > V_2$, the particle will catch up with the shock and cross it. After scattering, which conserves energy in the upstream scattering wave frame, it exits back downstream at angle ϑ' to the shock normal (see Fig. 6.8). The total energy in the downstream frame after this cycle[Forman and Webb, 1985] is

$$E' = E\left[\frac{1+u\Delta V\cos\theta/c^2}{1+u'\Delta V\cos\theta'/c^2}\right] \tag{6.1}$$

where $\Delta V = V_1 - V_2$ is the change in velocity at the shock for the restframes of the scattering centers. Since the particle does return, $0<\vartheta<\pi/2$ and $\pi/2<\vartheta'<\pi$, E' is always greater than E. If the particle escapes again upstream by scattering in the downstream plasma, this cycle can be repeated and further energy gain can be realized. This is the essence of first-order Fermi acceleration: a monotonic energy gain, with varying increments. The acceleration occurs because the particle can scatter in two scattering regions which converge with a speed ΔV at the shock. The basic physics of "diffusive" acceleration at shocks rests on repeated shock crossings made possible by scatttering in the upstream and downstream regions where the energy is conserved on each side of the shock in the plasma frame. The energy gain is drawn from the velocity difference ΔV, and derived from a Lorentz transformation between frames.

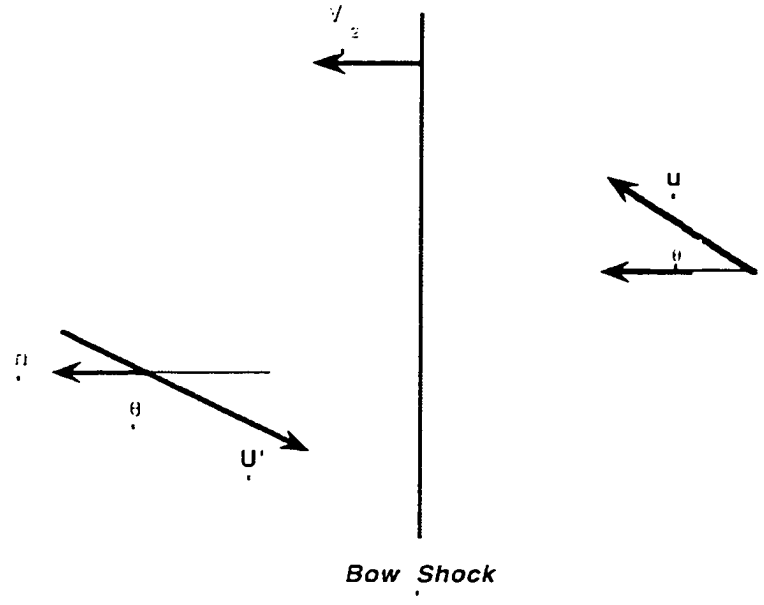

Fig. 6.8. Geometry showing the particle crossing a moving shock and scattering by the waves in either side of the bow shock.

6.2.2) Diffusive-Convective Transport Equation for Energetic Particles

Energetic particles, being a minor component in an already collisionless plasma can also be treated as collisionless. They move through the plasma on trajectories defined by the electric and magnetic fields. The fields, however, are usually composed of a mean field (averaged on some scale) plus a turbulent component on smaller scales due to hydromagnetic waves or other plasma waves in the plasma. The turbulent fields cause the

particle trajectories to deviate stochastically, i.e., to scatter randomly from the zeroth-order trajectories they would have in the mean fields alone. The waves do this by exerting on each particle random forces with zero average but nonzero correlation with the particle motion along the trajectory. Because of the helical turning of the particle velocity in the mean fields, the correlation of the random forces is proportional to the power spectrum of field fluctuations on the same scale as the helical zeroth-order orbit; that is, the power at wave number k such that $k|\mu|r_g = 1$, where μ is the cosine of the pitch angle and r_g the gyroradius in the mean field.

A starting point is the collisionless Boltzmann equation that describes, in principle, the evolution of the exact particle distribution function f $(\vec{r},\vec{p},t)$ in the exact electromagnetic field:

$$\frac{\partial f}{\partial t} + \vec{V}\cdot\frac{\partial f}{\partial \vec{x}} + Qe(\vec{V}\times\vec{B}/c + \vec{E})\cdot\frac{\partial f}{\partial \vec{p}} = 0 \qquad (6.2)$$

[Forman and Webb, 1985]. In the quasi-linear theory of weakly turbulent plasmas the electromagnetic fields are expressed as the sum of an averaged component and a perturbation. $\vec{B}$ and $\vec{E}$ consist of an average part plus a smaller fluctuating wave part whose average values are zero. The exact f can also be written as an average part f $(\vec{r},\vec{p},t)$ (also averaged over gyrophase) plus a smaller fluctuating part $f^{(1)}(\vec{r},\vec{p},t)$. When these linearized quantities are substituted into the Boltzmann equation, a plasma kinetic equation that describes diffusion in velocity space could be obtained:

$$\frac{\partial f}{\partial t} + \vec{V} \cdot \frac{\partial f}{\partial \vec{x}} + Qe(\vec{V} \times \vec{B}/c + \vec{E}) \cdot \frac{\partial f}{\partial \vec{p}} = \frac{\partial}{\partial \vec{p}} \cdot \vec{\vec{D}} \cdot \frac{\partial f}{\partial \vec{p}} \tag{6.3}$$

where $\vec{B}$ and $\vec{E}$ are now average fields, and $\vec{\vec{D}}$ is a diffusion tensor in momentum space that depends on the power spectrum of the field turbulence, as discussed by Kennel and Engelmann [1966], Hall and Sturrock [1967], Wu [1968], and Luhmann [1976]. This collisionlike term of the right hand side of eqn. (6.3) describes the effects of wave-particle interactions on f.

The diffusive or first-order Fermi acceleration mechanism has been described in considerable detail later by Krymsky [1977], Axford et al. [1977], Bell [1978], and Blandford and Ostriker [1978]. Its derivation is quite straightforward for a one-dimensional case. We picture the shock as an infinite, planar discontinuity in a flowing plasma. The plasma flows in from x = -∞ and out to x = ∞ with a discontinuous transition in flow speed from a supersonic upstream speed V_1, to a subsonic downstream speed V_2, at x = 0. Let us assume that the distribution function f $(\vec{x}, \vec{p})$ is omnidirectional distribution to first order in V/u, where V is the plasma flow velocity and u and p are the individual particle speed and momentum magnetude measured in the local plasma frame. Then for particles with u >>V the Boltzmann can be written in the form of a diffusion-convection equation [see Gleeson and Axford, 1967]

$$\frac{\partial f}{\partial t} + \vec{V} \cdot \frac{\partial f}{\partial x} - \frac{\partial}{\partial x} \kappa \frac{\partial f}{\partial x} - \frac{p}{3} \frac{dV}{dx} \frac{\partial f}{\partial p} = R\delta(x)\delta(p - p_0) \tag{6.4}$$

$\kappa = \kappa_{//}\cos^2\vartheta_{Bn} + \kappa_{\perp}\sin^2\vartheta_{Bn}$ is the diffusion coefficient in the direction normal to the shock, ϑ_{Bn} is the angle between the shock normal and the mean magnetic field, and $\kappa_{//}$ and $\kappa_{\perp}$ are the diffusion coefficients parallel and perpendicular to the magnetic field, respectively. Equation (6.4) holds for all ϑ_{Bn} and as long as scattering is strong enough to insure near isotropy and validate the assumptions of the diffusion-convection equation. The relation between κ and quasi-linear theory will be discussed in the following section. In order, the terms on the left-hand side of equation (6.4) represent time changes, convection, diffusion, and adiabatic deceleration. R is a source term, i.e., the rate with which particles are injected at the shock. We assume that particles are injected at some momentum p_0, i.e., $R\delta(x)\delta(p-p_0)$. The solution $f(p>p_0) \neq 0$ since $\nabla \cdot \vec{V} < 0$ at the shock.

6.2.3) Boundary Conditions for Diffusive Energetic Particle Transport

For simplicity, we assume in the model that the average magnetic field is parallel to the shock normal **n** and to the flow velocity; since all quantities depend only on x, perpendicular diffusion play no role. The nature of the solution is determined by the boundary conditions. We will consider two cases: a) leakage of ions from the magnetosphere as the only source injected into the system. Then the boundary condition at the magnetopause specifies the source in the magnetosphere, and no injection at the shock is considered. b) Local ion sources such as solar wind and interstellar pickup ions are injected at the shock and no leakage of ions from the magnetosphere participates in the

diffusion process. Then the boundary conditions exclude the source in the magnetosphere, and the injection rate at the shock is main factor in determining the solution of the equation. Of course, these two cases may also exist simultaneously. However, since the equation is linear in f, the ion distribution is given as a linear superposition of the two basic cases.

The boundary conditions at the shock are obtained by integrating the transport equation across the shock. The usual diffusive interface boundary condition applies as follows (Figure 6.9 shows the simple structure for the model): The particle number density in phase space is continuous, i.e., the ion distribution function in the region upstream is equal to that of in the region downstream of the shock: $f_1(-\varepsilon) = f_2(+\varepsilon)$. The normal component of the particle flux is continuous, if there is no surface source. It may change by an amount equal to the particle injection rate of a surface source, i.e., the difference between the downstream and upstream normal flux density equals the particle injection rate R. This condition reads

$$\left[(\kappa_1 - \kappa_2)\frac{\partial f}{\partial x} + \frac{p}{3}(V_1 - V_2)\frac{\partial f}{\partial p} = R\delta(p - p_0)\right]_{x=0} \tag{6.5}$$

The subscripts 1 and 2 refer to the region upstream and downstream of the shock, respectively [Scholer, 1985].

Axford et al.[1977] and Blandford and Ostriker[1978] have shown that for a wide range of

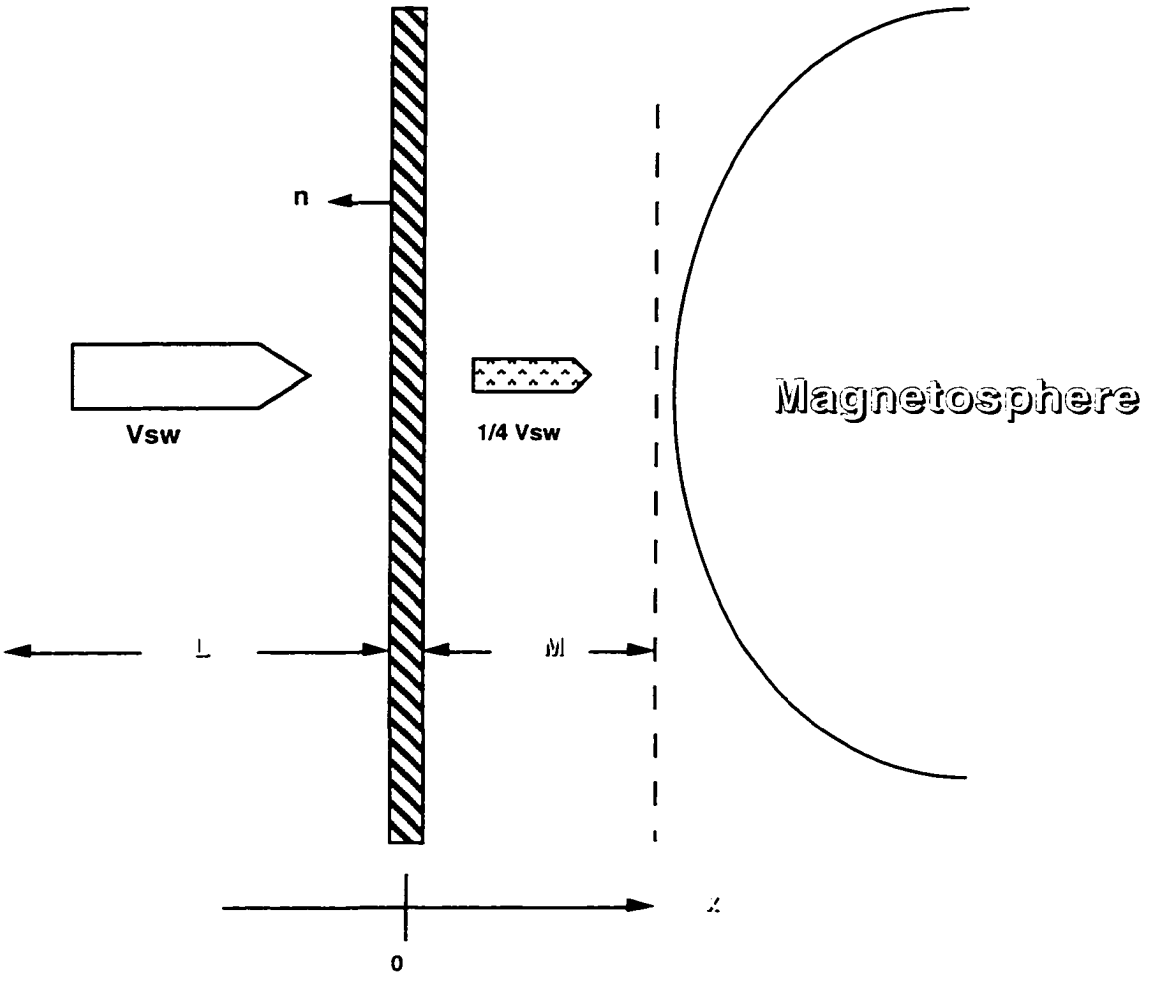

Fig. 6.9. Schematic representation of the configuration assumed in of the diffusive model.

background populations the accelerated particle distribution has a power law spectrum in momentum for an infinite planar shock. Such a power law spectrum is clearly not observed for the upstream particles [Ipavich et al., 1979]. The spectrum steepens toward higher energies and falls off rapidly above 200 keV. In order to explain such a steepening of the spectrum, Terasawa [1979] assumed that the accelerated particles have not reached the steady state and that the diffusion coefficient depends strongly on energy, $\kappa \propto E^{3}$ above 50 keV. Such a strong dependence on energy is inconsistent with observations.

Measurements indicate an approximately linear dependence of κ on E. ISEE 3 measurements [Scholer et al., 1980b] have shown that at 200 R_E upstream of Earth's bow shock, particles move essentially scatter free, indicating that particle scattering in the upstream wave field is limited to some region close to the shock. It is also observed that the upstream magnetic turbulence needed to scatter accelerated ions back to the shock decays with increasing distance from the shock. Michell et al. [1983] found within a distance of ~ 10 R_e from the bow shock distribution which, when transformed into the solar wind frame, are enhanced near 90^0 pitch angle and have equal fluxes Sunward and Earthward. At some point upstream, the level of turbulence may be low enough that ions will stream freely away from the shock. We will simulate the lack of sufficient scattering farther upstream by placing a free escape boundary(FEB) at a certain distance in front of the shock. The FEB is assumed to be at the same physical distance L for all ions, and ions that cross the FEB can freely stream away [Ellison et.al., 1987]. We approximate this behavior by a boundary condition that reads $f_1(-L) = 0$. This corresponds to a FEB which is equivalent to a perfectly absorbing wall.

Finally, a boundary condition has to be set for the magnetopause $f_2(M)$, where M is the width of the magnetosheath. For leakage from the magnetosphere, the distribution function at the magnetopause $f_2(M)$ will be determined by the distribution in the magnetosphere g(p). The boundary condition reads $f_2(+M) = g(p)$. L = 10 R_e, M = 4 R_e are used for all energies in the model.

6.2.4) Diffusion Coefficient

The value and the variation of the diffusion coefficient with particle species and energy is important for the determination of the solution. Diffusion coefficients have been described in the framework of a quasi-linear description that relates magnetic field fluctuations and particle scattering. Following of Drury [1983], Völk [1984], Forman and Webb [1985], and Blandford and Eichler [1987], particles are assumed to undergo many small angle perturbations in pitch angle by interacting with magnetic fluctuations, such as Alfvén waves and magnetoacoustic waves. If a particle traveling faster than the Alfvén velocity has a gyroradius, r_g = pc/(QeB) (B is the mean background magnetic field), comparable to the wavelength of the Alfvén wave or magnetic disturbance, it can interact resonantly, and its pitch angle can be changed most effectively. After a number of interactions with random phases, the particle may be turned around. A mean free path can be defined. For small wave amplitudes (i.e., $\delta B/B << 1$), the diffusion coefficient can be determined using a quasi-linear approximation. If the Alfvén waves can be characterized by a background turbulence spectrum with a power law $P = P_0 f^{-n}$ [Ellison, 1990], the spatial diffusion coefficient parallel to the magnetic field can be written as $\kappa_0 u^{3-n} (A/Q)^{2-n}$ [Scholer et al., 1976]. This is equivalent to $(E/Q)^{(3-n)/2} (A/Q)^{(1-n)/2}$. u is the particle speed, E the particle energy, Q the charge number, and A the atomic number. Now, the

proportionality constant κ_0 according to $\kappa_{//} = \kappa_0 (A/Q)^{(1-n)/2} (E/Q)^{(3-n)/2}$ remains to be determined.

The evaluation of κ_0 can be obtained from an analysis based on the data. According to the statistical analysis for diffuse energetic ions by Trattner and Adroler.[1994], the intensity of diffuse ions falls off approximately exponentially with distance upstream from the bow shock parallel to the magnetic field with e-folding distance which varies from 3.2±0.1 R_E at 10 keV to 9.3±0.1 R_E at 67.3 keV. The best correlation of the linear regression analysis was found for the diffuse ions at an energy of 11.9 keV. The e-folding distance for both species, protons and alpha particles, are almost the same at the same energy/charge and clearly increase with energy. This supports the fact that the diffusion coefficient of the ions in the upstream region is a function of particle energy per charge and that the more energetic particles can escape more easily into the upstream direction. This increase of the e-folding distance with energy generally leads to a harder spectrum further away from the bow shock compared to spectra immediately at the shock in agreement with previous observations by Scholer et al.[1981]. So we describe the spatial dependence of the omnidirectional distribution function f along the magnetic field by $f \sim f_0 \exp(-LV/\kappa_0)$ and choose the e-folding distance $l = 3.2\ R_E$ for a proton with $E_s = 10$ keV as our baseline, i.e.,

$$\kappa_0 = \kappa_p \approx l\, u\ (E_s = 10\ \text{keV}) \approx 2.85\times10^{17}\ \text{cm}^2/\text{s}$$

in the region upstream of the shock. To determine the spatial diffusion coefficient for all species at different energies we use

$$\kappa\,(E/Q,A/Q) = \kappa_p\,(A/Q)^{(1-n)/2}\,(E/E_S)^{(3-n)/2} \qquad (6.6)$$

For simplicity κ is assumed to be independent of the distance from the bow shock. Without knowledge of the diffusion coefficient in the magnetosheath we assume $\kappa_2 = 0.1\ \kappa_1$, because the field compression, the ratio of downstream to upstream magnetic field perturbation, is about 3, and is of the same order as the density compression ratio [Hada, 1985]. So the differential wave intensity in the downstream region is about 9 times that in the upstream region. Since the diffusion coefficient is inversely proportional to the wave intensity, our assumption is reasonable.

This leads us to the question which value to adopt for the spectral index of the wave spectrum n. To get a handle on the power spectrum of the fluctuations, the actual hydromagnetic wave intensities were determined from the full resolution magnetic field data (time resolution $\Delta t = 1/32$ s) during the upstream events under investigation. The wave power spectrum was derived by applying a fast Fourier transformation to the magnetic field data. Figure 6.10 shows a typical wave spectrum upstream of the shock, separated into compressive (X) and transverse components(Y, Z).

The power of the transverse components generally exceeds the power of the compressive

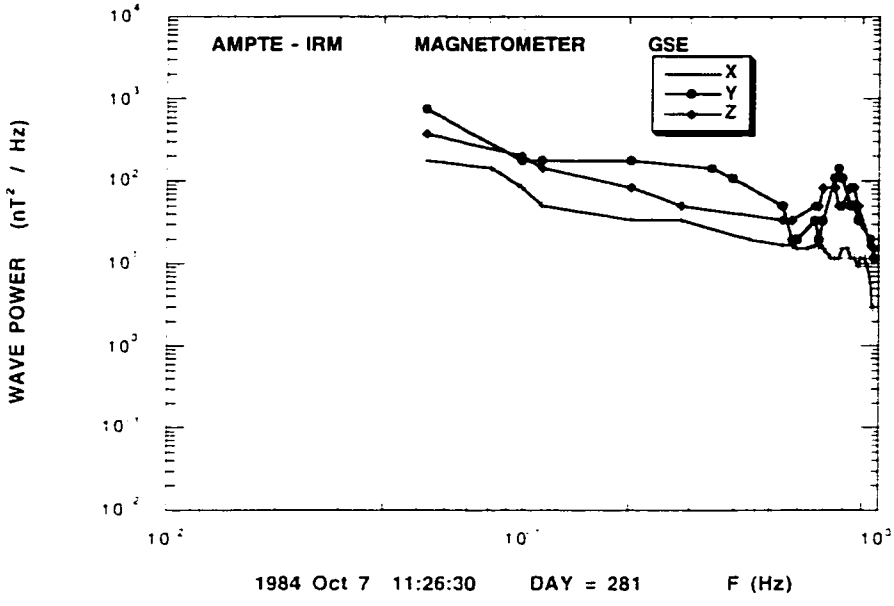

Fig. 6.10. Wave power (nT^2/Hz) versus frequency (hertz) separated into transversal and compressive parts. The spectrum was calculated for the October 7 event averaged from 1126 - 1136.

component, i.e., the fluctuations basically represent transverse Alfvén waves. The peak of the power spectrum is at about 0.77 Hz. The spectrum falls according to f^{11} between 0.77 HZ and 1.0 HZ so that n = 11 gives the inverse proportional dependence of κ on A/Q, which is inconsistent with our observations. The spectrum rises according to $f^{-9.6}$ between 0.57 Hz and 0.77 Hz. At frequencies below 0.57 Hz the spectrum falls roughly with $f^{-0.5}$. The peak reflects the resonant range of the waves that interact with protons at 20 - 30 keV, i.e., the maximum flux in the H^+ spectrum. For the ions under study heavier than protons, the resonant frequency should be much lower than 0.77 Hz. For example,

the resonant frequency of He^{2+} is 0.4 Hz, 0.2 Hz for He^{+} and 0.08 Hz for O^{+} at the same E/Q. Therefore we choose n = 0.5. Accordingly, the spatial diffusion coefficient for all species is described as

$$\kappa\,(E/Q,A/Q) = \kappa_p\,(A/Q)^{1/4}\,(E/E_S)^{5/4}. \qquad (6.7)$$

This implies that the diffusion coefficient increases with A/Q for a given energy per charge. We make the assumption that this form remains valid on both sides of the shock.

In the following we will discuss the influence of different ion sources, as well as the transport and acceleration of these ions separately in models which treat one source at a time.

6.3) Comparison of the Models with the Observations

6.3.1) *MODEL 1: Diffusive transport and acceleration with source in the magnetosphere*

Let us start our discussion by assuming that the only ion source is leakage of energetic ions (H^{+}, He^{2+}, He^{+}, O^{+}) from the magnetosphere, and that there is no local injection at the shock. Under this assumption, the boundary condition for the diffusive-transport equation can be written as follows: The ion distribution function at the magnetopause is equivalent to the source function g(p) in the magnetosphere so $f_2(M,p) = g(p)$. The continuity of f(x,p) at the bow shock (x = 0) reads $f_1(-\varepsilon,p) = f_2(+\varepsilon,p)$, and the continuity of the normal component of the ion flux at x= 0 without injection at the shock is

$$\left[(\kappa_1-\kappa_2)\frac{\partial f}{\partial x}+\frac{p}{3}(V_1-V_2)\frac{\partial f}{\partial p}=0\right]_{x=0} \qquad (6.8)$$

Finally, the ion distribution function in the upstream region vanishes at the FEB so that $f_1(-L,p) = 0$. The diffusive-transport equation is everywhere given:

$$V\frac{\partial f}{\partial x}-\frac{\partial}{\partial x}\kappa\frac{\partial f}{\partial x}-\frac{p}{3}\frac{dV}{dx}\frac{\partial f}{\partial p}=0 \tag{6.9}$$

We expect to answer the following question: How does the diffusive transport change the ion composition between the source and the upstream region? For simplicity, we further assume that the intensity of ion distribution function across the magnetopause is the same for all species.

Solution

We start by solving the transport equation separately on either side of the shock:

$$V_i\frac{\partial f_i}{\partial x}-\frac{\partial}{\partial x}\kappa_i\frac{\partial f_i}{\partial x}=0 \tag{6.10}$$

where i = (1, 2) refers to upstream and downstream. κ_i is the coefficient for diffusion parallel to the shock normal. Using the four boundary conditions, the general solution for the ion distribution function are (in the following we use E instead of p as our key variable, i.e., g(p) => G(E/Q), f(x,p) => F(x,E/Q)):

$$\begin{aligned}F_1(x,E/Q)&=\frac{\beta_1(x,E/Q)[G(E/Q)-Y(E/Q)]}{\alpha_1(E/Q)}\\ F_2(x,E/Q)&=G(E/Q)-\frac{\beta_2(x,E/Q)Y(E/Q)}{\alpha_2(E/Q))}\end{aligned} \tag{6.11}$$

where

$$\alpha_1(E/Q) = 1 - \exp\left(\frac{V_1 L}{\kappa_1(E/Q)}\right)$$

$$\alpha_2(E/Q) = \exp\left(\frac{V_2 M}{\kappa_2(E/Q)}\right) - 1$$

$$\beta_1(x, E/Q) = \exp\left(\frac{V_1 x}{\kappa_1(E/Q)}\right) - \exp\left(\frac{V_1 L}{\kappa_1(E/Q)}\right)$$

$$\beta_2(x, E/Q) = \exp\left(\frac{V_2 M}{\kappa_2(E/Q)}\right) - \exp\left(\frac{V_2 x}{\kappa_2(E/Q)}\right)$$

$$Y(E/Q) = A(E/Q)\left(\frac{E}{E_0}\right)^{3/4 \exp\left[-c\left(E/E_0\right)^{1/4}\right.}$$

and

$$A(E/Q) = \int_{E_0}^{E} \exp(cz^{\frac{5}{4}}) z^{\frac{3}{4}} \left[\frac{dG(z)}{dz} + \frac{2G(z)}{z\alpha_1(z)}\right]$$

Where c is the integration constant. We start with the simplifying assumption that all abundance ratios are 1, i.e., the distribution function G(E/Q) is the same at the same energy for all species before the ions leak from the magnetopause. Figure 6.11 shows the variation of the distribution functions of H^+, He^{2+}, He^+ and O^+ with distance from the magnetopause at 80 keV/Q. The horizontal axis represents the distance from the bow shock (x = 0) with the upstream region $x < 0$, and the magnetosheath $M > x > 0$. It is clear that the distribution function of O^+ decreases much slower with distance from the magnetopause than those of the other species. The sequence follows the mass/charge of the species. This implies that the abundance of energetic O^+ should always be larger in the

upstream region in comparison with its level in the magnetosphere if all species stem solely leakage from the magnetosphere. It indicates that the O^+ /He^+, and O^+/He^{2+} abundance ratios should always be higher in the upstream region than in the magnetosheath or magnetosphere. These results are obviously in contradiction with the observations shown in Fig. 6.6.

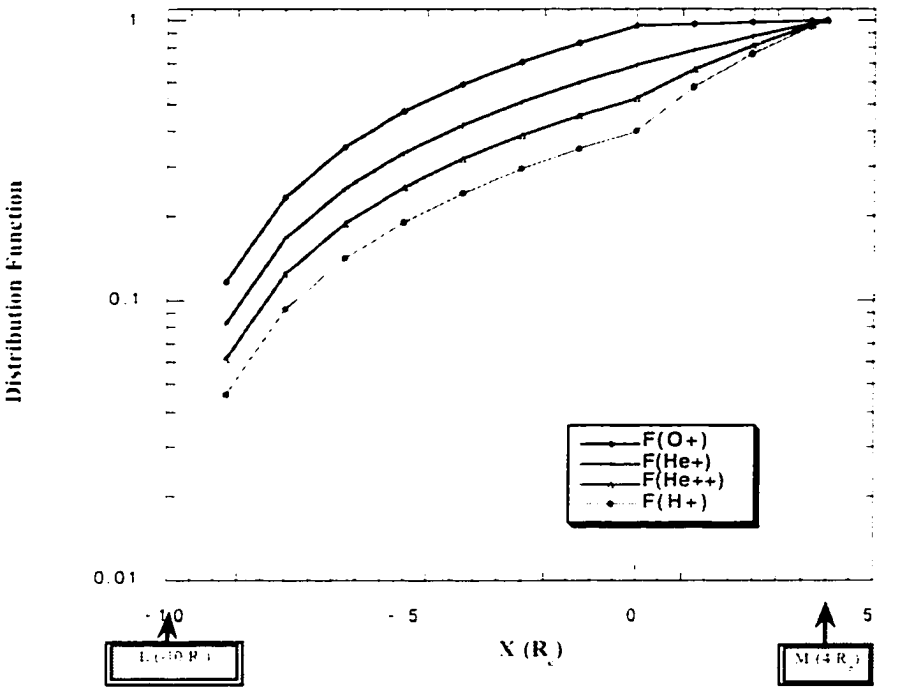

Fig. 6.11. Variation of the distribution functions resulting from model 1 with distance from the magnetopause at 80 keV/Q for H^+, He^{2+}, He^+ and O^+.

In order to substantiate our results we have carried out a detailed comparison of our model with the data for all four species. The steps of this comparison can be followed in Fig. 6.12. The solid triangle in the left panel of Fig. 6.12 indicates the final result of the model in the upstream region, after all free parameters were adjusted to best fit the data (solid circle). First we obtain a smooth spectrum for the apparent source function in the magnetosphere by assuming an exponential law and fitting the observed spectrum in the magnetosphere. We use this function as source function for our calculation to obtain the distribution f_I (x,p) in the upstream region. Then we compare the result with the data in the upstream region for the energy range 10 to 160 keV. For convenience 80 keV was

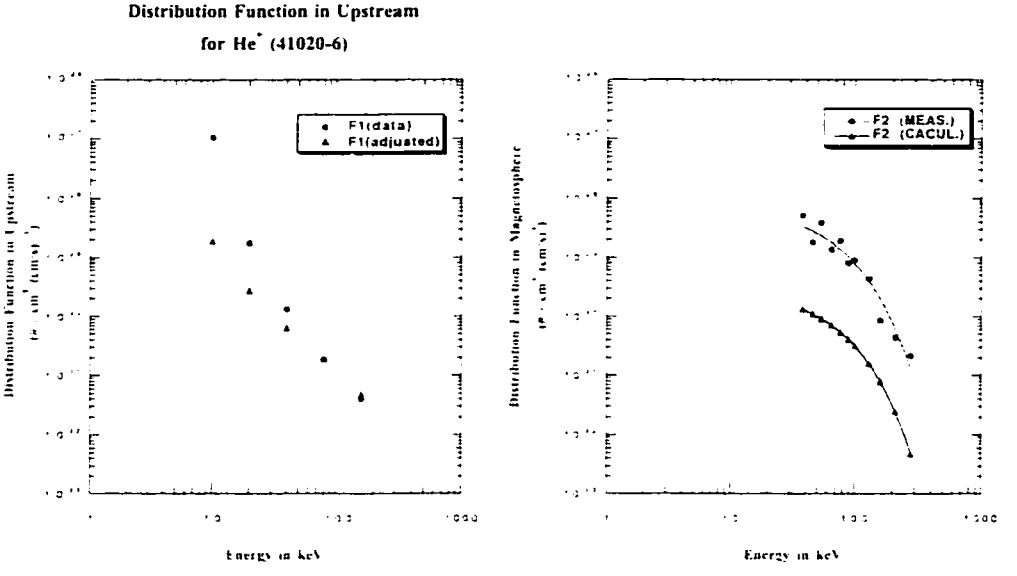

Fig. 6.12. Schematic representation of the steps to compare the measured data with the predictions of model 1. In the right panel the dot points represent the measurements while the triangle points indicate the adjusted calculations of the model.

chosen as the matching point for all species. In order to fit the data the absolute flux found in the model has to be reduced by a substantial factor.

A reasonable candidate for this reduction is a leakage efficiency ε out of the magnetosphere. We therefore use $G(E) * \varepsilon$ with $0 < \varepsilon < 1$ as the source function of the energetic ions at the magnetopause. The reduced source function is shown in the right panel of Fig. 6.12. A possible explanation for such a reduction would be that there is a strong coupling between the fluctuating magnetic field which has some net motion in the direction of the convecting magnetosheath plasma and the particles in the magnetosphere so that only a few magnetospheric particles will be able to leak out of the magnetopause [Luhmann et al., 1984].

It is interesting to compare the values of ε for different species under the assumption of pure magnetosphere leakage. These results are shown in the top panel of figure 6.13. The first impression is that, generally, ε is the lowest for O^+. There is one event lacking the data of O^+ at 80 keV in the original measurements by IRM. This impression is reemphasized in the bottom panel of Fig. 6.13 which contains the ratios of the leakage efficiencies. The $\varepsilon(O^+) / \varepsilon(H^+)$, $\varepsilon(O^+) / \varepsilon(He^{2+})$ and $\varepsilon(O^+) / \varepsilon(He^+)$ ratios are all lower than 1 with only two exceptions. If we were to interpret our results in terms of rigidity dependent transport out of the magnetosphere, it seems as if ions with higher rigidity are at a disadvantage to cross the magnetopause into the magnetosheath compared to other

species. The impression is that lower rigidity leads to more efficient leakage. However, this contradicts the general result that transport is enhanced for high rigidity particles.

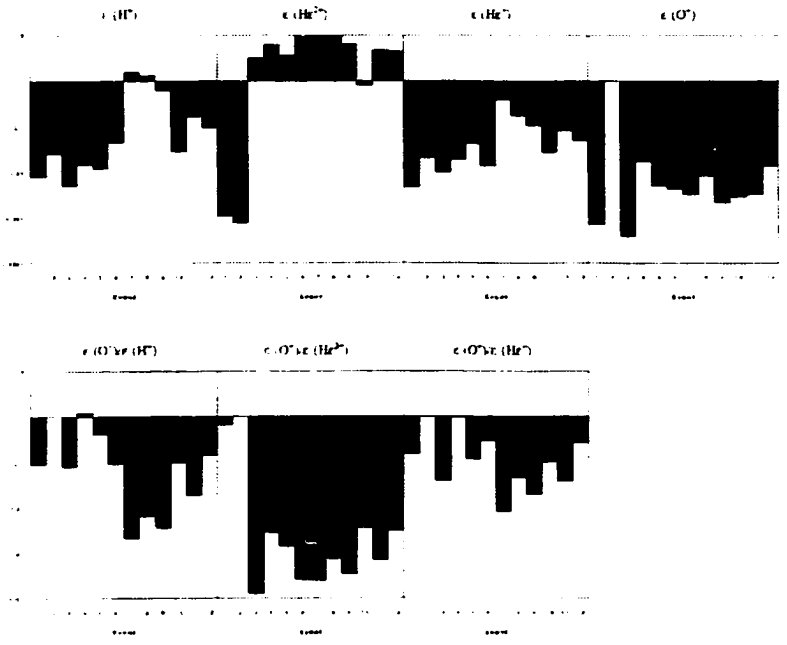

Fig. 6.13 (upper) Comparisons of leakage efficiency ε for H^+, He^{2+}, He^+ and O^+; (lower) Comparisons of the ratios of leakage efficiency for H^+, He^{2+} and He^+ to O^+, respectively.

It is still safe to assume that O^+ comes from the magnetosphere, since it is by far the strongest known source of O^+. In general terms, O^+, with higher rigidity, has a larger gyroradius, which makes it easier to leak out of the magnetosphere than for other species Therefore, the results as presented above should not be expected. However, as mentioned in chapter 2, H^+ and He^{2+} have already been identified as bow shock accelerated. From our analysis He^+ behaves similar to H^+ and He^{2+}, but different from O^+. Therefore, these results indicate that bow shock acceleration for He^+ is a plausible explanation. In addition,

He^+ pickup ions in the solar wind are an important source at the shock. Thus we have to turn our attention to this alternative source.

Based upon the conclusion from model 1, we now treat the He pickup ions as the source of energetic He^+ ions. We will use the following model to confirm the shock origin and to see what percentage of the pickup ions that encounter the shock can participate in the shock acceleration process.

6.3.2) MODEL 2: Diffusive transport and acceleration with a source at the bow shock

As mentioned before, since the downstream fluid is moving away from the shock subsonically, some hot ions are able to scatter back into the upstream region and are accelerated still further. In this way, a few particles will be "injected" into the diffusive shock acceleration process. By crossing the shock many times, they will be accelerated to high energy. The majority of the ions, however, enter the downstream region without gaining significant additional energy and are swept downstream to x=M. The result is a continuous particle distribution from thermal to the highest energies. It is important to note that this injection-acceleration process is a direct result of the assumption that all ions scatter elastically in the local plasma frame.

With local injection at the shock, from the solar wind for H^+ and He^{2+}, and from pickup ions for He^+, the stationary 1-D diffusive-transport equation is:

$$V\frac{\partial f}{\partial x}-\frac{\partial}{\partial x}\kappa\frac{\partial f}{\partial x}-\frac{p}{3}\frac{dV}{dx}\frac{\partial f}{\partial p}=R_s\delta(x)\delta(p-p_0) \tag{6.12}$$

with the boundary conditions as follows, We assume again the FEB as a perfectly absorting wall, so that the ion distribution function satisfies $f_1(-L,p) = 0$. No ions escape from the magnetosphere into the upstream region, i.e., $f_2(M,p) = 0$. The ion distribution function is continuous at the shock, $f_1(-\varepsilon,p) = f_2(+\varepsilon,p)$. The normal component of the particle flux changes by an amount equal to the particle injection rate at the shock surface, i.e., the difference between the downstream and upstream flux density normal to the shock equals the particle injection rate R. This condition is

$$\left[(\kappa_1-\kappa_2)\frac{\partial f}{\partial x}+\frac{p}{3}(V_1-V_2)\frac{\partial f}{\partial p}=R_s\delta(p-p_0)\right]_{x=0} \tag{6.13}$$

The differences between model 1 and model 2 are that there is no source in the magnetosphere ($g(p) = 0$) in model 2, while there is an injection R at the shock.

The method of solution is similar to model 1. In order to get insight into R_s, we note that the integration

$$\int 4\pi p^2 dpdx\frac{\partial f}{\partial t}\propto\frac{\#}{cm^2 s}$$

is an energy flux density, which can be set up for the unit of density times the solar wind velocity, while

$$\int 4\pi p^2 dp dx R_s \delta(x)\delta(p-p_0) = 4\pi p_0^2 R_s, \tag{6.14}$$

so that R_s represents the number of ions of species s injected per unit area per unit time per unit momentum area at the shock front with momentum p_0. Ions are, of course, "injected" with a range of energies; since the diffuse ion spectra at higher energies are not dependent on p_0 except for overall normalization according to the study of Lee [1982], the assumption of a monoenergetic injection can be made with impunity. We define the injection energy to point where we start to count the accelerated distribution. The analysis by Ellison et al. [1990] shows that the quasi-parallel bow shock can directly accelerate thermal ions. Since we are only interested in the overall acceleration efficiency, we can safely assume this be the incident solar wind energy, which is ~1 keV/Q for H^+ and ~2 keV/Q for He^{2+} [Ellison et al., 1987]. For He^+, although the pickup ions can in principle be injected into acceleration over the entire energy range from 0 to the cut-off energy, we define an "average" injection energy as at the solar wind energy. Let R_s be equivalent to $\zeta n V_1/4\ \pi p_0^2$, where ζ represents the injection efficiency with respect to the flux density of incident particles, n the density of the ions, p_0 the threshold momentum for injection, and V_1 the solar wind velocity in the upstream region.

Solution

The general solutions are

$$F_1(x,E) = \frac{\beta_1(x,E)Y(E)}{\alpha_1(E)}$$

$$F_2(x,E) = -\frac{\beta_2(x,E)Y(E)}{\alpha_2(E)} \qquad (6.15)$$

$$Y(E) = -\varsigma\frac{nm^3}{\pi p_0^3}\exp\left(-\int_{E_0}^{E}\left(\left(\frac{4}{\alpha_1(E)}+\frac{1}{\alpha_2(E)}\right)\frac{dE}{2E}\right)\right)$$

E_0 is the threshold energy responding to the threshold momentum p_0.

Now an estimate of the injection efficiency ζ can be obtained as follows. At the threshold energy E_0, the distribution function in the upstream region is

$$F_1(E_0) = \varsigma\frac{\beta_1(x,E_0)}{\alpha_1(E_0)}\frac{n}{\pi(2E_0/m)^{3/2}}.$$

Since the differential flux density $j(E_0) = 2E_0F_1(E_0)/m^2$ is known from the data, ζ is determined as

$$\varsigma = \pi\frac{\alpha_1(E_0)}{\beta_1(x,E_0)}\frac{j(E_0)}{n}\sqrt{2mE_0}\ . \qquad (6.16)$$

Finally we need to determine $j(E_0)$, the flux of the thermal plasma at E_0. The upstream proton spectra, generally, consist of two parts: a narrow distribution peaking at about 1.0 keV and a second higher energy component between ~10 and 200 keV. The lower-energy component is the unshocked solar wind while the high-energy component is identified as "diffuse ions" [Ellison et al., 1990]. Therefore, the incident thermal flux at 1 keV should be derived from the high-energy component. We obtain a smooth spectrum for the measurement by applying an exponential law, then calculate the flux at 1 keV according to the exponential equation. The same procedures are also used for He^{2+} and He^{+} pickup ions.

The number density n of He^{2+} is roughly estimated as 4% of that of H^{+}; the pickup ion number densities for He^{+} were calculated by integrating the differential number spectrum

over the energy range from zero to the cutoff energy (=1/2 m $(2V_{sw})^2$) in the data as follows, since

$$n = \int f v^2 dv d\Omega = \int f \sqrt{\frac{2E}{m}} \frac{dE}{m} d\Omega = 4\pi \int f \sqrt{\frac{2E}{m^3}} dE \tag{6.17}$$

with

$$\frac{\Delta j_N}{\Delta E \Delta \Omega} = f \frac{2E}{m^2} \tag{6.18}$$

This leads to

$$\frac{\Delta n}{\Delta E} = 4\pi \sqrt{\frac{m}{2E}} \left(\frac{\Delta j_N}{\Delta E \Delta \Omega} \right)_{pickup} \tag{6.19}$$

$$n_{pickup} = \int_0^{E_{cut-off}} \frac{\Delta n}{\Delta E} \Delta E . \tag{6.20}$$

Figure 6.14 shows the efficiencies for the different species. The injection efficiency of He^+ is significantly higher than that of H^+ and He^{2+}. Roughly, the average injection efficiency is about 1.3% for H^+, 0.5% for He^{2+} and 12% for He^+. This result, that the injection efficiency of He^+ is higher than that of He^{2+} is not unexpected, since the pickup ions start already with higher energies, although the differential flux densities of diffusive He^{2+} are higher than these of He^+ (see Fig. 6.3). In order to get more insight into the result, we define an overabundance factor and an energy gain factor for further comparison of the relative energization of He^{2+} and He^+. To be consistent, we choose the cut-off energy of He^+ as the threshold energy for our comparison, neglecting the ion distribution at the energy below the cut-off energy for H^+ and He^{2+} .

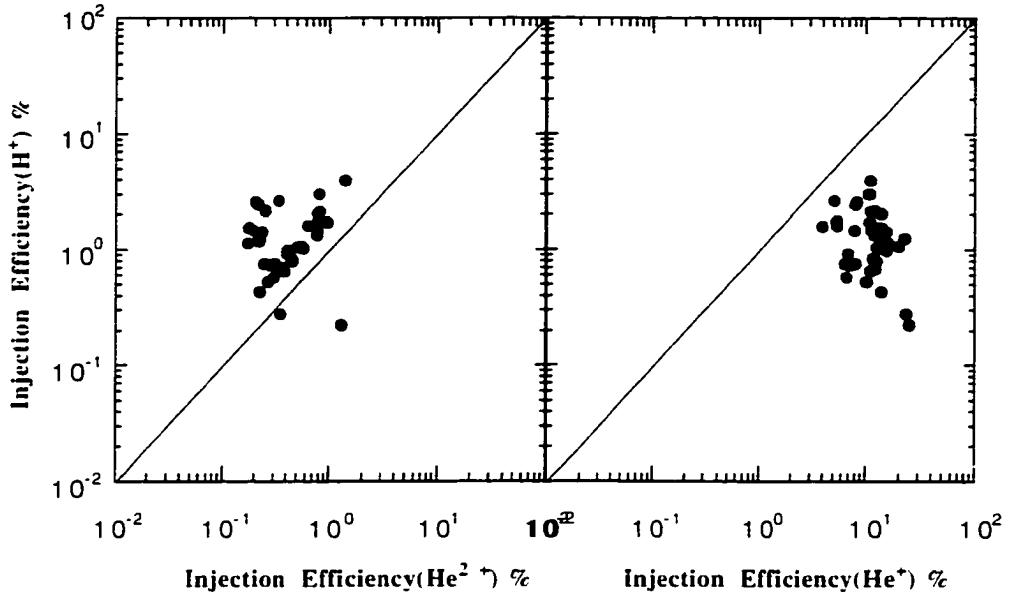

Fig. 6.14. Comparisons of injection efficiency between H^+, He^{2+} and He^+.

We define an abundance factor α for energetic ions

$$\alpha_{energetic} = \frac{\int_{E}^{\infty} j(E)dE}{\int_{E}^{\infty} j_H(E)dE} \tag{6.21}$$

where E_0 is taken as E_{cutoff}. It is the abundance of energetic ions. The average results are

$$\alpha_{energetic}(He^{2+}) \approx 9.0*10^{-2}$$

$$\alpha_{energetic}(He^{+}) \approx 4.0*10^{-3}$$

The average $\alpha_{pickup}(He^{+})$ which is calculated as follows:

$$\frac{\int_{0}^{E_{cutoff}} j_{pickup}(E)dE}{N_{SW} V_{SW}}. \qquad (6.22)$$

with the result

$$\alpha_{energetic}(He^{2+}) \approx 7.0*10^{-5}$$

Then we define an "overabundance" as the ratio of the abundance of energetic ions to the abundance of the ions in the solar wind. Since the ratio He^{2+}/H^{+} in the solar wind is about 0.04, therefore we get

$$\text{overabundance}(He^{2+}) = \alpha_{energetic}(He^{2+})/0.04 = 2.25$$

$$\text{overabundance}(He^{+}) = \alpha_{energetic}(He^{+})/\alpha_{picku}(He^{+}) = 57,$$

which means

$$\text{overabundance}(He^{+}) = 25 \times \text{overabundance}(He^{2+}).$$

Secondly, from the viewpoint of energy gain, we define an energy gain factor χ

$$\chi = \frac{\int_{E_{min}}^{\infty} Ej(E)dE}{\int_{0}^{E_{max}} Ej_{source}(E)dE}, \qquad (6.23)$$

where, $E_0 = E_{cutoff}$ for all species, to describe the capability of energy gain of each ion species. $\int_0^{E_{max}} Ej_{source}(E)dE$ is estimated for H^+ as $N_{sw}V_{sw}E_0$ (E_0 =1 keV/Q), for He^{2+} , $0.04N_{sw}V_{sw}E_0$ (E_0 =2 keV/Q). Figure 6.15 compares the energy gain factors for those ions.

It is clear that the energy gain factor for He^+ is higher roughly by a factor 16 compared with that of He^{2+}. This is consistent with the result of an enhanced overabundance factor of He^+. They are obviously reasonably consistent with the expectation that the injection efficiency of He^+ is higher than that of He^{2+}.

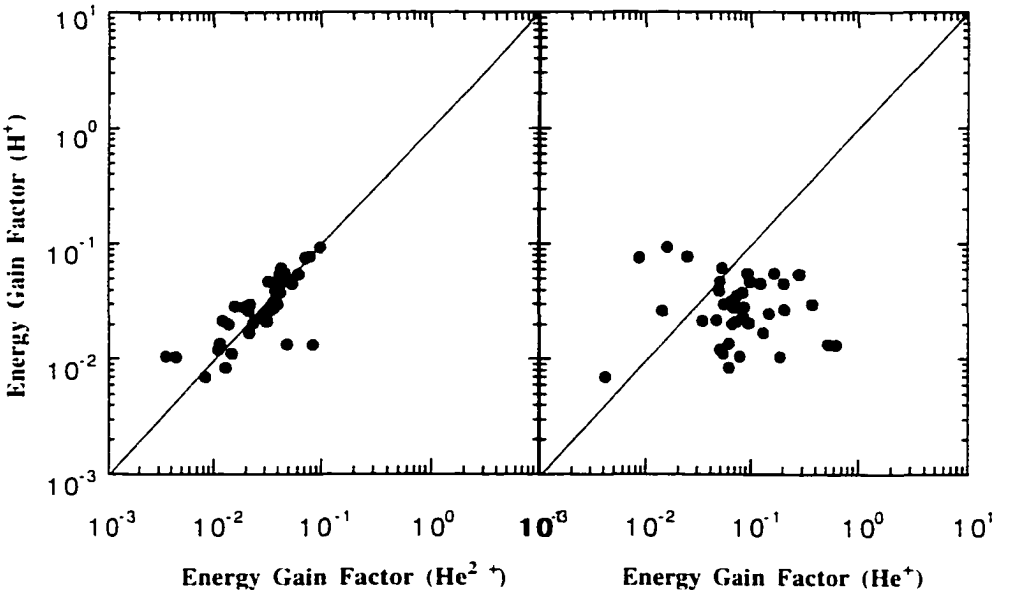

Fig 6.15. Comparisons of energy gain factors between H^+, He^{2+} and He^+.

6.4 Conclusions

In this chapter, the question about the origin of energetic He^+ ions observed at the quasi-parallel Earth's bow shock has been addressed. A statistical analysis of 38 upstream events with 10 of the 38 events also having simultaneous observations in the magnetosphere provides qualitative evidence that the pickup ion distribution is a more important source for the diffuse He^+ ions than the leakage from the magnetosphere. Based on the diffusion-convection equation, two models have been constructed with different boundary conditions. In the first model, we have compared the ratios of the leakage efficiencies from the magnetosphere for the different species and found that leakage efficiency for O^+ is the lowest in comparison with the other species. This is inconsistent with our general idea of a rigidity dependent transport. Combined with the known fact that H^+ and He^{2+} are bow shock accelerated, while O^+ comes from the magnetosphere, the results of model 1 confirm quantitatively that bow shock acceleration of He^+ ions is a more pausible explanation for their origin than the leakage of magnetospheric He^+ ions.

Model 2 treats the pickup He^+ ions as the source of energetic He^+ ions. The statistical result that the injection efficiency of He^+ is higher by a factor of 24 compared with that of He^{2+} is reasonable because the pickup ions start already with higher energy than that of He^{2+} in the solar wind. The calculations of overabundance and energy gain factor confirm the efficiency of He^+ acceleration.

CHAPTER 7

CONCLUSIONS

In this thesis we have presented the first detailed study of the sources and the acceleration of energetic He^+ ions in front of the Earth's bow shock, using data from AMPTE/IRM and AMPTE/CCE. Using numerical simulations of specular reflection at the quasi-perpendicular shock and diffusive shock acceleration at the quasi-parallel shock, we have shown that of He^+ pickup ions are the dominant source in both cases.

Based on observations of energetic He^+ ions during an event when the bow shock was an almost perfect perpendicular shock, we could identify specular reflection at the shock potential and magnetic reflection as contributing to the energization process. A high percentage (A+B %) of the original pickup ions get "specularly reflected" by these processes. Numerical simulations based on particle trajectory calculations are in basic agreement with the observed spectra and directional distributions and support the idea that multiple reflections with acceleration along the shock, the so called "surfing" of ions as pointed out by Lee et al.[1996], is indeed important.

At the quasi-parallel shock we first investigated whether the dominant source of energetic upstream He^+ ions is leakage of ions from the magnetosphere or acceleration of pickup ions at the bow shock. By calculating the omnidirectional distributions of H^+, He^{2+}, He^+ and O^+ ions upstream of the shock, as well as a comparison of the observed spectra upstream of the shock and in the magnetosphere with results from the calculations, we concluded that He^+ is locally accelerated. The subsequent modeling of the injection and diffusive acceleration at the shock presented evidence that pickup ions can be injected and accelerated more efficiently than solar wind plasma

In conclusion, we have found that in both cases, at the quasi-perpendicular bow shock as well as at the quasi-parallel shock, the energetic He^+ ions observed at the Earth's bow shock predominantly are accelerated out of the incident pickup ion distribution and that the injection processes are more efficient than for acceleration out of the solar wind. The abundance of He^+, however, showed a high variation from event to event. From the limited data set no clear dependence of this variation could be derived.

To study the variation of the related processes with the shock parameters, measurements with a more comprehensive data set are needed. Understanding such variation would then allow extrapolation of the results to other astrophysically relevant shocks. But this thesis presents the important finding that pickup ions are indeed accelerated very efficiently.

LIST OF REFERENCES

Asbridge, J.R., S. J. Bame, I.B. Strong, Outward flow of protons from the Earth's bow shock, J.Geophys. Res. 73,577,1668.

Asbridge, J.R., S. J. Bame, J.T. Gosling, G. Paschmann, and N. Sckopke, Energetic plasma ions within the Earth's magnetosheath, Geophys. Res. Lett., 5, 953, 1978

Axford, W.I., C.P. Sonnett, P.J. Coleman,Jr., J.M. Wilcox(eds), The solar wind, Nasa-SP308,609,1972.

Axford, W.I., E. Leer and G. Skadron, The acceleration of cosmic rays by shock waves, Proc. Int. Conf. Cosmic Rays 15th, 11, 132, 1977.

Axford, W.I., The acceleration of galactic cosmic rays, Origin of Cosmic Rays, Proc. 339, 1981.

Bame, S.J., J.R. Asbridge, W.C. Feldman, M.D. Montgomery and P.D. Kearney, Solar wind heavy ion abundances, Sol. Phys., 43, 463, 1975.

Bame, S.J., J.R. Asbridge, W.C. Feldman,J.T. Goslling, G. Paschmann and N. Sckopke, Deceleration of the solar wind upstream from the Earth's bow shock and the origin of the diffuse upstream ions, J.Geophys.Res., 85,2981,1980.

Barnes, A., theory of generation of bow-shock-assocoated waves in the upstream interplanetary medium, Cosmic Electr., 1,90, 1970.

Bell, A.R., The acceleration of cosmic rays in shock fronts, I. Mon. Not. R. Astron. Soc., 182, 147, 1980.

Bergess, D., Cyclic behavior at quasi-parallel collisionless shock, Geophys. Res. Lett., 16, 345, 1989.

Bertaux, J. -L., and J.E. Blamont, Astron. Satrophys., 11, 200, 1971.

Biskamp, D., Collisionless shock waves in plasmas, Nucl. Fusion,13,719-740,1973.

Blandford, R.D., and J.P. Ostriker, Ap. J. (Letters), 221, L29, 1978.

Blandford, R.D., and D. Eichler, Particle acceleration at astrophysical shocks, Phys.Rep., 154, 1, 1987.

Blum, P.M.and H.J. Fahr, Nature223,936,1969.

Bonifazi, C., and G. Morenno, Reflected and diffuse ions backstreaming from the Earth's bow shock, 1, Basic properties, J.Geophys.Res.86, 4397, 1981a.

Bonifazi, C., and G. Morenno, Reflected and diffuse ions backstreaming from the Earth's bow shock, 2, Origin, J.Geophys.Res.86, 4405, 1981b.

Burgess, D., Cyclic behavior at quasi-parallel collisionless shocks, Geophys.Res.Letter, 16, 345, 1989.

Cummings, J.R., A.C. Cummings, R.A. Mewaldt, R.S. Sclesnick, E.C. Stone, and T.T. Von Rosenvinge, New evidence for geomagnetically trapped anomalous codmic rays, Geophys. Res. Lett., 20, 2003, 1993.

Dalaudier, F., J.L. Bertaux, V.G. Kurt, and E.N. Mironova,
Astron. Astrophys., 134, 171, 1984.

Decker, R.B. and L. Vlahos, Modeling of ion acceleration through drift and diffusion at interplatary shocks, J.Geophys. Res., 91,13349, 1986a.

Decker, R.B. and L. Vlahos, Numericak studies of particle acceleration at turbulent, oblique shocks with an application to prompt ion acceleration during solar flares, Astrophys. J., 306, 710, 1986b.

Decker, R.B., The role of drifts in diffusive shock acceleration, Astrophys. J., 324, 566, 1988.

Drury,L.O'C., An introduction of the theory of diffusive shock acceleration of energetic particles in tenuous plasmas, Rep. Prog. Phys., Vol. 46, pp. 973, 1983.

Ellison, D.C., Monte carlo similation of charged particles upstream of the Earth's bow shock, Geophys.Res.Letters, 8, 991, 1981.

Ellison, D.C. and E. Möbius, Diffusive shock acceleration: Comparison of a unified shock model to bow shock observations, Astrophys.J., 318, 474, 1987.

Ellison, D.C. and E. Möbius and G. Paschmann, Particles injection and acceleration at Earth's bow shock: Comparison of upstream and downstream events, Astrophysical Journal, 352, 376, 1990.

Fairfield, D.H., Bow shock associated waves observed in the far upstream interplanetary medium, J. Geophys. Res. 74, 3541, 1969.

Fan, C.Y., G. Gloeckler, and D. Hovestadt, Ion and electron pulses observed in the magnetotail and rapid annihilation of magnetic field lines, Astrophys.J.,209,259,1976.

Fan, C.Y., G. Gloeckler, and D. Hovestadt, The composition of heavy ions in solar energetic particle events, Space Sci. Rev., 38, 143, 1984.

Fahr, H.J., Astrophys.Space Sci.,2474,1968.

Fisk, L.A., B. Koslovsky, and R. Ramaty, Astrophys. J. Lett., 190, L35, 1974.

Forman, M.A. and G.M. Webb, Acceleration of energetic particles, in: Collisionless Shocks in the Heliosphere: A Tutorial Review, Geophys. Mono. Ser., Vol. 34, ed. by B.T. Tsyrytani and R.G. Stone, pp. 91, AGU, Washington D.C., 1985.

Frank, L.A., W.R. Paterson, K.L. Ackerson, F.V. Cortini, ans V.M. Vasyliunas, Plasma observation at Venus with Galileo, Science, v53, 1528, 1991.

Fuselier, S.A., M.F. Thomsen, J.T. Gosling, S.J. Bame, C.T. Russell, Gyrating and intermediate ion distributions upstream from the Earth's bow shock, J. Geophys. Res., 91, 91, 1986a.

Fuselier, S.A., J.T. Gosling and M.F. Thomsen, The motion of ions specular reflected off a quasi-parallel shock in the presence of large amplitude, monochromatic MHD waves, J. Geophys. Res., 91, 4163, 1986b.

Fuselier, S.A., M.F. Thomsen, S.P.Gary, S. J. Rame, C.T. Russell, and G. K. Parks,The phase relationship between gyrophase-bunched ions and MHD-Like waves, Geophys. Res. Lett., 13, 60, 1986c.

Fuselier, S.A., O.W. Lennartsson, M.F. Thomsen and C.T. Russel, Specularly reflected He^{2+} at high mach number quasi-parallel shocks, J. Geophys. Res., 95, 4319, 1990.

Fuselier, S.A., O.W. Lennartsson, M.F. Thomsen and C.T. Russel, He^{2+} heating at quasi-parallel shock, J. Geophys. Res., 96, A6, 9805,1991.

Fuselier, S.A., and M.F.Thomsen, He^{++} in field aligned beams: ISEE results, Geophys. Res. Letters, 19, 437, 1992.

Fuselier, S.A., Suprathermal ions upstream and downstream from the Earth's bow shock, American Geophys. Union, pp. 107, 1994.

Garcia-Munoz, M., G.M. Mason, and J.A. Simpson, Astrophys. J. Lett., 182, L81, 1973. 274, L93, 1983

Gary, S.P., J.T. Gosling amd D.W. Forslund, The electromagnetic ion beam instability upstream of the Earth's bow shock, J. Geophys. Res., 86, 6691, 1981.

Geiss, J., G. Gloeckler, U. Mall, R. von Steiger, A.B. Galvin, and K.W. Ogilvie, Astron. Astrophys., 1993.

Geiss, J., G. Gloeskler, U. Mall, et al., A$A 282, 924, 1994.

Geiss, J., G. Gloeskler, and R. von Steiger, Space Sci. Rev., 1996.

Giacalone, J., D. Burgress, S.J. Schwartz, and D.C. Ellison, Hybrid simulations of protons strongly accelerated by a parallel collisionless shock, Geophys. Res. Lett., 19, 433, 1992.

Giacalone, J., D. Burgress, S.J. Schwartz, and D.C. Ellison, Ion injection and acceleration at parallel shocks: Comparison of self-consistent plasma simulations with existing theories, Astrophys. J., 402, 550, 1993.

Gleeson, L.J. amd W.I. Axford, Cosmic rays in the interplanetary medium, Astrophys. J., 149, L115,1967.

Gloeckler, G., B. Wilken, W. Stüdemann, F. M. Ipavich, D. Hovestadt, D. C. Hamilton and G. Kremser, Geophys. Res. Lett., 12,325, 1985.

Gloeckler, G. and D.C. Hamilton, AMPTE Ion Composition Results, Physica Scripta. Vol. T18, 73, 1987.

Gloeckler, G., L.A. Fisk, and N. Schwardron, Weak pitch angle scattering of few MV regidity ions from measurements of anisotropies in the distribution function of intersterllar pickup hydrogen, Geophys. Res. Lett., 22, 2665, 1995.

Gloeckler, G., J. Geiss, H. Balsiger, L.A. Fisk, A.B. Galvin, F.M. Ipavich, K.W. Ogilvie, R. von Steiger, and B. Wilken, Astron. Astrophys. Suppl., ser. 92, 267, 1992.

Gloeckler, G., J. Geiss, H. Balsiger, L.A. Fisk, A.B. Galvin, F.M. Ipavich, K.W. Ogilvie, R. von Steiger, and B. Wilken, Science, 261, 70, 1993.

Gosling, J.T., J.R. Asbridge, S.J. Bame, G. Paschmann and N. Sckopke, Observation of two distinct populations of bow shock ions in the upstream solar wind, Geophys .Res. Letters, 5, 957, 1978.

Gosling, J. T., M. F. Thomsen, S. J. Bame, W. C. Feldman, G. Paschmann, and N. Sckopke, Evidence for specularly reflected ions upstream from the quasi-parallel shock, Geophys. Res. Lett., 9, 1333, 1982.

Gosling, J.T.and A.E. Robson, Ion reflection, Gyrating, and dissipation at supercritical shocks, in Collisionless shocks in the helisphere: Reviews of current research, Edt BruceT. Tsurutani and Robert G.Stone, AGU, Washington, D.C.,1985.

Gosling, J. T., M.F. Thomsen, S.J. Bame, And C.T. Russell, Ion reflection and downstream thermalization at the quasi-parallel bow shock, J. Geophys. Res. 94, A8, 10027, 1989a.

Gosling, J. T., M.F.Thomsen, S.J. Bame, And C.T.Russell, On the source of diffuse, superathermal ions observed in the vicinity of the Earth's bow shock, J. Geophys. Res., 94, 3555, 1989b.

Greenstadt, E. W., Phenomenology of the Earth's bow shock system. A summary description of experimental results in magnetospheric particles and fields, edited by B. M. McCormac, pp. 13-28, D. Reidel Publishing company, Dordrecht-Holland, 1976.

Hall, D.E., and P.A. Sturrock, Diffusion, scattering and acceleration of particles by stochastic magnetic fields, Phys. Fluids, 10, 2620, 1967.

Hada, T., Nonlinear evolution of waves and shocks in the solar wind, Thesis, University of California, 1985.

Hinteregger, H.E., Atm.Terr. Phys., 38,791, 1976.

Holzer, T. E., Interacton of the solar wind with the neutral component of the interstellar gas, J. Geophys. Res., 77, 5407, 1972.

Holzer, T. E., Rev. Geophys. Space. Phys. 15, 467, 1977.

Hoppe, M.M., C.T. Russell, L.A. Frank, T.E. Eastman, E.W. Greenstadt, Upstream hydromagnetic waves and their association with backstreaming ions population:ISEE-1 and ISEE-2 observations, J. Geophys. Res., Vol. 86, No.A4, 4471, 1981.

Hoppe, M.M., and C.T.Russell, Plasma rest fame fewquencies and polarizations of the low-frequency upstream waves: ISEE 1 and ISEE 2 observations, J. Geophys. Res., 88, 2021, 1983.

Hoshino, M. and T. Terasawa, Numerical study of the upstream wave excitation mechanism 1 Nonlinear phase bunching of beam ions, J. Geophys. Res., 90, 57, 1985.

Hovestadt, D., D. Vollmer, G. Gloeckler, And C.Y. Fan, Differential energy spectra of low-energy (<8.5 MeV per nucleon) heavy cosmic rays during solar quiet times, Phys. Res. Lett., J. 31, 650, 1973.

Hundhausen, A.J., Coronal Expansion and Solar wind, Springer Verlag, Berlin, 1972.

Ipavich, F.M., G. Gloeckler, C.Y. Fan, L.A. Fisk, D. Hocvestadt, B. Klecker, J.J. O'Gallagher and M. Sholer, Initial observations of low energy charged particles near the earth's bow shock on ISEE-1 , Space Sci. Rev., 23, 93, 1979.

Ipavich, F.M., A.B. Galvin, G. Gloeckler, M. Scholer and D. Hovestatd, A statistical survey of ions ovserved upstream of the Earth's bow shock: energy spectra, composition and spatial variations, J. Geophys. Res., Vol. 86. No.A6, 4337,1981.

Ipavich, F.M., J.T. Gosling and M. Scholer, Correlation between the He/H ratios in the upstream particle events and in the solar wind, J. Geophys. Res., Vol. 89, No.A3, 1501, 1984.

Ipavich, F.M., G. Gloeckler, D.C. Hamilton, L.M. Kistler, J.T. Gosling, Protons and alpha particled in field-aligned beams upstream of the bow shock, Geophys. Res. Letters, Vol.15, No.10, 1153, 1988.

Isenberg, P.A., J.Geophys. Res., 92, 1067, 1987.

Jokipii, J.R., Particle drift, diffusion, and acceleration at shocks, Astrophys.J., 255, 716, 1982.

Jokipii, J.R., Rate of energy gain and maximum energy in diffusive shoack acceleration, Astrophys. J., 313, 842, 1987.

Jokipii, J.R., The anomalous component of cosmic rays in physics of the outer heliosphere, edited by S.Grzedzielski and D.E. Page, pp. 169, COSPAR, Pergamon, New york, 1990.

Jones, J.F., and D.C. Ellison, The plasma physics of shock acceleration, Space Sci. Rev., 58, 259, 1991.

Kennel, C.F., and F. Englemann, Velocity space diffusion from weak plasma in a magnetic fiels, Phys. Fluids, 9, 2377, 1966.

Krymsky, G.F., Soviet phys. Dokl., 22, 327, 1977.

Kucharek, H. and M. Scholer, Origin of diffuse superthermal ions at quasi-parallel supercritical collisionless shocks, J. Geophys. Res., 96, 21195, 1991.

Lallement, R., J.-L. Bertaux, and J.T. Clarke, Science, 260, 1095, 1993.

Lee, M. A. and G. Skadron, A simple model for the formation of "reflected", "intermediate", and "diffuse" ion distributions upstream of Earth's bow shock, J. Geophys. Res., 9, A1, 39, 1985.

Lee, M. A., Coupled hydromagnetic wave excitation and ion acceleration upstream of the Earth's supercritical bow shocks, J. Geophys. Res., 87, 5093, 1982.

Lee, M. A., V. Shapiro, R. Z. Sagdeev, Pickup ion energization by shock surface, J. Geophys. Res., 101, A3, 4777, 1996.

Leroy, M. M., C. C. Goodrich, D. Winske, C. S. Wu, and K. Papadopoulos, Simulation of a perpendicular bow shock, Geophy. Res. Lett., 8, 1269, 1981.

Leroy, M. M., D. Winske, C. C. Goodrich, C. S. Wu, and K. Papadopoulos, The structure of perpendicular bow shock, J. Geophys. Res., 87, 5081, 1982.

Lin, R. P., C. I. Meng, and K. A. Anderson, 30 to 100 KeV protons upstream from the earth's bow shock, J. Geophys. Res., 79, 489, 1974.

Luhman, J.G., A quasi-linear equation for cosmic rays in the interplanetary medium, J. Geophys. Res., 81, 2089, 1976.

Luhman, J.G., R.J. Walker, C.T. Russel, J.R. Spreiter, S.S. Stanhara, a,d D.J. willisms, Mapping the magnetosheath field between the magnetopause and the bow shock: implication for the magnetospheric particle leakage, J. Geophys. Res., 89, A8, 6829, 1984.

Lühr, H., N. Klöcker, W. Oelschlägel, B. Häusler, and M. Acuna, The IRM fluxgate magnetometer, IEEE Transsction on Geoscience and Remote Sensing, GE-23(3), 259, 1985.

Lyu, L.H., and J.R. Kan, Ion leakage, ion reflection, ion heating and shock reformation in a simuleted supercritical quasi-parallel collisionless shock, Geophys. Res. Letters, 17, 1041, 1990.

McDonald, F.B., et al., Astrolhys. J. Lett., 185, L105, 1974.

Mitchell, D. G., E. C. Roelof, T. R. Sanderson, R. Reinhard and K. P. Wenzel, ISEE/IRP observations of simultanaous upstream ion events, J. Geophys. Res., 88, 5635, 1983.

Möbius, E., G. Gloeckler, D. Hovestadt, F.M. Ipavich, B. Klercker, M. Scholer, H. Arbringer, H. Höfner, E. Künneth, P. Laeverenz, A. Luhn, E.O. Tums and H. Waldleben, The time-of-flight spectrometer SULEICA for ions in the energy range 5-270 Kev/charge on AMPTE/IRM, IEEE Transaction on Geoscience and Remote Sensing, Vol. GE-23(3), 274, 1985a.

Möbius, E., D. Hovestadt, B. Klecker, M. Scholer, G. Gloeckler, and F. M. Ipavich, Direct observation of He+ pickup ions of interstellar origin in thr solar wind, Nature 318, 426, 1985b.

Möbius, E., D. Hovestadt, B. Klecker, M. Scholer, F. M. Ipavich,.C.W. Carlson, R.P. Lin, A burst of energetic O+ ions duriong an upstream particle event, Geophys.Res. Letters, Vol. 13, No. 13, 1372, 1986.

Möbius, E., Pick-up of interstellar neutrals by the solar wind, Adv.Space Res.Vol.6, No.1, pp. 199-208, 1986.

Möbius, E., M. Scholer, N. Sckople, H. Lühr, G. Paschmann and D. Hovestadt, The distribution function of diffuse ions and the magnetic field power spectrum upstream of the Earth's bow shock, Geophys. Res. Letters, Vol. 14, No. 7, 681, 1987.

Möbius, E., B. Klecker, D. Hovestadt, and M. Sholer, Interaction of interstellar pick-up ions with the solar wind, Astrophys. Space Sci., 144, 487, 1988.

Möbius, E., S. Grzedzielski, and D.E. Page eds, Physics of the outer Heliosphere, Pergamon, 345, 1990.

Möbius, E., D. Rucinski, D. Hovestadt, B. Klecker, The hilium parameters of the very local interstellar medium as derived from the distribution of He+ pick up ions in the solar wind, Astron. Astrophys., 304, 505, 1995a.

Möbius, E., M.A. Lee, P.A. Iswnberg, D. Rucinski,and B. Klecker, EOS Trans., 76(17), S229, 1995b.

Möbius, E., D. Rucinski, P.A. Isenberg, M.A. Lee, Ann. Geophys., 14, 492, 1996.

Moore, K.R., D.J. McComas, C.T. Russell, and J.D. Mihalov, Superathermal ions observed upstream of the Venus bow shock, J .Geophys. Res., 94, 3743, 1989.

Onsager, T.G., M.F. Thomsen, J.T. Gosling, S.J. Bame, and C.T. Russell, Survey of coherent ion reflection at the quasi parallel bow shock, J. Geophys. Res., 95, 2261, 1990.

Onsager, T.G., D. Winske and M.F. Thomsen, Ion interaction simulations of quasi parallel shock reformation, J. Geophys. Res., 96, 21, 183, 1991.

Paschmann, G., N. Sckopke, S. J. Bame, J. R. Asbridge, J. T. Gosling, C.T. Russell and E.W. Greenstadt, Association of low-frequency waves with suprathemal ions in the upstream solar wind, Geophys. Res. Letters, 6, 209, 1979.

Paschmann, G., N. Sckopke, J. R. Asbridge, S. J. Bame, and J. T. Gosling, Energization of solar wind ions by reflection from the earth's bow shock, J. Geophys. Res., 85, 4689, 1980.

Paschmann, G., N. Sckopke, S. J. Bame, and J. T. Gosling, Observations of gyrating ions in the foot of the nearly perpendicular bow shock, Geophys. Res. Lett., 9, 881, 1982.

Paschmann, G., H. Loidl, P. Obermayer, M. Ertl, R. Laborenz, N. Sckopke, W. Baumjohann, C.W. Carlson and D.W. Curtis, The Plasma Instrument for AMPTE/IRM, IEEE Transaction on Geoscience and Remote Sensing, Vol. GE-23, No.3, 262, 1985.

Quett, K. B., Theory and simulation of collisionless parallel shocks, J. Geophys. Res., 93, 9649, 1988.

Russell, C. T., and E. W. Greenstadt, Initial ISEE magnetometer results: Shock observations, Space Sci. Res., 23, 3, 1979.

Russell, C. T., J.G. Luhmann, T.J. Odera, and W.F. Stuart, The rate of occurrence of dayside PC 3,4 pulsations: The L-value dependence of the IMF Cone angle effect, Geophys. Res. Lett., 10, 663, 1983.

Sarris, E.T., S.M. Krimigis and T.P. Armstrong, Observation of magnetospheric bursts of high-energy protons and electrons at ~35 R_E with IMP 7, J. Geophys. Res., 81, 2341, 1976.

Scholer, M., and G. Morfill, On the Alpha to proton ratio changes in energetic storm particle events, J. Geophys. Res., 81, 28, 5027, 1976.

Scholer, M., G.Gloeckler, F.M. Ipavich, D. Hovestadt, B.Klecker, Pitch angle distributions of energetic protons neat the earth's bow shock. Geophys. Res. Letters, Vol.6, No.9, 707,1979.

Scholer, M., F.M. Ipavich, G. Gloeckler, and D. Hovestadt, Conditions for acceleration of energetic ions ≥ 30 keV associated with the earth's bow shock, J. Geophys. Res., 85, 4602, 1980a.

Scholer, M., F.M. Ipavich, G. Gloeckler, D. Hovestadt, and B. Klecker, Upstream particle events close to the earth shock and far upstream: ISEE-1 and ISEE-3 observations, Geophys. Res. Letter, Vol.7, No.1, 73, 1980b.

Scholer, M., F.M. Ipavich, G. Gloeckler, and D. Hovestadt, Simultaneous observations of energetic protons close to the bow shock and far upstream, J. Geophys., 49, 186, 1981.

Scholer, M., Diffusive acceleration, in Collisionless Shock in the Heliosphere: Review of Current Research, pp. 287, American Geophysical Union, 1985.

Scholer, M. and T. Terasawa, Ion reflection and dissipation at quasi-parallel collisionless shocks, Geophys. Res. Letters, 7, 119, 1990.

Scholer, M., and D. Burgess, The role of upstream waves in supwecritical quasi-parallel shock reformation, J. Geophys. Res., 97, 8319, 1992.

Sckopke, N., G. Paschmann, S. J. Bame, J. T. Gosling, and C. T. Russell, Evolution of ion distributions across the nearly perpendicular bow shock: Specularly and nonspecularly reflected ions, J. Geophys. Res., 88, 6121, 1983.

Siscoe, G.L., N.R. Mukherjee, J. Geophys. Res., 77, 6042, 1972.

Sonnerup, B. U. O., Acceleration of particles reflected at a shock front, J. Geophys. Res., 74, 1301-1304, 1969.

Schwartz, S.J., and D. Burgess, On the theoretical/observational comparison of field-aligned ion beams in the Earth's foreshock, J. Geophys. Res., 89, 2381, 1984.

Schwartz, S.J., M.F. Thomsen, On the theoretical/observational comparison of field-aligned ion beams in the Earth's foreshock, J. Geophys. Res., 89, 2381, 1984.

Terasawa, T., Energy spectrum and pitch angle distribution of particles reflected by MHD shock waves of fast mode, Planet. Space Sci., 27, 193, 1979.

Thosmas, G.E., and Siscoe, G.L., J. Geophys. Res., 81, 1247,1976.

Thomas, V.A., D. Winske and N. Omidi, Re-forming supercritical quasi-parallel shocks, I. one and two dimensional simulations, J. Geophys. Res., 95, A11, 18809, 1990.

Thomsen, M.F., J.T. Gosling, S.J. Bame, T.G. Onsager and C.T. Russell, Gyrating and large-amplitude momochromatic MHD waves upstream Earth's bow shock, J. Geophys. Res., 90, 267, 1985.

Thomsen, M.F., J.T. Gosling, S.J. Bame, T.G. Onsager and C.T. Russell, Two-stage ion heating at quasi-parallel shocks, J. Geophys. Res., 95, 6363, 1990.

Trattner, K.J. And M. Scholer, Diffuse minor ions upstream of simulated quasi-parallel shocks, J. Geophys. Res., 99, A4, 6637,1994.

Trattner, K.J. And M. Scholer, Diffuse alpha particles upstream of simulated quasi-parallel supercritical collisionless shocks, Geophys. Res. Lett., 18, 1817, 1991.

Völk, H.J., Nonlinear theory of cosmic ray acceleration in shock waves, in: High Ener. Cosmic Rays, ed: J. Audouze, 1984.

Vasyliunas, V. M., and G. L. Siscoe, On the flux and energy spectrum of interstellar ions in the solar system, J. Geophys. Res., 81, 1247, 1976.

West, H. I., and R. M. Buck, Observations of > 100 Kev protons in the earth's magnetosheath, J. Geophys. Res., 81, 569, 1976.

Winske, D., C.S. Wu, Y.Y. Li, Z.Z. Mou, S.V. Guo, J. Geophys. Res., 90, 2713, 1985.

Witte, M., H. Rosenbauer, M. Banazkiewicz, and H.J. Fahr, Adv. Space Res., 1993.

Wu, C.S., Unified theory of weakly turbulent plasmas, Phys. Fluids, 11, 1733, 1968.

Wu, C.S., and R.C. Davidson, J. Geophys. Res., 77, 5399, 1972.

Wu, C.S., R.E. Hartle, and K.W. Ogilvie, J.Geophys. Res., 78, 306, 1973.

Zwickl, R.D., S.M. Krimigis, J.F. Carbary, E.P. Keath, T.P. Armstrong, D.C. Hamilton and G. Gloeckler, Energetic particle events (≥ 30 keV) of the Jovian origin ovserved by Voyager 1 and 2 in interplanetary space, J. Geophys. Res., 86, 8125, 1981.

IMAGE EVALUATION
TEST TARGET (QA-3)

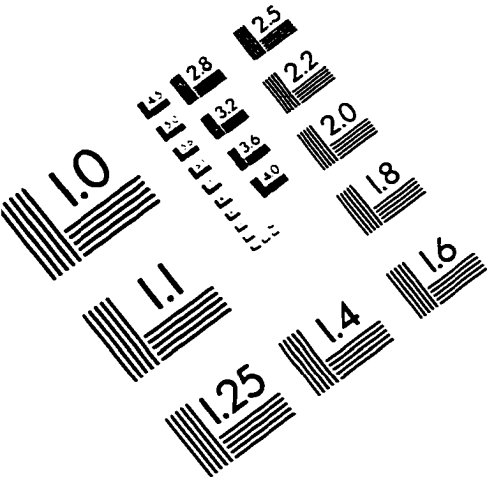

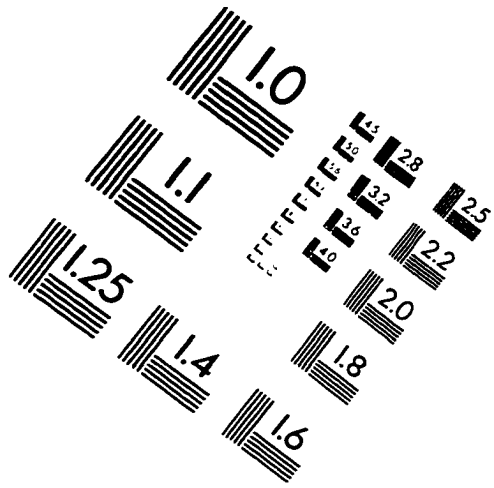

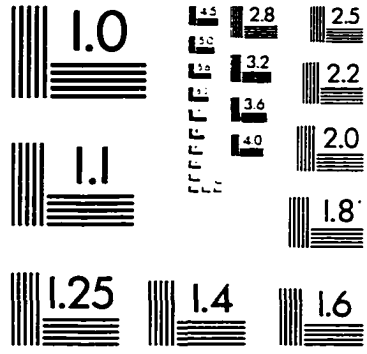

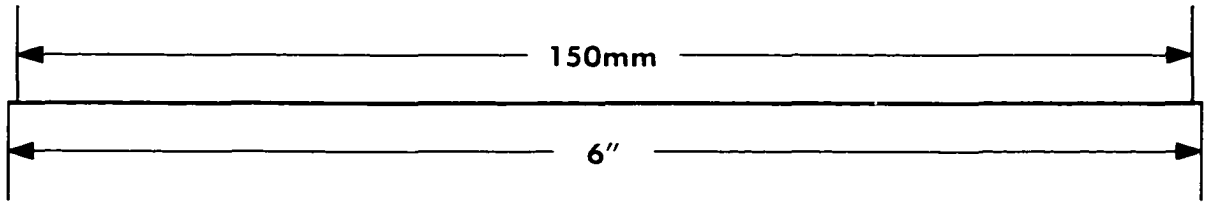

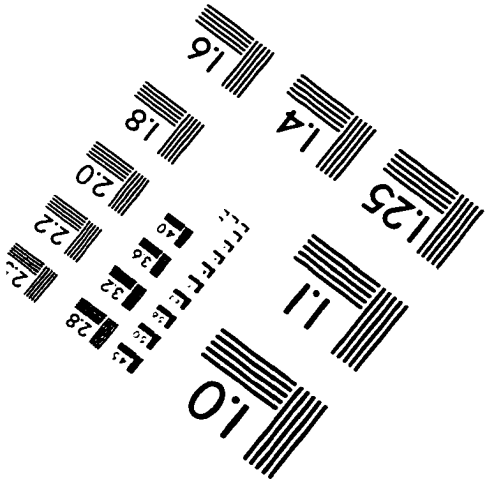

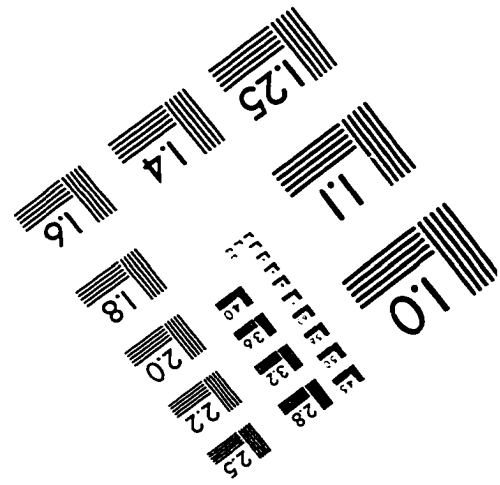

APPLIED IMAGE, Inc
1653 East Main Street
Rochester, NY 14609 USA
Phone: 716/482-0300
Fax: 716/288-5989